ANL-6231
Chemical Separations Processes
for Plutonium and Uranium
(TID-4500, 16th Ed.)
AEC Research and
Development Report

ARGONNE NATIONAL LABORATORY
9700 South Cass Avenue
Argonne, Illinois

CHEMICAL ENGINEERING DIVISION SUMMARY REPORT

July, August, September, 1960

Stephen Lawroski, Division Director
R. C. Vogel, Associate Division Director
V. H. Munnecke, Assistant Division Director

Preceding Quarterly Reports:

ANL-6183	April, May, June, 1960
ANL-6145	January, February, March, 1960
ANL-6101	October, November, December, 1959

Operated by The University of Chicago
under
Contract W-31-109-eng-38

DISCLAIMER

This report was prepared as an account of work sponsored by an agency of the United States Government. Neither the United States Government nor any agency thereof, nor any of their employees, make any warranty, express or implied, or assumes any legal liability or responsibility for the accuracy, completeness, or usefulness of any information, apparatus, product, or process disclosed, or represents that its use would not infringe privately owned rights. Reference herein to any specific commercial product, process, or service by trade name, trademark, manufacturer, or otherwise does not necessarily constitute or imply its endorsement, recommendation, or favoring by the United States Government or any agency thereof. The views and opinions of authors expressed herein do not necessarily state or reflect those of the United States Government or any agency thereof.

DISCLAIMER

Portions of this document may be illegible in electronic image products. Images are produced from the best available original document.

TABLE OF CONTENTS

	Page
SUMMARY	9
I. CHEMICAL-METALLURGICAL PROCESSING	22
A. Fuel Processing Facilities for EBR-II	26
1. Design, Development, and Construction of Buildings and Equipment	26
2. EBR-II Fuel Processing Mockup	33
B. Pyrometallurgical Development	38
1. Melt Refining	38
2. Liquid Metal Solvents Process Development	53
C. Pyrometallurgical Research	67
1. Chemistry of Liquid Metal Solvents	67
2. Calorimetry	80
II. FUEL CYCLE APPLICATIONS OF VOLATILITY AND FLUIDIZATION TECHNIQUES	90
A. Laboratory Investigations of Fluoride Volatility Processes	93
1. Fluorine Chemistry and Fluoride Separation Studies	94
2. Metal Fluorination Studies	104
B. Engineering-scale Investigations of Fluoride Volatility Processes	108
1. Direct Fluorination Process for Oxide Fuels	109
2. Direct Fluorination Process for Uranium-Zirconium Alloys	117
3. Direct Fluorination Process for Stainless Steel-clad or Matrix Fuels	123
4. Fused Salt Processing of Zirconium Matrix Fuels	127
C. Conversion of Uranium Hexafluoride to Uranium Dioxide	132
D. Multistage Fluidization	135
III. REACTOR SAFETY	136
A. Metal Oxidation and Ignition Kinetics	138
1. Ignition Studies by the Burning-curve Method	138
2. Burning-propagation Studies	150
3. The Kinetics of Uranium Oxidation	153

TABLE OF CONTENTS

		Page
	B. Metal-Water Reactions	155
	1. Laboratory Studies: Condenser-discharge Method	155
	2. In-pile Testing in the TREAT Reactor	159
IV.	REACTOR CHEMISTRY	166
	A. Determination of Nuclear Constants	167
	1. Fast Neutron Capture in Uranium-236	167
	2. Capture and Fission Cross Sections of Uranium and Plutonium Isotopes in EBR-I, Mark III	167
	B. Slurrex Chemical Supporting Program	168
	C. Reactor Decontamination	168
	1. Laboratory Studies	169
	2. Loop Operations	173
	3. Present Status of the Work	179
	D. Structural Materials for Nuclear Superheaters	181
V.	ROUTINE OPERATIONS	182
	A. Radioactive Waste Processing	182
	B. High-level Gamma Irradiation Facility	182

LIST OF TABLES

No.	Title	Page
1.	Nitridation of Uranium and Uranium-Fissium Pins	48
2.	Effect of Sodium on Ingot Yield	50
3.	Comparison of Various Thermal Insulation Modifications in the Melt-refining Assembly	52
4.	Some Fission Product Concentrations in Skull Oxides	56
5.	Summary of Small-scale Magnesium Reductions of Uranium Oxide	59
6.	Performance of Tantalum as a Container Material for Retorting Uranium-Zinc Systems	64
7.	Solubility of Zirconium in Cadmium	69
8.	Solubility of Samarium in Cadmium	71
9.	Solubility of Yttrium in Cadmium	73
10.	Distribution Data for Lead-Zinc System	74
11.	Results of Molybdenum Combustions in Fluorine	83
12.	Combustion of Boron in Fluorine	86
13.	Reaction of Plutonium Hexafluoride and Sulfur Tetrafluoride	97
14.	Reaction of Sulfur Tetrafluoride and Plutonium Dioxide	99
15.	Reaction of 90 Per Cent Hydrogen Fluoride - 10 Per Cent Hydrogen Chloride Gas Mixtures with Uranium Dioxide	102
16.	The Corrosion of A-Nickel by a Gas Mixture of 90 Volume Per Cent Hydrogen Fluoride and 10 Volume Per Cent Hydrogen Chloride	107
17.	Gas-phase Decladding of Zircaloy-clad Elements	110
18.	Effect of Baffles on Back-mixing in a Fluidized Bed	119
19.	Summary of Hydrochlorination-Hydrofluorination Runs for the Two-zone Process	121
20.	Results of Fluorination Experiments on Solids from Hydrochlorination-Hydrofluorination of Uranium-Zirconium Alloys	122
21.	Results of Pellet Fabrication Experiments on Uranium Dioxide Prepared by Fluid-bed Conversion of Uranium Hexafluoride	134

LIST OF TABLES

No.	Title	Page
22.	Comparison of Ignition Temperatures of Individual Specimens and Aggregates for Uranium in Oxygen	140
23.	The Effect of Halogenated Hydrocarbons on the Burning Properties of Uranium Foils in Air	141
24.	Size Distribution of Subsieve Spherical Uranium Powder	145
25.	Size Distribution of Subsieve Irregular Uranium Powder	146
26.	Theoretical Ignition Temperatures of Uranium Based on Frank-Kamenetskii Theory of Thermal Explosions	150
27.	Burning-propagation Rates at Elevated Ambient Temperatures	151
28.	The Effect of Various Gas Contaminants on the Burning-propagation Rate in Air of Zirconium and Plutonium Foils	152
29.	Zirconium-Water Reaction Data from High-pressure Condenser Discharge Apparatus	157
30.	Summary of Results of Recent In-pile Metal-Water Experiments	159
31.	Specific Fission Product Decontamination by the Alkaline Permanganate Procedure	170
32.	Distribution of Fission Product Activity after an Autoclave Contamination Run	172
33.	Corrosion of Chromium-Molybdenum Steel in Alkaline Permanganate-Citrate Solutions	173
34.	Half-lives and Principal Gamma Energies of Fission Products Observed in Loop Runs	175
35.	Comparison of Individual Fission Product Content of Loop Drainings and Residues	177
36.	Removal of Uranium and Beta Activities from Loop following Run U-1	180
37.	Removal of Uranium and Gamma Activities from Loop following Run U-2	180
38.	Summary of Irradiations Performed in Rack M-1 during July through September, 1960	182

LIST OF FIGURES

No.	Title	Page
1.	Thermocouple Locations on Prototype Service Plug and Sleeve	35
2.	Heating Curves for Prototype Service Plug for Argon Cell, Run No. 7	36
3.	Heating Curves for Prototype Service Plug for Argon Cell, Run No. 8	36
4.	Furnace for Heating Highly Irradiated Uranium Alloy Pins	43
5.	Experimental Furnace Auxiliary System	44
6.	Xenon and Krypton Evolution from Highly Irradiated Uranium Alloy Pin	45
7.	Photographs of Irradiated Uranium Alloy Pin during Fission Gas-release Experiment	46
8.	Composition and Size Distribution of Skull Oxides	55
9.	Skull Oxide Reduction by Zinc-10 Weight Per Cent Magnesium	57
10.	Liquid Metal Process for Reclamation of Melt-refining Skulls	60
11.	Solubility of Titanium in Liquid Cadmium	68
12.	Solubility of Zirconium in Cadmium	70
13.	Solubility of Samarium in Cadmium	72
14.	Solubility of Yttrium in Cadmium	73
15.	Temperature Dependence of Uranium Distribution in the Lead-Zinc System	75
16.	Emf as a Function of Temperature of the Uranium-Thallium Cell	77
17.	Emf as a Function of Temperature for the Cerium-Zinc Cell	79
18.	Sample Support Method for Molybdenum Combustions in Fluorine	84
19.	Photomicrograph (280 X) of Autoradiograph of Nickel Oxide Scale Containing Nickel-63	105
20.	Photomicrograph (600 X) of Nickel Oxide Scale Showing Porosity	106

LIST OF FIGURES

No.	Title	Page
21.	Heat Transfer from a Small Cylinder to a Fluidized Bed: Effect of Gas Velocity on Heat Transfer Coefficient, h	113
22.	Heat Transfer from a Small Cylinder to a Fluidized Solid in Beds Containing Nonfluidized Packing	114
23.	Configuration Used in Heat Transfer Studies in Packed Fluidized Bed	115
24.	Heat Transfer to a Fluidized Bed Containing Packing and Multiple Heaters	116
25.	Individual Heat Transfer Coefficients for Three Pellet Heaters in the Same Fluid Bed	117
26.	Uranium Removal during Fluorination of Zirconium-Uranium Fluorides	123
27.	Reaction of 304 Stainless Steel with 50 Mole Per Cent Chlorine in Nitrogen	124
28.	Synthetic Zircaloy Fuel Element	127
29.	Dissolution of Zircaloy Element in Fused Salt: Off-Gas Record	127
30.	Frozen Salt in the Dissolver Lampblack Layer	129
31.	Internal Damage to Graphite Components in Salt Remelt Test	130
32.	Relationship Between Sample Specific Area and Ignition Temperature for Uranium in Air and in Oxygen	139
33.	Effect of Sample Height on the Ignition Temperature of -18 +20 Mesh Spherical Uranium Powder	143
34.	Effect of Sample Height on the Ignition Temperature of -80 +100 Mesh Spherical Uranium Powder	144
35.	Effect of Specific Area of Spherical Uranium Powders on Experimental Ignition Temperatures	145
36.	Rate-determining Data for a Typical Uranium Oxidation Run	154
37.	High-pressure Condenser Discharge Apparatus	156
38.	Results of Condenser Discharge Runs with 60-mil Zirconium Wires (nonexplosive runs)	158
39.	Zircaloy-2-jacketed, Oxide-core Pin after Transient CEN-28	160

LIST OF FIGURES

No.	Title	Page
40.	Zircaloy-2-jacketed, Oxide-core Pin after Transient CEN-29	161
41.	Zircaloy-2-jacketed, Oxide-core Pin after Transient CEN-30	161
42.	Radiograph of Zircaloy-2-jacketed, Oxide-core Fuel Pin after Transient CEN-28	162
43.	Cermet-core, Zircaloy-2-jacketed Pin after Transient CEN-31	163
44.	Unused Pin and Melted Pin from Transient CEN-37, Unjacketed Cermet	163
45.	Unused Pin and Melted Pin from Transient CEN-38, Unjacketed Cermet	164
46.	Oscillograph Record of CEN-38	164
47.	Neutron Capture Cross Section of Uranium-236	168
48.	Disengaging Section of Loop Showing Elevation of Components Relative to Reference	174
49.	Gamma-energy Spectrum of Loop Water from Run U-1	175
50.	Composition of Loop Water during Run U-2	176
51.	Deposition of Fission Products on Metal Sample Strip during Run U-1	178
52.	Deposition of Fission Products on Metal Sample Strip during Run U-2	178

CHEMICAL ENGINEERING DIVISION
SUMMARY REPORT

July, August, September, 1960

SUMMARY

I. Chemical-Metallurgical Processing (pages 22 to 89)

A direct-cycle fuel-reprocessing plant using pyrometallurgical procedures is being designed and constructed as part of the Experimental Breeder Reactor No. II (EBR-II) project. A Laboratory and Service Building is also included. Melt refining, liquid metal extraction, and processes involving fractional crystallization from liquid metal systems are methods being examined for the recovery and purification of EBR-II fuels. Based on these studies, process equipment is being designed and tested.

The construction of the Laboratory and Service Building was completed on August 3, 1960, when the building was accepted by the U. S. Atomic Energy Commission. Equipment is being installed in the building.

Construction of the Fuel Cycle Facility Building is continuing. The structure, which was 20 per cent completed by June 6, was 40 per cent completed by September 6, three months later.

The five-ton cranes for the Fuel Cycle Facility have been shipped to the Idaho site. The majority of the drawings for the eight operating manipulators have been approved. Fabrication of the manipulators has started.

The prototype small air lock and component parts were tested in the mockup area. Operation with the manipulator was not completely satisfactory, and, therefore, revisions are required. Work continues on other equipment items for the Fuel Cycle Facility.

As of September 15, 1960, eighty-seven per cent of the total order of Process Cell windows had been delivered to the Idaho site. All the steel window liners are now cast in the concrete of the cell walls.

Irradiation of mineral-insulated (MI) cables sealed with Temporell No. 741 is continuing. Moisture problems have caused insulation resistances to drop; however, for nonpermanent installations using MI cables,

the Temporell would suffice as a sealant. Tests of manipulator power feed cable after irradiation have indicated that the expected life of the cable in the cell might be six years. Bearing tests in which irradiated grease was the lubricant have been run for 300 hours without incident.

Enriched fuel ingot production was resumed and ingots 59 through 80 were poured successfully in mockup equipment. In addition, 14 ingots were poured from melts of pin scraps.

The molded Fiberfrax fume trap has been used successfully during uranium melting and pouring operations.

The first of a series of demonstrations at high-activity levels of the melt-refining process for EBR-II core fuel has been completed. Uranium-five weight per cent fissium fuel pins, ten per cent enriched in uranium-235, were irradiated in CP-5 to a total atom burnup of about 0.6 per cent and cooled approximately 30 days. A 400-gram charge of the irradiated material was melt refined for three hours at 1400 C. Although there was no pin-shell formation and the surface of the ingot had a clean metallic appearance, initial attempts to pour the molten metal were unsuccessful. After the unpoured charge was permitted to cool to room temperature, then remelted, a successful pour was obtained. Analytical information on the fission product behavior is not yet available.

An experiment was also completed on the evolution of fission product krypton and xenon from an irradiated fuel pin as it was heated to a temperature above the melting point. The uranium-fissium pin had been cooled for 49 days prior to the time of the experiment. On heating at a rate of 5 C per minute, the diameter of the pin increased about 40 per cent between temperatures of 650 and 800 C. Rapid evolution of krypton-85 and xenon-133 also began during this period and ended when the pin had reached a temperature of about 1020 C. At this temperature the pin began to lose its cylindrical shape, and at 1080 C melting appeared to be complete.

In the process cell of the EBR-II Fuel Cycle Facility, the argon atmosphere may contain as much as five per cent nitrogen. Since the declad sodium-coated fuel pins are expected to reach a temperature of roughly 300 C during storage as a result of fission product decay heat, the probable extent of uranium nitride formation under these conditions has been considered. Laboratory experiments with uranium and uranium-fissium alloy pins show that the extent of nitridation is significant under these conditions and that it is increased by sodium coatings. In two melt-refining runs on a two-kilogram scale, prior storage of the sodium-coated fissium alloy pins at 300 C in an argon atmosphere containing five per cent nitrogen for 15 and 66 hours, respectively, lowered the melt-refining yield to about 80 per cent. Runs with sodium-coated pins not exposed to the nitrogen-containing atmosphere and melt refined on a one- and two-kilogram scale under conditions

of minimum oxygen contamination produced yields of about 97 per cent. In these runs no rare earths were included.

In tests of alternate materials for use in a melt-refining furnace, a fibrous potassium titanate grain retainer was found to be a very effective heat insulator, but to have less strength than rigid Fiberfrax retainers. Carbon wool was not as effective an insulating material as silicon carbide, graphite, or carbon black powders.

The "skull" remaining in the zirconia crucible after a melt-refining operation must be processed to recover, as partially purified metal, the fissionable material for return to the fuel cycle. Work was continued on the development of this process, which is generally called the "dragout" process.

It is planned to effect removal of skull material by converting it to a free-flowing oxide powder by oxidation in a 20 per cent oxygen-argon atmosphere. Skulls from three plant-scale runs were readily oxidized and the oxide products were easily poured out, with yields of about 99 per cent. As in previous runs, cerium was concentrated in the fine particles while ruthenium and molybdenum were concentrated in the coarse particles.

The possibility of volatilizing certain fission product oxides (those of ruthenium, molybdenum, technetium, and tellurium) during oxidation of skull material was further studied. It has been found that the presence of cerium in the skull decreases the volatilization of molybdenum, probably through a chemical interaction of the two oxides. The volatilization of ruthenium is difficult, requiring flowing oxygen and temperatures above 800 C, and is not affected by the presence of cerium. Preliminary results indicate that technetium behaves much like ruthenium. No volatilization of tellurium has occurred under process conditions.

Several essentially quantitative reductions of uranium dioxide and skull oxides have been achieved in times of less than eight hours at 800 C in dilute magnesium-zinc solutions and in magnesium containing a small percentage (0.5 to 2) of sodium as a wetting agent. In one experiment the presence of a chloride flux increased the reduction rate.

The low and erratic results which were previously obtained in the reductions may be attributed, at least in part, to the use of Vycor sampling tubes. The sampling tubes introduced impurities which precipitated uranium and led to low analyses for uranium. Tantalum sampling tubes are currently being employed and are proving very satisfactory.

Several additional retorting runs were performed in tantalum for recovery of uranium from zinc systems. The uranium metal sinter cake was found to stick to the tantalum crucible when the charge was prepared directly in the retorting crucible, but not when the charge was prepared in

a separate crucible and transferred as an ingot to the retorting crucible. This is probably related to a better opportunity for wetting in the first case. Product removal has almost always been readily accomplished when ceramic or ceramic-coated graphite crucibles are employed.

Evaluation of materials for pyrometallurgical equipment is continuing. The work includes: (1) development of corrosion information, (2) effect of various materials on stability of liquid metal solutions, and (3) accumulation of extensive information on fabrication techniques for the materials of interest.

Among the basic physicochemical data being determined in support of the process development activities are the solubilities of various fissile, fission product, and other elements in liquid metals. The solubility of titanium in liquid cadmium over the temperature range 325 to 650 C may be represented by the equation

$$\log (\text{atom per cent titanium}) = 3.237 - 5333\ T^{-1} + 1.468 \times 10^{6}\ T^{-2} \quad .$$

The solubility of zirconium in cadmium may be represented by the equations

$$(325 \text{ to } 452\ \text{C})\ \log (\text{weight per cent zirconium}) = 3.058 - 2750\ T^{-1}$$

and

$$(452 \text{ to } 575\ \text{C})\ \log (\text{weight per cent zirconium}) = 1.079 - 1314\ T^{-1} \quad .$$

The solubility of samarium in liquid cadmium may be represented by two equations. For the compound $SmCd_{11}$, in equilibrium with the melt below 420.5 C, the solubility is given by

$$(325 \text{ to } 420\ \text{C})\ \log (\text{atom per cent samarium}) = 7.0729 - 4878.2\ T^{-1} \quad .$$

Above 420 C the solubility is given by

$$(420 \text{ to } 609\ \text{C})\ \log (\text{atom per cent samarium}) = 3.0911 - 2116.1\ T^{-1} \quad .$$

The solubility of yttrium in liquid cadmium may be represented by the equation

$$(325 \text{ to } 600\ \text{C})\ \log (\text{weight per cent yttrium}) = 4.8539 - 4687.5\ T^{-1} + 0.7520 \times 10^{6}\ T^{-2} \quad .$$

The partition coefficients of a number of representative fissile and fission product elements between the two immiscible liquids, lead and zinc, at about 735 C have been measured. Values of the coefficients (weight per cent in zinc phase/weight per cent in lead phase) were: uranium, 31.9; palladium, 150; cerium, 3.7; and strontium, 0.14. The coefficient for uranium

was found to vary from 31.9 at 734 C to 270 at 647 C.

The free energy of formation of the uranium-thallium intermetallic compound UTl_3 was measured using a galvanic cell method. Over the temperature range from 370 to 670 C, the results may be represented by the equation

$$\Delta F_f^\circ = -13{,}376 + 12.008\ T \quad .$$

Galvanic cell measurements with the cerium-zinc system over the temperature range from 443 to 742 C were made. The free energy of formation of $CeZn_{11}$ may be represented by the equation

$$\Delta F_f^\circ = -79{,}257 + 25.046\ T + 0.01157\ T^2 \quad ;$$

the activity coefficient of cerium in saturated zinc solutions is given by the equation

$$\log \gamma_{Ce} = -9442\ T^{-1} - 0.8269 + 3.2095 \times 10^{-3}\ T \quad .$$

The study of the heat of formation of tungsten disulfide is being continued. Combustions of tungsten and sulfur in oxygen are being carried out to obtain auxiliary data to complement the data already obtained for combustions of tungsten disulfide in oxygen.

Trial combustions of two uranium nitrides and zirconium dihydride have been carried out preparatory to calorimetric determinations of the heats of formation of these compounds.

The determination of the heat of formation of zirconium tetrafluoride by combustions of zirconium in fluorine has been completed. The following values have been determined for the reaction $Zr(c) + 2F_2(gas) \rightarrow ZrF_4(c,\beta)$ at 25 C: the energy change for reaction or the energy of formation, $\Delta E_c^\circ = \Delta E_f^\circ = -455.71$ kcal/mole; the standard heat of formation, $\Delta H_f^\circ = -456.29$ kcal/mole; and the standard free energy of formation, $\Delta F_f^\circ = -432.63$ kcal/mole.

The experimental work on the determination of the heat of formation of molybdenum hexafluoride by combustion of molybdenum in fluorine has been completed. A preliminary value of -372.44 kcal/mole for $\Delta H_f^\circ(MoF_6\ gas)$ has been obtained.

Calorimetric combustions of boron in fluorine are being continued. Exploratory combustions of magnesium, aluminum, zinc, and cadmium are being carried out.

II. Fuel Cycle Application of Volatility and Fluidization Techniques (pages 90 to 135)

Several processes, in which advantage is taken of the volatilities of uranium and plutonium hexafluoride and in which fluidization techniques are used, have been proposed for the recovery of uranium and plutonium from irradiated reactor fuels. These include a Direct Fluorination Process and the Fused Fluoride Volatility Process.

The Direct Fluorination Volatility Process is being developed to recover uranium and plutonium from spent uranium oxide, Zircaloy-clad, fuel elements. A proposed processing procedure utilizes the reaction of zirconium with a mixture of hydrogen fluoride and hydrogen chloride for decladding. Plutonium and uranium hexafluorides, which result from the reaction of the oxide fuel with fluorine, may be separated using a combination of the variability of the rates of fluorination of the plutonium and uranium compounds and chemical reactivities of the hexafluorides. Equipment has been constructed and is in operation to study the process steps with multigram amounts (10 to 100 grams) of plutonium.

An investigation of the kinetics and mechanism of the decomposition of plutonium hexafluoride vapor suggests that the reaction is heterogeneous at 161 C.

Investigation of the stoichiometry of the reaction of plutonium hexafluoride with sulfur tetrafluoride has been completed. The resultant products are sulfur hexafluoride and plutonium tetrafluoride. The reaction of sulfur tetrafluoride with plutonium dioxide at 600 C to produce plutonium tetrafluoride was found to be slow. The investigation of the stoichiometry of the reactions of sulfur tetrafluoride with uranium trioxide, uranium dioxide, uranyl fluoride, and U_3O_8 has been completed. Uranium hexafluoride is produced equivalent in amount to uranium in the plus six valence state in these compounds.

Radiation decomposition of plutonium hexafluoride in the presence of uranium hexafluoride, 2.6 per cent per day, was found to be very similar to the value obtained for plutonium hexafluoride alone. Uranium hexafluoride decomposed to the extent of 0.3 per cent per day in the gas mixture.

The solubility of hydrogen chloride in liquid hydrogen fluoride at condenser temperatures would be an important process variable in the decladding step of the Direct Fluorination Volatility process. In terms of weight per cent hydrogen chloride, the solubility of hydrogen chloride in liquid hydrogen fluoride is 0.7 at -38 C and 2.4 at -78 C.

An investigation of the corrosive effect of hydrogen fluoride-hydrogen chloride gas mixtures on A-nickel has been initiated. At 500 C, with

a 90 volume per cent hydrogen chloride mixture, after six days, intergranular attack of 0.4 to 1.0 mil was noted. Under these same conditions the penetration rate was 0.023 mil per day as calculated from the weight change of the test coupons. Due to the short durations of these experiments the values should be considered preliminary in nature.

Additional studies of metal fluorinations have been concerned with the mechanisms of the nickel-fluorine and nickel-oxygen reactions. The fluorine reaction appears to occur at the nickel fluoride-nickel interface. In the nickel-oxygen reaction, nickel ions migrate through the nickel oxide and the reaction with oxygen occurs at the nickel oxide-nickel interface.

Work has continued on engineering-scale studies of the Direct Fluorination Process applied to dense uranium dioxide pellet fuel. Two decladding runs were made to investigate the effect of close packing of fuel elements on operation of the fluid-bed reactor. One-half-inch diameter Zircaloy-2 tubing elements containing uranium dioxide pellets were reacted at 500 C with 10 mole per cent hydrogen chloride-90 mole per cent hydrogen fluoride gas. Fourteen-inch lengths of these 30-mil wall tubing elements were submerged vertically in a calcium fluoride fluidized bed. Decladding was successful in both runs. For a near-maximum packing in which the cross-sectional area of the tubes was 55 per cent of the reactor area, formation of a firm cake raised the pressure differential across the bed and prevented free flowing of the bed at the end of the run. When the number of tubes was reduced to half that used in the above run, essentially no caking or pressure increase was found, and the bed was free flowing. No significant pellet degradation or fines production was observed in these runs.

In a shakedown run in the new forced-air-cooled reactor, pellets were fluorinated at substantially higher rates than previously reported (ANL-6183, page 98). It was found that heat transfer was limited by large temperature differentials from the wall to the bed rather than by the external heat transfer surfaces. Fluorination studies are in progress.

Mockup tests of heat transfer from the surface of fixed packing submerged in a fluid bed were made to determine the effects of bed height and gas velocity. The bed of 1/4-inch nickel balls and 140 to 200 mesh copper shot gave heat transfer coefficients in the range from 81 to 125 Btu/(hr)(sq ft)(F) for gas rates sufficient to fluidize the finer material. These heat transfer coefficients were five to eight times higher than with the non-fluidized packing alone and 0.6 to 0.9 of those obtained for fluidized material without packing.

Direct Fluorination Processes are also being studied as a means of recovering uranium from highly enriched uranium-zirconium alloy fuels. In general, the processes involve conversion of the element to fluoride salts by means of hydrogen chloride and hydrogen fluoride. In this step the elements are submerged in a fluidized bed of inert material which serves as

the heat transfer medium. The next step, fluorination with elemental fluorine, is expected to volatilize the uranium as the hexafluoride and permit separation. Emphasis during this quarter was shifted from reactions of the metallic fuel with dilute mixtures of hydrogen chloride in hydrogen fluoride to separate reactions with these gases in a two-zone, fluid-bed reactor. The initial reaction is hydrochlorination, forming the volatile zirconium tetrachloride. The volatile material is converted to the solid tetrafluoride by anhydrous hydrogen fluoride which is admitted in the upper section of the reactor. Baffling between the two reaction zones has been found to reduce gas back-mixing which resulted in gas mixtures of low reactivity. Eighty-five to 94 per cent of a multiplate assembly (1.5 weight per cent uranium-zirconium alloy) was converted to fluorides in about 12 hours by means of this procedure at a temperature of 400 C.

Initial fluorination studies on these reaction products achieved about 85 to 90 per cent removal in two hours at 600 C, in four hours at 550 C, and in eight hours at 500 C. Additional exposure of the fluorinated residues to fluorine at 500 C resulted in increased removal to 96 per cent.

In the Fused Salt Volatility Process for recovery of uranium from zirconium matrix fuels, the alloy fuel elements are dissolved in a molten sodium fluoride-zirconium fluoride mixture at 600 to 700 C with a hydrogen fluoride sparge. A final dissolution was performed in a series of dissolutions of synthetic fuel assemblies to demonstrate operation of the graphite pilot-plant dissolver. A 10-plate Zircaloy-2 fuel element was 90 per cent dissolved in 10.7 hours and 99 per cent dissolved in 13.4 hours. This dissolution rate was slower than previously obtained for pure zirconium and salt without alloy constituents. Nickel fluoride, which had been added to the molten salt, was substantially removed from the salt, probably by reduction on the Zircaloy.

Examination of the walls of the graphite dissolver showed the expected presence of fused salt in the middle of the lampblack insulating zone. No salt had contacted the outer metal shell. About 30 lb of salt were so deposited in the walls.

A fused salt charge was allowed to freeze in the dissolver to determine the effect that this would have on dissolver components. This charge was then remelted in the dissolver. Extensive damage to internal graphite downlines and heaters was found. The fuel element support plate (graphite) was eroded. There was no evidence of mechanical damage to the graphite crucible or chemical attack of any graphite components.

In all of the dissolver runs, entrained solids were removed from the dissolver off-gas by a bed packed with $\frac{3}{16}$-inch sodium fluoride pellets followed

by grade 60 porous carbon filters. The carbon filters were successful in removing all fines that passed the absorber bed.

The reaction of stainless steel with various gases is being investigated as an initial step in the processing of stainless steel-clad or matrix fuels. Studies carried out in a one-inch horizontal tube furnace showed the initial reaction rates of chlorine and stainless steel, determined by weight loss of the test specimen, were 5.0 mils/hr at 570 C and 9.7 mils/hr at 600 C. The effect of nitrogen dilution was found to be negligible at chlorine concentrations above 50 per cent. A mixture of chlorine and hydrogen fluoride showed a much lower penetration rate than did the chlorine alone. Monel equipment was found to be severely corroded by chlorine. This was caused by leaching of the copper component as cuprous chloride. A single experiment on the reaction of fluorine gas with a 304 stainless steel specimen at 550 C in a fluid-bed reactor gave a low penetration rate, 0.7 mil/hr.

The conversion of uranium hexafluoride to uranium dioxide by reaction with steam and hydrogen in a fluid bed is being studied. A short run at a high temperature (650 C) and high hexafluoride rate, 217 lb/(hr)(sq ft reactor cross section), confirmed that essentially complete conversion (99.99 per cent) to solids is readily achieved, but a second step is required to produce specification-grade (low fluoride) powder by further reaction of the solid with steam and hydrogen. Installation of a three-inch diameter column which will be used for additional studies of the second step is almost complete. Pellet fabrication tests performed by the ANL Ceramics Group achieved about 94.5 to 97 per cent theoretical density for dioxide prepared by this process. One-kilogram samples of dioxide powder prepared from uranium hexafluoride by the direct conversion process have been furnished to seven industrial concerns that wish to evaluate the material.

A mass transfer study of the adsorption of water vapor by silica gel is being made to evaluate the characteristics of the new multistage fluidized-bed reactor, as the second phase of a doctoral thesis research problem.

III. Reactor Safety (pages 136 to 165)

The oxidation, ignition, and combustion processes of uranium, zirconium, plutonium, and thorium are being studied to provide information to aid in minimizing the hazards associated with handling these metals.

In the continued study of the ignition of uranium it has been confirmed that an aggregate or array of pieces ignites at a considerably lower temperature than an individual piece of the same specific area. The condition of decreased heat loss from an interior piece surrounded by other pieces which are also generating heat by reaction may be the explanation of some of the uranium fires which have occurred.

The results of sample geometry studies on the ignition behavior of uranium powder show that constant ignition temperature values are obtained for a given particle size powder when the powder exceeds a critical height, independent of the container diameter. With fine spherical uranium powder (-200 + 230 mesh), the critical height was estimated to be approximately 1 to 2 millimeters based on geometry studies; intermediate powder (-80 + 100 mesh), approximately 3 millimeters; and coarse powder (-18 + 20 mesh), approximately 7 millimeters. Using experimental ignition temperatures and corresponding critical-height values, one can estimate the effective thermal conductivities of uranium powder beds based on the Frank-Kamenetskii theory of thermal explosions. The calculated effective thermal conductivities were found to be in agreement with values expected for powders. Extrapolated critical height and effective thermal conductivity values can be used to estimate ignition temperatures over a wide range of specific area powders on the basis of Frank-Kamenetskii theory.

The use of nickel sulfate or zinc chloride solutions to decrease the pyrophoricity of uranium powder has been attempted. No evidence of increasing the ignition temperature of spherical or irregular 200 mesh powder or 0.13-mm (5-mil) foil was observed from burning-curve experiments after treatment with either solution.

Continued studies of the effects of halogenated hydrocarbons on the burning propagation of uranium and zirconium foils indicate the possibility of preventing continued combustion of individual zirconium foils or turnings thicker than 0.05 mm (2 mils). This may include the entire practical range of thicknesses of turnings. Preliminary studies of the effects of various gas contaminants on the burning propagation rates of a plutonium alloy indicate that dibromomethane (CH_2Br_2) and bromochloromethane (CH_2BrCl) are markedly effective in decreasing the burning rate.

A self-consistent mechanism for the isothermal oxidation of uranium has been devised; this explains most of the observations, such as linear rate, pressure dependence, and absence of higher oxides. The rate-controlling step in the oxidation occurs on the exterior surface of the oxide and may be ionization, dissociation, or surface diffusion. The increased rate of the second stage is attributed to the increased exterior surface area due to nodule growth and development.

The experimental program to determine rates of reaction of molten reactor fuel and cladding metals with water is continuing. The principal laboratory-scale method involves the rapid melting and dispersion of metal wires in a water or steam environment by a surge current from a bank of condensers. Construction of a high-pressure reaction cell has been completed. A series of runs with 60-mil zirconium wires was carried out in the new apparatus. The runs were made at initial metal temperatures in the region of the melting point. Solid zirconium at temperatures near the

melting point reacted to the extent of four to five per cent with room temperature water (vapor pressure ca 0.5 psia). At saturated vapor pressures of from five to 230 psia, eight to nine per cent reaction occurred. Liquid metal at the melting point gave about eight per cent reaction with room temperature water, whereas 30 per cent reaction was observed at pressures from 16 to 140 psia.

The results indicate that the overall reaction depends strongly on the pressure of water vapor up to some point between 0.5 and 5 psia. A further increase in pressure causes no additional reaction. This limit suggests that the reaction becomes controlled by the transport of water vapor through a film of hydrogen generated by reaction. This latter process would be expected to be relatively independent of pressure

A series of in-pile experiments was conducted in TREAT with oxide-core pins, cermet core pins and uranium wires. Each transient with the oxide-core pins resulted in rupturing and melting of the Zircaloy 2 jacket. The extent of metal water reaction increased from 4.1 to 14.0 per cent as the reactor bursts became more energetic. It was concluded tentatively from the results of runs with the oxide core metal-clad pins that the Zircaloy 2 jacket was more readily ruptured and melted than the stainless steel jacket. It was also noted by comparing runs with clad and unclad cermet core pins, that dispersion of the fuel into particles is favored by the use of a jacket. An experiment with a fully enriched uranium wire, 34 mils in diameter gave 28.3 per cent reaction with complete conversion of the metal into particles. Tests on a "radiation resistant unbonded strain gage pressure transducer showed that the pickup did respond to the transient radiation and that the radiation signal was decreased by using an AC carrier system rather than DC.

IV. Reactor Chemistry (pages 166 to 181)

Data are being obtained on the neutron capture cross sections of uranium-236 as a function of neutron energy. Cross sections have been obtained for neutron energies ranging from 0.475 to 1.74 Mev.

The Slurrex Reactor chemical supporting program has been terminated and a final report is being written.

The Reactor Decontamination Program has two main objectives (1) to determine the seriousness of fuel ruptures in boiling water reactors as measured by the quantities of radioactive materials which deposit in the steam system, and (2) to determine what methods of decontamination can be used to remove these deposited activities. The first study is being made with a stainless steel loop that simulates the action of a boiling water reactor into which mixed fission products can be introduced. Quantities and types of

fission products deposited are monitored by several methods. A second study is being made in the laboratory to find suitable means of removing deposited activities.

In the laboratory, it was found that the presence of oxygen during the contamination portion of an experiment reduced the effectiveness of decontamination by the alkaline permanganate-citrate procedure. This effect was greater when 30-day-cooled uranium was used for the experiment than it was with 60-day-cooled uranium.

Corrosion studies of various turbine materials in typical decontamination reagents were continued. Pitting of chromium-molybdenum steels in citrate solutions adjusted to pH 10 was found to be appreciably reduced when hexamethylenetetramine was added as an inhibitor.

In additional laboratory runs, analyses of supernatant and uranium dioxide particulate produced by reaction of irradiated uranium with water at high temperature indicated that two per cent of the total gamma activity was extracted into the water. The latter contained 52 per cent of the iodine, 0.9 per cent of the cerium, and 0.05 per cent of the ruthenium.

In the loop runs, radioactivity was introduced in the form of irradiated uranium which reacted with the hot water to simulate a fuel rupture. Analysis of loop liquid over a 12-day period indicated that the concentrations of uranium and fission products did not remain constant but exhibited variations both upward and downward.

Total gamma activity in steam samples was low and difficult to measure accurately. Calculated disengaging factors* were 2×10^3 for total gamma counts to 9×10^4 for zirconium-95. Disengaging factors for other fission products fell in between these two values.

The fission products zirconium-95, ruthenium-103, and barium-140-lanthanum-140 were deposited on the metal sample strip in the disengaging section in the same relative proportions as they were present in the circulating liquid. Cerium-141 deposition in the liquid phase was lower than that suggested by its relative content in the circulating liquid.

---

* "Disengaging factor" is defined as the ratio of activity in the liquid phase to that in the steam phase. This factor is often called a "decontamination factor" in the literature but is not so called herein to avoid confusion with the "decontamination factors" reported which are the ratios of activities on solid surfaces before and after various chemical treatments.

Gamma spectra of loop water and residual undissolved uranium oxide indicated that iodine-131 was preferentially leached into the water.

The program for studying the effects of steam on structural materials for nuclear superheaters has been terminated and a final report is being written.

V. Routine Operations (page 182)

The operation of the radioactive waste-processing facility and the gamma-irradiation facility continued without incident.

I. CHEMICAL-METALLURGICAL PROCESSING

A direct-cycle fuel-reprocessing plant using pyrometallurgical procedures is being designed and constructed as part of the Experimental Breeder Reactor No. II (EBR-II) project. A Laboratory and Service Building is also included. Melt refining, liquid metal extraction, and processes involving fractional crystallization from liquid metal systems are methods being examined for the recovery and purification of EBR-II fuels. Based on these studies, process equipment is being designed and tested.

The construction of the Laboratory and Service Building was completed on August 3, 1960, when the building was accepted by the U.S. Atomic Energy Commission. Equipment is being installed in the building.

Construction of the Fuel Cycle Facility Building is continuing. The structure, which was 20 per cent completed by June 6, was 40 per cent completed by September 6, three months later.

The five-ton cranes for the Fuel Cycle Facility have been shipped to the Idaho site. The majority of the drawings for the eight operating manipulators have been approved. Fabrication of the manipulators has started.

The prototype small air lock and component parts were tested in the mockup area. Operation with the manipulator was not completely satisfactory, and, therefore, revisions are required. Work continues on other equipment items for the Fuel Cycle Facility.

As of September 15, 1960, eighty-seven per cent of the total order of Process Cell windows had been delivered to the Idaho site. All the steel window liners are now cast in the concrete of the cell walls.

Irradiation of mineral-insulated (MI) cables sealed with Temporell No. 741 is continuing. Moisture problems have caused insulation resistances to drop; however, for nonpermanent installations using MI cables, the Temporell would suffice as a sealant. Tests of manipulator power feed cable after irradiation have indicated that the expected life of the cable in the cell might be six years. Bearing tests in which irradiated grease was the lubricant have been run for 300 hours without incident.

Enriched fuel ingot production was resumed and ingots 59 through 80 were poured successfully in mockup equipment. In addition, 14 ingots were poured from melts of pin scraps.

The molded Fiberfrax fume trap has been used successfully during uranium melting and pouring operations.

The first of a series of demonstrations at high-activity levels of the melt-refining process for EBR-II core fuel has been completed. Uranium-five weight per cent fissium fuel pins, ten per cent enriched in uranium-235, were irradiated in CP-5 to a total atom burnup of about 0.6 per cent and cooled approximately 30 days. A 400-gram charge of the irradiated material was melt refined for three hours at 1400 C. Although there was no pinshell formation and the surface of the ingot had a clean metallic appearance, initial attempts to pour the molten metal were unsuccessful. After the unpoured charge was permitted to cool to room temperature, then remelted, a successful pour was obtained. Analytical information on the fission product behavior is not yet available.

An experiment was also completed on the evolution of fission product krypton and xenon from an irradiated fuel pin as it was heated to a temperature above the melting point. The uranium-fissium pin had been cooled for 49 days prior to the time of the experiment. On heating at a rate of 5 C per minute, the diameter of the pin increased about 40 per cent between temperatures of 650 and 800 C. Rapid evolution of krypton-85 and xenon-133 also began during this period and ended when the pin had reached a temperature of about 1020 C At this temperature the pin began to lose its cylindrical shape, and at 1080 C melting appeared to be complete.

In the process cell of the EBR-II Fuel Cycle Facility, the argon atmosphere may contain as much as five per cent nitrogen. Since the declad sodium-coated fuel pins are expected to reach a temperature of roughly 300 C during storage as a result of fission product decay heat, the probable extent of uranium nitride formation under these conditions has been considered. Laboratory experiments with uranium and uranium-fissium alloy pins show that the extent of nitridation is significant under these conditions and that it is increased by sodium coatings. In two melt-refining runs on a two-kilogram scale, prior storage of the sodium-coated fissium alloy pins at 300 C in an argon atmosphere containing five per cent nitrogen for 15 and 66 hours, respectively, lowered the melt-refining yield to about 80 per cent. Runs with sodium-coated pins not exposed to the nitrogen-containing atmosphere and melt refined on a one- and two-kilogram scale under conditions of minimum oxygen contamination produced yields of about 97 per cent. In these runs no rare earths were included.

In tests of alternate materials for use in a melt-refining furnace, a fibrous potassium titanate grain retainer was found to be a very effective heat insulator, but to have less strength than rigid Fiberfrax retainers. Carbon wool was not as effective an insulating material as silicon carbide, graphite, or carbon black powders.

The "skull" remaining in the zirconia crucible after a melt-refining operation must be processed to recover, as partially purified metal, the fissionable material for return to the fuel cycle. Work was continued on the development of this process, which is generally called the "dragout" process.

It is planned to effect removal of skull material by converting it to a free-flowing oxide powder by oxidation in a 20 per cent oxygen-argon atmosphere. Skulls from three plant-scale runs were readily oxidized and the oxide products were easily poured out, with yields of about 99 per cent. As in previous runs, cerium was concentrated in the fine particles while ruthenium and molybdenum were concentrated in the coarse particles.

The possibility of volatilizing certain fission product oxides (those of ruthenium, molybdenum, technetium, and tellurium) during oxidation of skull material was further studied. It has been found that the presence of cerium in the skull decreases the volatilization of molybdenum, probably through a chemical interaction of the two oxides. The volatilization of ruthenium is difficult, requiring flowing oxygen and temperatures above 800 C, and is not affected by the presence of cerium. Preliminary results indicate that technetium behaves much like ruthenium. No volatilization of tellurium has occurred under process conditions.

Several essentially quantitative reductions of uranium dioxide and skull oxides have been achieved in times of less than eight hours at 800 C in dilute magnesium-zinc solutions and in magnesium containing a small percentage (0.5 to 2) of sodium as a wetting agent. In one experiment the presence of a chloride flux increased the reduction rate.

The low and erratic results which were previously obtained in the reductions may be attributed, at least in part, to the use of Vycor sampling tubes. The sampling tubes introduced impurities which precipitated uranium and led to low analyses for uranium. Tantalum sampling tubes are currently being employed and are proving very satisfactory.

Several additional retorting runs were performed in tantalum for recovery of uranium from zinc systems. The uranium metal sinter cake was found to stick to the tantalum crucible when the charge was prepared directly in the retorting crucible, but not when the charge was prepared in a separate crucible and transferred as an ingot to the retorting crucible. This is probably related to a better opportunity for wetting in the first case. Product removal has almost always been readily accomplished when ceramic or ceramic-coated graphite crucibles are employed.

Evaluation of materials for pyrometallurgical equipment is continuing. The work includes: (1) development of corrosion information, (2) effect of various materials on stability of liquid metal solutions, and (3) accumulation of extensive information on fabrication techniques for the materials of interest.

Among the basic physicochemical data being determined in support of the process development activities are the solubilities of various fissile, fission product, and other elements in liquid metals. The solubility of titanium in liquid cadmium over the temperature range 325 to 650 C may be represented by the equation

$$\log \text{(atom per cent titanium)} = 3.237 - 5333\ T^{-1} + 1.468 \times 10^6\ T^{-2} \quad .$$

The solubility of zirconium in cadmium may be represented by the equations

$$\text{(325 to 452 C)} \log \text{(weight per cent zirconium)} = 3.058 - 2750\ T^{-1}$$

and

$$\text{(452 to 575 C)} \log \text{(weight per cent zirconium)} = 1.079 - 1314\ T^{-1} \quad .$$

The solubility of samarium in liquid cadmium may be represented by two equations. For the compound $SmCd_{11}$, in equilibrium with the melt below 420.5 C, the solubility is given by

$$\text{(325 to 420 C)} \log \text{(atom per cent samarium)} = 7.0729 - 4878.2\ T^{-1} \ .$$

Above 420 C the solubility is given by

$$\text{(420 to 609 C)} \log \text{(atom per cent samarium)} = 3.0911 - 2116.1\ T^{-1} \ .$$

The solubility of yttrium in liquid cadmium may be represented by the equation

$$\text{(325 to 600 C)} \log \text{(weight per cent yttrium)} = 4.8539 - 4687.5\ T^{-1} + 0.7520 \times 10^6\ T^{-2} \quad .$$

The partition coefficients of a number of representative fissile and fission product elements between the two immiscible liquids, lead and zinc, at about 735 C have been measured. Values of the coefficients (weight per cent in zinc phase/weight per cent in lead phase) were: uranium, 31.9; palladium, 150; cerium, 3.7; and strontium, 0.14. The coefficient for uranium was found to vary from 31.9 at 734 C to 270 at 647 C.

The free energy of formation of the uranium-thallium intermetallic compound UTl_3 was measured using a galvanic cell method. Over the temperature range from 370 to 670 C, the results may be represented by the equation

$$\Delta F_f^0 = -13{,}376 + 12.008\ T \quad .$$

Galvanic cell measurements on the cerium-zinc system over the temperature range from 443 to 742 C were made. The free energy of formation of $CeZn_{11}$ may be represented by the equation

$$\Delta F_f^0 = -79{,}257 + 25.046\ T + 0.01157\ T^2 \quad ;$$

the activity coefficient of cerium in saturated zinc solutions is given by the equation

$$\log \gamma_{Ce} = -9442\ T^{-1} - 0.8269 + 3.2095 \times 10^{-3}\ T \quad .$$

The study of the heat of formation of tungsten disulfide is being continued. Combustions of tungsten and sulfur in oxygen are being carried out to obtain auxiliary data to complement the data already obtained for combustions of tungsten disulfide in oxygen.

Trial combustions of two uranium nitrides and zirconium dihydride have been carried out preparatory to calorimetric determinations of the heats of formation of these compounds.

The determination of the heat of formation of zirconium tetrafluoride by combustions of zirconium in fluorine has been completed. The following values have been determined for the reaction $Zr(c) + 2F_2(gas) \longrightarrow ZrF_4(c,s)$ at 25 C: the energy change for reaction or the energy of formation, $\Delta E_c^0 = \Delta E_f^0 = -455.71$ kcal/mole; the standard heat of formation, $\Delta H_f^0 = -456.29$ kcal/mole; and the standard free energy of formation, $\Delta F_f^0 = -432.63$ kcal/mole.

The experimental work on the determination of the heat of formation of molybdenum hexafluoride by combustion of molybdenum in fluorine has been completed. A preliminary value of -372.44 kcal/mole for ΔH_f^0 (MoF_6 gas) has been obtained.

Calorimetric combustions of boron in fluorine are being continued. Exploratory combustions of magnesium, aluminum, zinc, and cadmium are being carried out.

A. Fuel Processing Facilities for EBR-II
(J. H. Schraidt, M. Levenson)

1. Design, Development, and Construction of Buildings and Equipment

The Fuel Cycle Facility and the Laboratory and Service Building are described in previous quarterly reports (ANL-5789 and ANL-5820). The former building will be used for the processing of EBR-II fuel, and the latter will provide radiochemical analytical and related facilities for the entire Idaho Division of Argonne National Laboratory.

a. Status of Laboratory and Service Building Construction and Equipment
(G. J. Bernstein, A. A. Chilenskas, E. J. Petkus, H. L. Stethers)

The Laboratory and Service Building was accepted by the U.S. Atomic Energy Commission on August 3, 1960. This completed the

Package 1A contract with the James K. Stewart Company. The J. F. Pritchard Company is now installing equipment under the direction of Argonne personnel.

Installation of equipment, wiring, and piping for the Solidification Cell has been completed. The Solidification Cell, which is located in the basement of the Laboratory and Service Building, is to be used to solidify, for safer disposal, the high-level radioactive analytical wastes which are generated in the Junior Cave. These wastes are collected via a hot drain system beginning inside the caves and terminating in hot drain tanks located in the Solidification Cell. The collected wastes are sampled by means of a shielded sampling system. After analysis a measured amount (about five gallons) is transferred from the tanks to a metering tank from which discharge occurs through a spout into a 30-gallon or 55-gallon polyethylene-lined steel drum containing sufficient vermiculite to absorb the liquid. The drum is sealed remotely with a gasketed cap. During these operations and the transfer of the drum to the National Reactor Testing Station burial ground, the drum is held within a five-ton transfer shield. The transfer shield provides four inches of lead shielding for the 30-gallon drum or two inches of lead shielding for the 55-gallon drum. Operating procedures for the cell have been prepared and sent to the operating group in Idaho.

A waste evaporator is located in the basement of the Laboratory and Service Building and provides a means of disposal for liquid wastes, which are collected in the suspect-waste tanks, and which are too active for disposal directly to the leaching pit located on the site grounds. The evaporator is designed to process 1500 gallons of waste per eight-hour shift and to yield a decontamination factor (cpm per ml of feed/cpm per ml of distillate) of at least 10^5 with a feed having a total solids concentration of 2.2 per cent. The evaporator operates with a constant level of waste in the evaporator. The concentrated waste, approximately 30 gallons in volume and containing 40 to 50 per cent solids, is discharged to a shielded 30-gallon or 55-gallon drum where it is expected to solidify upon cooling. If necessary, vermiculite can be added to the drum to take up any liquid remaining after cooling. The drum of solidified waste contained in the five-ton transfer shield is transferred to the burial grounds where the drum is remotely removed from the shield and buried.

The waste evaporator has been tested and has been accepted by ANL. The decontamination efficiency of the evaporator was determined with an inactive solution of sodium sulfate. The tests showed that for a bottom composition of 8.87×10^4 ppm of sodium (35.5 per cent solids) the overhead effluent contained less than 0.1 ppm sodium. The decontamination factor of 8.87×10^5 meets specification.

The Model 8 manipulators and the acid-fuming scrubber have been installed in the Junior Cave.

b. Status of Fuel Cycle Facility Building Design and Construction
(E. J. Petkus, H. L. Stethers)

The Fuel Cycle Facility was more than 40 per cent completed as of September 6, 1960, as compared to 20 per cent on June 6, 1960. During this quarter the first floor concrete slab was completed and extensive work has been done on the Argon and Air Cells. In addition, most of the structural steel for the outer walls of the Facility has been erected.

The floor and most of the outer wall of the Argon Cell liner have been installed. Vacuum-box testing of the liner welds has been completed for the floor and is continuing for the walls. (Vacuum-box testing consists of placing a vacuum box over a weld which has been covered with soap solution and evacuating to 2.5 psia. The weld area is then observed for bubbles.) Concrete has been placed around the outside of the liner to a height of 11 ft 4 in. above the operating floor. The concrete for the walls of the Air Cell has been poured.

c. Cranes and Manipulators
(J. Graae)

The five-ton cranes for the Air Cell and Argon Cell have been shipped to the site at Idaho.

Lifting tools for crane and manipulator bridge drives have been built.

A standard General Mills Model 300 manipulator arm (articulated arm only, exclusive of carriage, bridge, and controls) for testing with the prototype operating manipulator in the mockup has been received. Some of the necessary additional controls and adapter for automatic plug-in on the prototype manipulator have been received.

Most of the drawings for the eight operating manipulators have been approved. Procurement and fabrication has started.

Control cabinets and switchboard for manipulators, cranes, and blister have been completed, except for installation of switchboard cables. Checkout equipment is being built.

d. Process Cell Windows
(T W. Eckels)

All of the window liners and most of the glass-containing components of the process cell windows (87 per cent of the total order) had been delivered to Idaho as of September 15 All the steel window liners are now cast in the concrete walls of the cells In the field, welding repairs to several of the Argon Cell liners were necessary prior to the pouring of concrete The glass containing components will be stored at the site for a period of nine months to possibly a year Pittsburgh Plate Glass Co. wished to monitor the effectiveness of a protective film covering glass surfaces of the components without disturbing the crated components They now have ready for shipment to Idaho a set of polished and acid-leached test plates, each 6 x 6 x 1/2 inch, of their 4966 glass as used in Slab B These plates are coated with Tygon film such as has been applied to all glass surfaces of the window components exposed to the air These plates will be kept at the site under the same storage conditions as the window components. After each two month period one plate will be shipped back to Pittsburgh for evaluation of the integrity and protective qualities of the film This precaution is necessary in view of the extended storage period There has been no previous experience in storing shielding window components for longer than sixty days under these conditions

e. Miscellaneous Fuel Cycle Facility Equipment
(G I Bernstein R H. Jahnke M A. Slawecki)

A prototype of the small air locks which will connect the Argon and Air Cells has been built and operationally tested with the manipulator The manipulator was able to close and lock the air-lock door quite easily but considerable difficulty was encountered in unlocking the door. Moreover, the operating cycle was much longer than anticipated. Further design studies resulted in a revision of the method of operation, changing from operation by the manipulator to a motor drive The remotely replaceable electric drive, complete with shielding, will be the same as the one used on the shielding window shutters

Design drawings for the degassing furnace have been completed This furnace will be used to remove adsorbed water and oxygen from such items as crucibles, molds fume traps, and insulation before they are transferred into the Argon Cell.

Because of the results of recent tests, 1000-MCM* MI** cable will be used instead of $\frac{1}{4}$ x 4-in. copper bus bar for power leads from

*MCM One thousand circular mils.

**Type MI cable One or more electrical conductors insulated with a highly compressed refractory mineral insulation and enclosed in a liquid-tight and gas-tight tube sheathing. Sheath and conductors are of electrolytic copper and mineral insulation is magnesium oxide for the cable mentioned.

the work station to the service sleeves. The 1000-MCM MI cable is composed of a 1-in. OD solid copper conductor surrounded by a layer of swaged magnesium oxide insulation about 0.176 in. thick. The insulation is in turn enclosed by a seamless copper tube of about 1.5-in. OD and about 0.084 in. thick. Results of investigations showed that the impedance of the MI cable is lower than that of the bus bars with 0.5-in. spacing between bars; this is the smallest spacing practical, consistent with the rating of the generator and the insulation between the bars. The lower impedance of the cable makes the system capable of delivering more power to the furnace for the same length of transmission line. Moreover, the cable is easier to install than the bus bar system.

f. Materials Testing*
(G J. Bernstein, A. A. Chilenskas, M. A. Slawecki)

Since the use of conventional rubber booting with Model 8 manipulators becomes impractical because of radiation damage after a dose of 1×10^8 rad, four reinforced plastic sheet samples were evaluated for possible use as disposable manipulator booting. Each material was gamma irradiated and examined after doses of 1.9×10^8 rad, 3×10^8 rad, and 4×10^8 rad The sample designated as S-10 ($\frac{1}{4}$-mil Mylar, Dacron Scrim**) exhibited the least damage. Its use would be satisfactory up to 3×10^8 rad. At 4×10^8 rad it was judged too brittle for satisfactory service Sample S-15 (Dacron Scrim between $\frac{1}{3}$-mil and $\frac{1}{4}$-mil Mylar) was satisfactory at 2×10^8 rad, but not at 3×10^8 rad. Scotchpac appeared to have marginal utility at 2×10^8 rad, while S-31 ($\frac{1}{3}$-mil Mylar, 1.85-oz Nylon Scrim) did not meet requirements at this level. A manipulator boot made of material that is satisfactory for a dose of up to 3×10^8 rad would require replacement every two months in the Air Cell.

Irradiation of the MI cable samples sealed with Temporell No. 741 potting compound is continuing. After receivng an accumulated dose of 4.4×10^9 rad, the samples showed little visual change since startup. Insulation resistance of the samples, however, decreased to between 10 and 20 megohms from an initial resistance of greater than 200 megohms. When the samples were baked at 100 C for about six hours, the insulation resistance increased to greater than 200 megohms. The decrease in resistance was attributed to absorbed moisture. The samples were sealed with an overcoat of Sterling Varnish P-74 over the Temporell, but moisture still

*The materials tested were subjected to test conditions for which they were not specifically designed, and the results of the tests do not constitute an endorsement or a criticism of any product tested.

**A woven reinforcement.

found its way into the cables. To date the Temporell appears to be the most promising sealant for MI cables used in semipermanent installations (i.e., installations that could be changed or revised if need be) in the Argon or Air Cells, even though some moisture pickup occurs.

The asbestos-covered alloy wire has been irradiated to 1.3×10^{10} rad. The insulation showed little visual change. The insulation resistance of the cables decreased to between 2 and 5 megohms from an initial resistance of more than 200 megohms. However, after slight heating the insulation resistance of each sample was restored to greater than 200 megohms.

Wire samples with types AI, AIA, and AA insulation* have been irradiated. Irradiation of types AI and AIA wires was discontinued after 3.3×10^9 rad. The insulation of these samples became very stiff and brittle, and their insulation resistance decreased to below 0.1 megohm from a resistance greater than 200 megohms. The type AA samples have been irradiated to 4.5×10^9 rad. Their insulation resistance decreased to between 5 and 15 megohms (initial resistance greater than 200 megohms), even though the insulation appeared satisfactory. However, after slight heating of the samples, their insulation resistance was restored to greater than 200 megohms.

Irradiation of samples of aluminum paint is continuing. The paints being irradiated at the present time are all products of the Tropical Paint Co. "Elastikote Heat Resisting Interior" aluminum paint has been irradiated to 1.28×10^{10} rad. The paint has become discolored but otherwise has held up quite well. "Elastikote Heat Resisting Exterior," "Tropelite," and "Thermalite" have been irradiated to 5.6×10^9 rad with only slight discoloration and blistering. "Dri-Spray Aluminum" samples have been irradiated to 9.9×10^9 rad. Again, only slight discoloration has taken place.

The $\frac{1}{10}$-hp Howard motors (Model SPN 74435) have been tested to determine brush life in dry high-purity argon. These motors will be installed in the articulated arm attachment for use with the operating manipulator. The brushes in these motors were recently redesigned by the manufacturer. Previous tests on the earlier design (Model SPW 73660) showed that a brush life of 250 operating hours could be anticipated. The latest test, of 10-hour duration, suggests the new design will have an expected life of about 500 operating hours. The expected life is determined by dividing the usable length of a new brush by the rate of wear determined in the test period.

---

*Types AI, AIA, and AA insulated wires: Type AI insulation is a felted asbestos insulation saturated with flame-, heat-, and moisture-resistant compounds. Type AIA is identical to type AI with the addition of a saturated asbestos braid outer covering. Type AA is identical to type AIA except for the absence of moisture-resistant compounds.

In the Argon Cell the six manipulators revolve about a central pivot and receive their power through flexible cables suspended from the top of and passing through a Pivot Tower. These cables are about 15 feet long, of which approximately 10 feet are shielded by the Pivot Tower and 5 feet are exposed. The manipulators are designed to rotate 270 degrees in either direction from a neutral position.

It is estimated that the section of cable shielded by the Pivot Tower will be subjected to a radiation level of 5×10^3 rad/hr and the exposed section to 5×10^4 rad/hr.

A special 54-conductor cable has been procured in which the conductor insulation and jacket contain a material (Antiox 4010) which retards radiation hardening. Electrical tests on cable samples have shown that insulation resistance remained above 200 megohms after irradiation to 2.3×10^9 rad.

Engineering studies have shown that remote changing of manipulator cables within the sealed Argon Cell will be extremely difficult. Accordingly, tests were conducted to indicate the usable life of these cables as limited by radiation hardening. It was assumed that the cables would function satisfactorily as long as the exposed section was sufficiently strong to transmit the necessary force required to twist the shielded section of cable through 270 degrees.

Bending and twisting tests were conducted on three cable samples irradiated to 5×10^8, 9×10^8 and 2.3×10^9 rad. With one end of the cable clamped in a vise, a load was applied to the free end of each of the test cables at a distance of 10 inches from the fixed end. The cables broke under loads of 84, 179, and 104 pounds, respectively. The cables were bent 7, 2.5, and 1 inch, respectively, at time of breakage.

To determine the torque required to twist a cable, the unbroken length of the cable irradiated to 9×10^8 rad was clamped in a vise and force was applied on a 10-inch moment arm 6 inches from the clamp. With a 30-pound force applied to the moment arm, the cable twisted 19 degrees in 6 inches. This is equivalent to 380 degrees in a 10-foot length.

Under anticipated radiation levels in the Argon Cell, an exposed cable would reach a total dose of 2.3×10^9 rad in about a six-year period. The shielded section of cable would receive a dose of about 2.3×10^8 rad in the same period. The above tests show that under these circumstances the exposed section could transmit the required torque to twist the shielded section.

Design studies are continuing toward development of a remote cable-changing device to be used if replacement of the cable is required for reasons other than hardening. Such devices will require a degree of flexibility in the cable much higher than shown by the sample irradiated to 2.3×10^9 rad. Remote cable replacement would have to be made before the cables had been exposed for two or three years.

2. EBR-II Fuel Processing Mockup

a. Manipulator and Manipulator Removal Blister
(D. C. Hampson, J. Graae)

A new, noncoated, Timken tapered roller bearing (No. 432 cup - No. 438 cone) lubricated with fresh radiation resistant grease NRRG 235, a product of Standard Oil of California,* ran for 306 hours at 40 rpm and 800 pounds axial load without heating or other incidents. It is estimated that the 306 hours corresponds to roughly four years of expected Fuel Cycle Facility operation. The bearing, rated at 2500 pounds, was open (without dust or grease shields) and was operated with the axis of rotation vertical. After the run was terminated the bearing was inspected. Bearing surfaces were shiny, and fluorescence indicated that they were covered by very thin layers of grease.

Another grease, NRRG-159, a product of Standard Oil of California, has been γ-irradiated to an accumulated dose of 3×10^9 rad. A fresh, noncoated, Timken roller bearing, similar to the one used previously, was lubricated with the irradiated grease, and a test run, using the same conditions as in the first test, was started. This bearing has been running for more than 300 hours without incident or heating.

It is recognized that these tests do not entirely duplicate the operating conditions which will prevail in the EBR-II Fuel Cycle Facility. The Air Cell conditions will involve working of the grease in the bearings while it is simultaneously exposed to air and γ radiation. Under these circumstances it has been shown[1] that grease will deteriorate at a more rapid rate. In the Argon Cell the oxygen concentration will be kept below 100 ppm. Dynamic tests[2] of lubricants under an inert atmosphere indicate an increase in service life over that found by static tests. Working of the lubricant may in itself be beneficial, but oxygen has a detrimental effect on the lubricant, which is increased by working.

---

*Developed by California Research Corporation and identified thus in ANL-6183.

[1] Burkhard, E. L., Combined Environmental Effects, Nucleonics, 18 (No. 9), 86 (September 1960).

[2] Carroll, J. G. and Bolt, R. O., Radiation Effects on Organic Materials, Nucleonics, 18 (No. 9) 79 (September 1960).

b. Melt-refining Furnaces
(D. C. Hampson, W. E. Miller, L. F. Coleman)

(1) Equipment Performance

(a) Crucibles

Crucible testing has been completed. In addition to the work reported last quarter (ANL-6183), twelve more crucibles were tested. Experience indicates that the manufacturing history of a crucible may be the most important variable in determining whether or not a crucible will fail.

Six crucibles of a new batch received from Norton (made from Norton Z-300 mix, stabilized zirconia) have been heated empty, with uranium, and with uranium-cerium alloy. In no case has any significant crack been noted, even with the top rim of the crucible uninsulated (under these conditions, all crucibles previously received from Norton cracked at the top rim). Evidently, Norton is now supplying a crucible which is superior to any previously supplied by them.

Three crucibles produced by another manufacturer (from a mix similar to Norton Z-300, stabilized zirconia) failed by cracking when heated empty (to 1400 C) in the same manner as in the previously reported Norton crucible tests (ANL-6183, page 30).

Three Norton thin-wall crucibles ($\frac{3}{8}$-inch thick wall, as compared to standard $\frac{5}{8}$-inch thick wall) were tested. One was heated empty, one was heated with a uranium charge, and one was heated with a uranium-cerium charge. All were heated to 1400 C and held at this temperature for two to four hours. The crucible containing the uranium-cerium melt was the only one that cracked. These results are similar to those previously obtained with thin-wall crucibles manufactured by the Laboratory Equipment Company.

(b) Sodium Vapor Fume Trap

Molded Fiberfrax fume traps, which have proved satisfactory in sorbing sodium vapors in trapping tests, have been applied to uranium melting and pouring operations. Initial experience was not good because heavy slags formed on the melts. These slags prevented pouring or caused delayed pouring and metal spills. However, when the traps were thoroughly degassed prior to their use in uranium-pouring operations, no pouring difficulties were encountered.

The traps were degassed in a furnace built for this purpose. The Fiberfrax wall temperature during the degassing step was

1000 C. Six successful uranium-pouring tests were made, using a new degassed trap as a furnace top cover in each case. The traps are now being used as a furnace top cover in the EBR-II fuel alloy preparation runs.

(c) Power Feed through Mockup

Service plugs installed in service sleeves will be employed in the Argon Cell to transmit high-frequency power through the concrete cell floor to induction furnaces located within the cell. Heat generation within the service plug will cause a rise in temperature, as well as thermal stresses between the service plug and the power conductor and between the plug and the sleeve. Time-temperature data were collected on a prototype service plug in air and are presented below. The results are being extrapolated to plugs installed in concrete.

The prototype assembly consists of (1) a stepped outer shell made from 6-inch and $5\frac{1}{2}$-inch tubing, flanged at both ends and 5 ft long between the flange faces; (2) a removable plug made from $5\frac{1}{2}$-inch and $4\frac{3}{4}$-inch tubing, with a flange welded to the top end and a removable and adjustable flange at the bottom end to facilitate sealing in the outer shell. A 1000-MCM coaxial MI cable runs down the center of the removable plug. The MI cable is brazed to the flange on the top end and is secured at the bottom end with an "O" ring seal. The annulus between the MI cable and the plug wall was filled with 160 pounds of copper shot. Figure 1 is a sketch of the plug, showing locations of the thermocouples from which temperature data were obtained.

FIGURE 1
THERMOCOUPLE LOCATIONS ON PROTOTYPE SERVICE PLUG AND SLEEVE

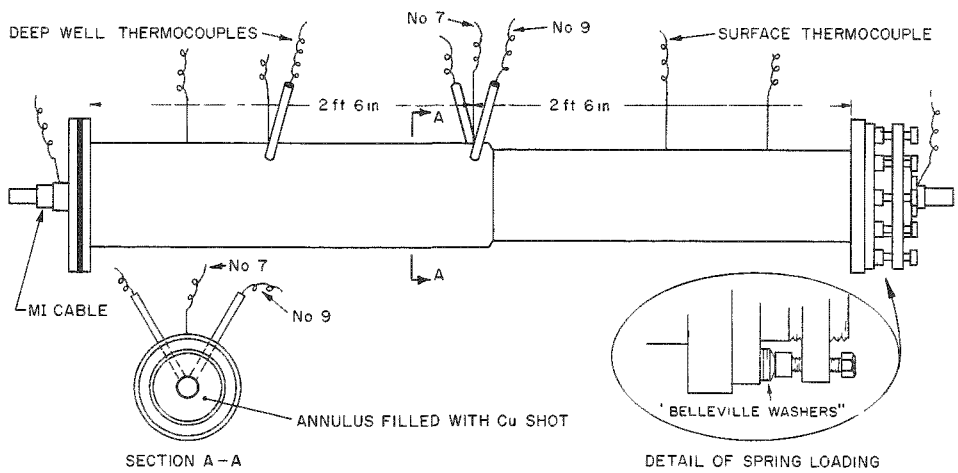

Figures 2 and 3 are typical of the temperature-time data collected. Run No. 7 was made with a steady current of 441 amperes. This is the value of the peak current required in the prototype melt-refining furnace. Run No. 8 was made with a current of 844 amperes.

FIGURE 2
HEATING CURVES FOR PROTOTYPE
SERVICE PLUG FOR ARGON CELL
Run No. 7

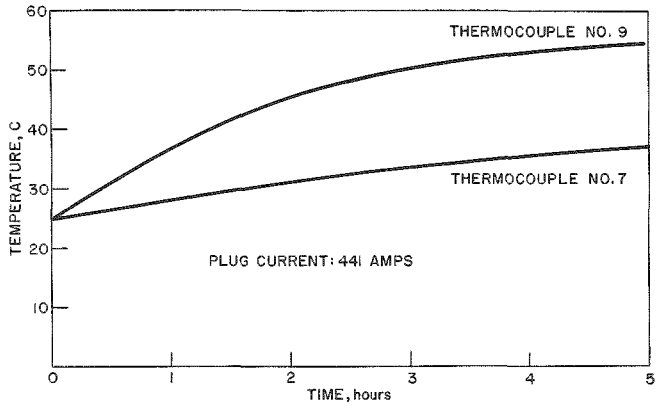

Thermocouple No. 9 was attached to the sheath of the MI cable at a spot where the sum of the radial thermal resistances was a maximum. The geometry of the service sleeve and plug was such that this spot was midway between the ends of the service sleeve. Therefore, the temperature measured by Thermocouple No. 9 was the maximum sheath temperature. Thermocouple No. 7 was located in the same radial plane as Thermocouple No. 9.

FIGURE 3
HEATING CURVES FOR PROTOTYPE
SERVICE PLUG FOR ARGON CELL
Run No. 8

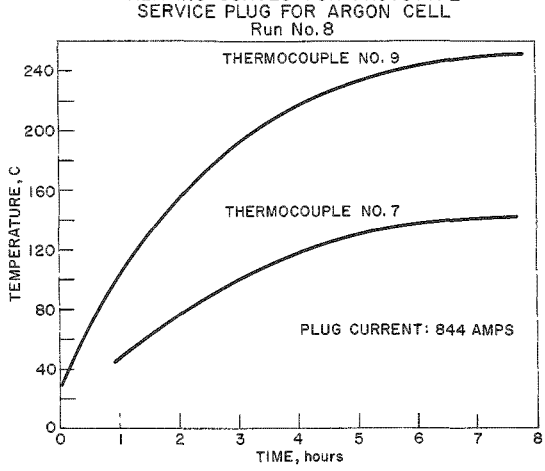

The temperature of the MI cable near the "O" ring seal at the bottom end was a maximum of 52 C when the current was 441 amperes and 227 C when the current was 844 amperes.

The difference in expansion of the service sleeve and the MI cable relative to the service plug was measured as the temperatures increased. The maximum difference in expansion between the sleeve and the plug was <0.001 inch when the current was 441 amperes and -0.005 inch when the current was 844 amperes. The maximum difference in expansion between the MI cable and the plug was +0.014 inch when the current was 441 amperes and +0.040 inch when the current was 844 amperes.

The data from these experiments are sufficient for the design of a service plug with a power feedthrough adequate for 844 amperes from a 10-kc power supply. While operation in concrete will cause changes in component temperatures from those measured in these experiments, the differences in temperatures and hence the relative expansions will remain essentially the same. The elevated temperature at the "O" ring seal at the bottom is too high for satisfactory operation with most elastomers. This seal will be accomplished with a bellows, sized to permit a 0.040-inch movement. The temperature of the MI cable sheath is too high to permit operation in air. Therefore, the plug will be filled with an inert gas prior to sealing. The annulus between the service plug and seal will be pressurized with argon after an initial argon purge. The effect of differential expansion between the plug and sleeve upon gasket compression will be overcome by the use of Belleville spring assemblies (dish springs), sized to permit a 0.005-inch deflection while maintaining a proper gasket compressive stress. Final drawings of this service plug are being prepared.

(2) EBR-II Fuel Alloy Production

Since the crucible cracking problem was solved, the production of enriched ingots for EBR-II fuel manufacture was resumed. Ingots 59 through 80 were produced. Analyses of additional ingots have been completed. The average amounts of various fissium elements in ingots 49 through 80 were found to be as follows:

Element	Nominal Composition (wt percent)	Ingot Analyses (wt percent)
Molybdenum	2.46	2.16 ± 0.20[a]
Ruthenium	1.96	1.97 ± 0.15
Rhodium	0.28	0.23 ± 0.02
Palladium	0.19	0.16 ± 0.02
Zirconium	0.10	0.11 ± 0.02

[a] $\sigma = \sqrt{\frac{\Sigma(x - \bar{x})^2}{n - 1}}$

Isotopic analyses for uranium-235 content have been received for the same batch of ingots. The average uranium-235 content

was 48.1 per cent. The highest value was 48.3 per cent and the lowest was 47.9 per cent. Each analysis was accurate to ±0.5 per cent. The nominal composition was 48.13 per cent uranium-235.

The average pouring yield for ingots 49 through 80 was 97.2 per cent. The highest yield was 98.0 per cent and the lowest yield was 96.0 per cent. The high yields that were obtained are attributed to the absence of cerium in the melt

In addition to blending the ingredients and producing the original fuel alloy, pin scrap is now being received from Metallurgy and is being melted down into ingots. Fourteen ten-kilogram ingots have been made from this scrap. The average pouring yield for these ingots was 92.4 per cent. The highest yield was 94.0 per cent and the lowest was 91.0 per cent.

B. Pyrometallurgical Development

1. Melt Refining
(R. K. Steunenberg, L. Burris, Jr.)

The melt-refining process will be used to recover the 50 per cent enriched uranium fuel alloy in the first core loading of EBR-II. In this process, the fuel pins are dejacketed, sheared into short lengths, melted in a zirconia crucible, and held at a temperature of about 1400 C for a period of three to four hours. Approximately two-thirds of the fission products are removed by this treatment through the mechanisms of volatilization and selective oxidation by the crucible. The molten metal is separated by top-pouring into a graphite-coated mold. The resulting ingot of purified metal is used for the refabrication of new fuel elements. A separate process is required to recover the unpoured metal and oxide remaining in the crucible. Development work has been continued on the following aspects of the melt-refining process: (1) a melt-refining demonstration run utilizing a 400-gram charge of highly irradiated uranium-fissium alloy, (2) an experiment on the evolution of the noble gas fission products, krypton and xenon, during the heating and melting of a highly irradiated fuel pin, (3) studies of the nitridation of sodium-coated pins in a nitrogen-argon atmosphere, (4) melt-refining runs with unirradiated sodium-coated pins, and (5) an investigation of alternative materials and designs for melt-refining furnaces.

a. High-activity Level Melt-refining Experiments
(V. G. Trice, W. H. Spicer)

In previous development work on the melt-refining process, experiments were performed with inactive alloys, alloys with tracer activity, lightly irradiated uranium, and uranium irradiated to 0.4 total atom per cent burnup and cooled for 318 days. As the final stage in the laboratory-scale

development of the process, a series of experiments have been started utilizing 400-gram charges of uranium-five weight per cent fissium alloy irradiated to between one and two total atom per cent burnup and cooled about 30 days. It is expected that these experiments will confirm the chemical and physical behavior of fission product elements observed in the earlier studies. In addition they will provide the first opportunity to evaluate any interactions between the various fission products in fully irradiated material and will afford observations of the physical behavior of highly irradiated uranium-fissium fuel alloy during charge preparation, melt-refining, and product-handling operations.

The equipment for these experiments has been installed in a 10,000-curie cave located in the Chemical Engineering Building. The principal item is a furnace covered by a metal bell jar and provided with an exhaust line to a vacuum pump, an inlet gas-supply line, high-frequency current for induction heating, 60-cycle current for resistance heating, and six thermocouple leads. The auxiliary equipment includes a torsion balance, a jar mill, a grinding and blending machine, and numerous tools adapted for use with the Model 3 electronic manipulators which serve the cave.

The fuel for these experiments is irradiated in the CP-5 and MTR reactors. Each irradiation capsule contains about 200 or 400 grams of 95 per cent uranium-5 per cent fissium alloy enriched to 10.73 per cent in uranium-235. The fuel, in the form of 0.144-inch diameter rods, is loaded bare into a sodium- or NaK-filled capsule and irradiated to between one and two total atom per cent burnup. The irradiated fuel is removed from the stainless steel capsules in a shielded facility by cutting off the top with a pipe cutter and melting out the sodium in a heated paraffin bath or pouring out the NaK in an inert atmosphere. The fuel pins are cleaned by washing with kerosene, butyl alcohol, and acetone, followed by buffing with alumina abrasive in the jar mill.

The cleaned pins are then melt refined in a zirconia crucible (Norton Mix RZ 5601) for three hours at 1400 C. The purified metal is separated by top pouring into a graphite-coated copper mold. The skull (a mixture of oxides and unpoured metal remaining in the crucible) is powdered by air oxidation at about 600 C in the resistance furnace and poured from the crucible. To provide material for analysis that is amenable to aqueous dissolution, the skull oxide is reduced by hydrogen at 700 C. The reduced skull oxide is then ground and blended in an electric mortar to provide a homogeneous powder from which representative analytical samples can be obtained.

Observations on the First High-activity Level Melt-refining Experiments

One high-activity level melt-refining experiment has been completed. Discussion of this experiment is limited to the physical aspects, since complete analytical data are not yet available. The 387 6 grams of

fuel alloy used in the experiment were irradiated to about 0.6 total atom per cent burnup in a sodium-filled stainless steel capsule. The combined effects of thermal cycling and irradiation damage produced considerable distortion of the unrestrained uranium-five per cent fissium fuel.* Measured displacements over pins three inches in length were as great as $\frac{5}{8}$ inch; the diameters of the pins, however, remained uniform at 0.143 inch. Embrittlement of the alloy was apparent from the ease with which the pins could be fractured. The irradiated pins were buffed in a jar mill for two hours with 60-mesh alumina abrasive to remove any surface coating which might produce pin shells on melt refining. The buffed pins were free of all traces of black oxide and had a metallic dull-gray appearance. It is planned to evaluate the pin-shell problem in other experiments.

The fuel was melt refined for three hours at 1400 C under an argon atmosphere. The yield of purified metal in the cast ingot was 72.4 per cent. Although this yield is considerably lower than the 85 to 90 per cent obtained previously with unirradiated fuel, it is considered adequate for the first active run of the series and for the small size of the melt. A yield of 86.7 per cent was obtained in a "dummy" run which preceded the active run and which employed the same operating procedure and equipment as the active run, with the exception of the crucible and thermocouples.

During the active melt-refining experiment, a continuous crust developed on the melt, with sufficient strength to prevent pouring on the first attempt. The melt was permitted to cool and solidify in the crucible Visual examination revealed complete consolidation of the fuel with no evidence of pin-shell formation. The surface of the ingot had a smooth metallic appearance. Since the crucible appeared free from damage, it was returned to the furnace with the solidified melt undisturbed and heated to 1400 C under one atmosphere of argon pressure. On raising the crucible to the pouring position and applying vacuum to the system, a pour was obtained, apparently through hair-line ruptures in the surface crust. After these operations the crucible was examined and found to be free from visible cracks. With the completion of additional melt-refining experiments in this series, it will be established whether or not the development of a surface crust is a typical phenomenon characteristic of high-burnup fuel.

Observations on Air Oxidation and Hydrogen Reduction of a High-burnup Melt-refining Skull

The skull produced in the high-activity level melt-refining experiment was powdered by air oxidation to facilitate removal from the crucible It was then treated with hydrogen, primarily to reduce ruthenium

*Fuel composition before irradiation in weight per cent: U, 94.73; Mo, 2.59; Ru, 2.11; Rh, 0.26; Pd, 0.19; Zr, 0.12; and Nb, 0.01.

dioxide to the metal, which can then be dissolved in aqueous solutions. The oxidation-reduction was performed in a small resistance-heated furnace which, for purposes of atmosphere control, was installed in the bell jar of the melt-refining equipment.

The behavior of the highly irradiated skull during oxidation-reduction was markedly different from that observed in previous work with unirradiated alloy. In the case of unirradiated alloy, six to eight hours of air oxidation at 700 C were required to powder a 50-gram skull. In the run with highly irradiated alloy, the 107-gram skull was completely powdered in $2\frac{1}{2}$ hours Hydrogen reduction of the unirradiated skull oxide at 700 mm of hydrogen pressure and 700 C proceeded smoothly without rapid evolution of heat. In the case of the irradiated skull oxide, however, the introduction of 100 mm of hydrogen pressure at 700 C produced a temperature excursion of 150 C.

Fuel Irradiations

Two capsules, containing about 400 grams of fuel each, were irradiated in CP-5. One capsule, which had been in the reactor since September 10, 1959, developed a small leak on June 14, 1960 and was removed from the reactor. No appreciable quantity of fission products was released to the reactor The capsules were cylindrical stainless steel cans, $1\frac{1}{4}$ inches in diameter and 21 inches long. The top of the capsule was welded on after the fuel pins and sodium were loaded. The irradiations were conducted in sealed, helium-pressurized water thimbles in the core of the reactor with instrumentation consisting of a helium-pressure monitor and three thermocouples in the capsules. It is believed that during irradiation the fuel pins reached a temperature in the neighborhood of 350 C.

The capsule rupture was detected by the thimble-pressure monitor. On removal of the capsule, it was found that the leak had occurred in the weld joining the top to the body of the capsule. It is believed that with each power cycle of the reactor a small amount of water entered the capsule, reacted with the contents and released hydrogen, thereby increasing the pressure in the thimble. In three reactor power cycles the thimble pressure increased from 200 psi to 350 psi The pressure buildup was terminated in the third cycle by shutdown of the reactor. On examination of the ruptured capsule, the fuel was indeed found to be destroyed by extensive reactions.

The fuel used in the first high-activity level melt-refining experiment was obtained from the second capsule, which was removed from the reactor on June 29, 1960 No evidence of corrosion of the capsule was detected.

b. Fission Gas-release Studies
(N. R. Chellew, C. C. Honesty, G. W. Smith,* D. W. Mongan*)

The first of a series of experiments on the release of krypton and xenon during the heating and melting of highly irradiated uranium-fissium pins has been completed. The objectives of the initial experiment were two-fold: (1) to follow the evolution of the fission product gases as the alloy is heated until fully molten, and (2) to observe physical changes in the metal during heating. The value of this information to the melt-refining process has been discussed previously (ANL-6145, page 35).

Calculations show that the uranium-fissium fuel alloy to be used in the first EBR-II core loading will contain about 2800 ppm of xenon plus krypton at two total atom per cent burnup. The volume of gas, if released quantitatively at 1000 C during melt refining, would amount to approximately 40 cc per cc of molten alloy. A previously reported experiment (ANL-5896, page 124), utilizing irradiated uranium containing 140 ppm of xenon plus krypton, showed that the evolution of krypton is essentially complete shortly after melting. The availability of highly irradiated uranium-five per cent fissium alloy has permitted a similar investigation with material which simulates much more closely the fuel that will be discharged from EBR-II.

The furnace and auxiliary gas-handling train used in the experiment are illustrated in Figures 4 and 5. The components containing highly radioactive material were mounted on a steel table and installed in Cell A of the Senior Cave Facility in Building 205. Nonbrowning optical flats at each end of the resistance-heated furnace tube served as sight ports. Dimensional changes and the appearance of the fuel pin during the experiment were observed and photographed by means of a Kollmorgen cave-wall periscope equipped with a filar eyepiece. A previous calibration of the viewing equipment, using inactive material (unwarped pins), indicated that the error in measuring the diameter of an active pin should be within ±0.004 inch. The temperature of the fuel pin was measured with a platinum-platinum 10 per cent rhodium thermocouple located in the heated zone near the pin. Provisions were made for circulating the furnace atmosphere at a measured rate through a 7-cc Pyrex bulb located in a gas counting assembly. Gamma-ray spectra of the activities present in the bulb were determined with a 256-channel gamma-ray spectrometer equipped with a 2 x 2-inch sodium iodide crystal. The system was arranged to permit counting of the gas under conditions of constant volume.

The material used in the preliminary fission gas release experiment was prepared by irradiating uranium-five per cent fissium alloy in CP-5 to a total atom burnup of approximately 0.6 per cent. The composition of the alloy prior to irradiation was as follows, in weight per cent:

*Analytical Group

FIGURE 4

FURNACE FOR HEATING HIGHLY IRRADIATED URANIUM ALLOY PINS

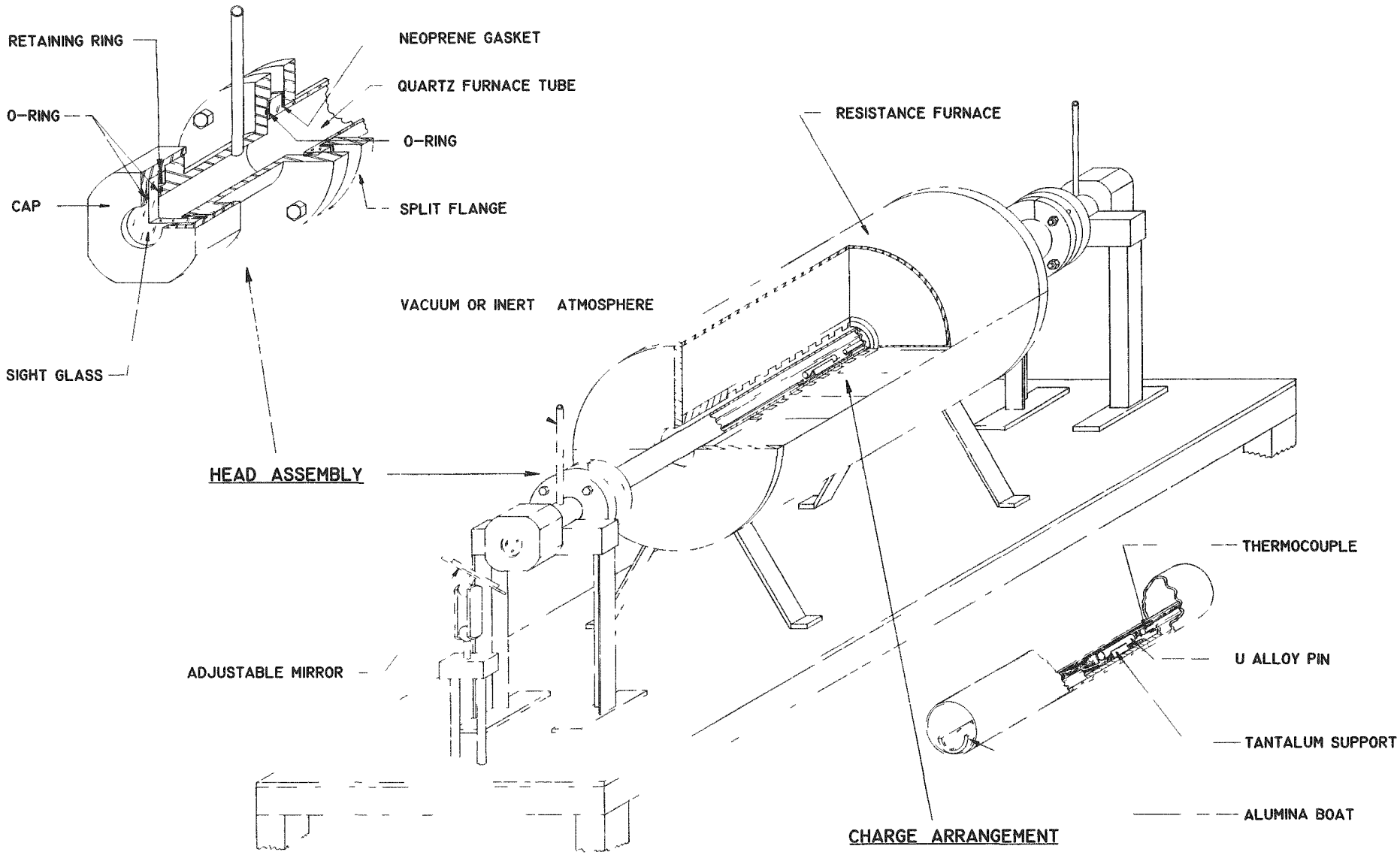

uranium-238, 84; uranium-235, 10.73; molybdenum, 2.59; ruthenium, 2.11; rhodium, 0.26; palladium, ~0.19; zirconium, ~0.12; and niobium, ~0.01. The irradiated fuel pin was 1.5 inches long, 0.143 inch in diameter, and weighed 7.17 grams. The cooling time prior to the experiment was 49 days, and the total content of krypton and xenon was calculated to be ~800 ppm.

FIGURE 5
EXPERIMENTAL FURNACE AUXILIARY SYSTEM

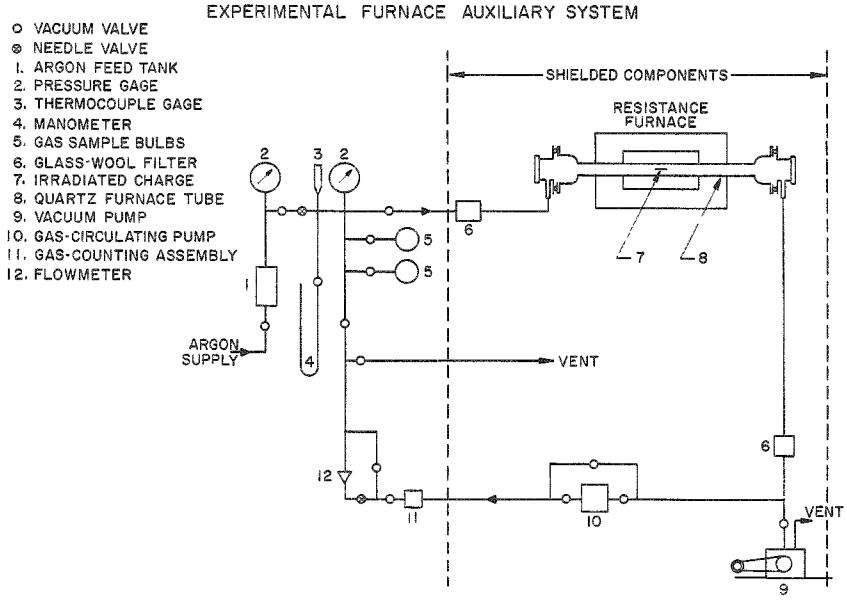

The experimental procedure was as follows. The pin was located on a tantalum support in an alumina boat which had been degassed previously at 1200 C. This assembly, shown in Figure 4, when inserted into the tube furnace, permitted viewing of the unrestrained pin during heating. Before a known volume of argon was added to the closed system, the materials in the furnace tube were degassed for 85 minutes at 100 C and a pressure of 40 microns. In the course of the experiment, the pressure of the system varied from 685 to 790 mm Hg as a result of temperature variation. Since the gas was at constant volume, counting-rate corrections due to temperature changes were unnecessary. It was necessary, however, to apply corrections for the time lag in transporting the activity from the furnace tube to the counting assembly. These corrections were applied when counting rates were used to obtain the cumulative totals of activities evolved as a function of temperature and time of heating. This time lag amounted to four minutes for the gas circulation rate of 120 cc per minute used in the experiment.

The conditions employed and the results of the experiment are reported in Figure 6. Although both xenon-133 and krypton-85 were identified in the gas stream when the fuel pin was heated between 400 and 650 C, their concentrations were less than 0.1 per cent of the final values shown in Figure 6. The period of rapid evolution of both isotopes began and ended at similar temperatures, starting at about 700 C and ending in

the vicinity of 1000 C. During this period, the pin diameter increased about 40 per cent. The pin appeared to retain its cylindrical shape until it had reached a temperature of about 1020 C, at which there was evidence of sagging. When the temperature exceeded 1080 C, the alloy began to flow, wetting the tantalum support. No further release of gas was found when heating was continued at a temperature higher than 1050 C for 90 minutes, or when the pin was cooled rapidly from 1150 to 800 C. In Figure 6 the scatter in the activity data at the beginning of the plateau in the curve may have resulted from incomplete mixing of the fission gases with the circulating argon in the system. Separate tests are being made to determine the rate of mixing.

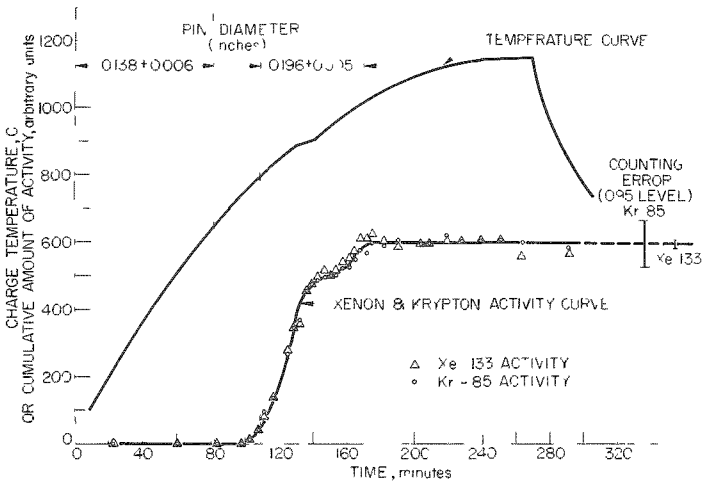

A photographic record of the irradiated pin at various temperatures is shown in Figure 7. During the experiment, the horizontally supported pin gradually crept toward the front of the tantalum bracket and assumed a tilted position. This is attributed to vibration of the furnace tube by the gas circulating pump. Photographs B and C show the pin prior to and during the period of rapid gas evolution, respectively. When photograph D was taken, the evolution of gases had subsided and the metal had softened. Prior to reaching this temperature the pin, although deformed by swelling, had retained its cylindrical shape. In photograph E the bulk of the metal had flowed from the tantalum support to the alumina boat.

Some additional observations which may be of process interest are as follows:

(1) There was no indication of spattering of molten metal as a result of gas evolution during the heating period. This result was confirmed by inspection of the alumina boat at the end of the experiment.

FIGURE 7

PHOTOGRAPHS OF IRRADIATED URANIUM ALLOY PIN DURING FISSION GAS-RELEASE EXPERIMENT

Charge History: See Figure 6
Magnification: ~2X

A

to 370 C

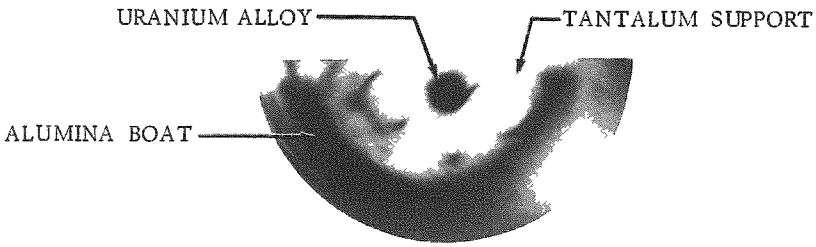

B

370 C

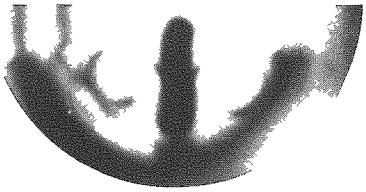

C

860 C

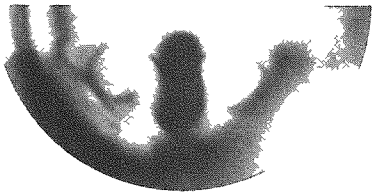

D

1020 C

E

1120 C

(2) Relatively little activity was deposited on the view port which was located 20 inches from the fuel pin and was maintained at a temperature below 100 C during the experiment. A smear taken from this component showed 25 milliroentgens per hour of hard and soft activity at a distance of two inches.

(3) During the experiment, activities present in the in-line counting chamber other than xenon-133 and krypton-85 were negligible. Cesium and iodine activities were absent. With intermittent flushing and evacuation of the system after the fuel pin had cooled at the end of the experiment, the only activity transported to this zone was iodine-131.

(4) The rate of noble gas evolution prior to melting was significantly slower than that observed in an earlier study conducted with irradiated uranium containing 140 ppm of xenon and krypton (ANL-5896, page 124). In the previous experiment, however, the rate of heating during this period was 20 C per minute, or roughly four times the rate in the present experiment. An additional study is planned to obtain information on the effect of heating rate on the evolution of krypton-85 from highly irradiated uranium-five per cent fissium alloy.

(5) It is of interest to note that the rapid evolution of fission gases and the expansion of the irradiated uranium-five weight per cent fissium pin occurred near a temperature of 725 C, where similar unirradiated alloy is reported to undergo a phase transformation; above this temperature single-phase gamma is stable.[3]

c. Nitride Formation on Sodium-coated Fuel Pins
(J. P. LaPlante)

The design specifications for the process cell of the EBR-II Fuel Cycle Facility limit the nitrogen content of the purified argon atmosphere to five volume per cent. During the fuel decladding and other operations preceding the melt-refining step, it has been estimated that the fuel pins will reach a temperature of 300 C as a result of fission product decay heat.[4] While the nitrogen content of the cell atmosphere may, in fact, be much less than five per cent, an investigation of the tendency of fuel pins to form uranium nitride coatings at the five per cent concentration level is appropriate. The formation of nitride shells on the fuel pins could cause serious difficulties in achieving coalescence of the metal in the melt-refining operation. Data are available on the nitridation rate of uranium, but little is known about the influence of fissium constituents, sodium coatings, and irradiation on the rate.

---

[3] Nevitt, M. V. and Zegler, S. T., Journal of Nuclear Materials, 1, 6 (1959).

[4] Chilenskas, A. A., private communication.

Experiments were performed on the nitridation of sodium-coated uranium and uranium-five per cent fissium pins at 308 C in an argon atmosphere containing 5.39 per cent nitrogen. The oxide coatings on the surfaces of the pins were removed by a polishing wheel until a smooth bright metallic finish was obtained. The sodium coatings were prepared by subliming sodium onto the clean pins until a uniform surface was evident. The pins were attached to a movable rod so that they could be raised from the lower part of the furnace tube to the center, where they were heated in the nitrogen-argon atmosphere.

The nitridation results are summarized in Table 1, in which the relative amounts of nitrogen consumed are compared for coated and uncoated uranium and uranium-fissium pins. The absolute rate of nitridation of uncoated uranium pins, based on an estimated area, agrees with rates reported in the literature[5] and in ANL-5974, page 187. Both the uranium and uranium-fissium pins were nitrided at a significant rate at 308 C, and the rate was increased by the sodium coatings in both cases.

Table 1

NITRIDATION OF URANIUM AND URANIUM-FISSIUM PINS

Temperature: 308 C
Time: 17.5 hr

Type of Pins	Weight of Pins (g)	Quantity of Nitrogen (moles x 10^4)		Nitrogen Reacted (per cent)
		Initial	Final	
Uranium	95.4	5.80	4.40	24.0
Uranium[a]	102.3	5.89	2.36	60.0
Uranium-Fissium	82.3	5.89	4.47	25.0
Uranium-Fissium[a]	90.4	5.94	3.21	46.0

[a] Sodium coated.

A dull black film was evident on the nitrided pins which were not coated with sodium. The coated pins had an uneven film with black and metallic areas when the sodium was removed. X-ray diffraction results showed the coating in both areas to be primarily uranium dinitride. An attempt was made to remove the nitride film from the uranium pins by buffing them for two hours in a jar mill, using a 60 mesh alundum abrasive. The buffing was ineffective in removing the film, suggesting that the nitrides are somewhat harder than oxide films, which are removed by this treatment.

[5] Adda, Y., Investigation of the Kinetics of the Reactions of Oxidation, Nitridation and Hydridation of Uranium, Gauthier-Villars, Editeur, Impriment Libraire, Paris (1958).

These results indicate that exposure of the fuel pins to the cell atmosphere during storage may have to be limited in order to avoid the formation of uranium nitride pinshells during melt refining.

d. Melt Refining of Sodium-coated Pins
(G. A. Bennett, W. A. Pehl)

In EBR-II, sodium is used to effect a thermal bond between the fuel pin and the stainless steel container. The question of whether the presence of this sodium will have a material effect on the melt-refining process has been raised.

Melt Refining under Conditions of Low Oxygen Contamination

Preliminary results were presented previously (ANL-6145, page 36) on the effect of oxygen contamination on the pouring yield of sodium-coated pins during melt refining. These results showed that when oxygen contamination occurred during the melt refining of sodium-coated pins, a yield decrease of about 10 per cent, accompanied by pinshell formation, could be expected; if oxygen contamination was reduced considerably, however, no such yield decrease was observed.

These results, previously reported on an 800-gram basis, have now been confirmed on a scale of two kilograms. In this latter run, in which sodium-coated fissium pins were melt refined for one hour at 1400 C, the ingot yield was 97.4 per cent. This yield is the same as that obtained when starting with massive uranium or uranium-fissium alloys alone (Table 2). No pinshells were formed in this run. In the above runs, no cerium was present as a stand-in for all rare earths. The presence of cerium would have decreased the yield slightly (by about two per cent).

The procedure used was that described in ANL-6145, page 36, except that the sodium was removed at a pressure of about two to five inches of water above atmospheric. In addition, precautions were taken to eliminate not only external sources of oxygen, nitrogen, and water vapor from the charge as previously described, but also all possible sources of contamination from within the furnace. The only disquieting note is that the tantalum susceptor disintegrated at some time during the run, probably due to attack by sodium. This effect had been observed previously.

Table 2

EFFECT OF SODIUM ON INGOT YIELD

Conditions: Liquation Temperature: 1400 C
Liquation Time: 1 hr
Crucible: Dry-pressed zirconia (degassed)
Atmosphere: High-purity argon

Charge			
Material	Weight (g)	Sodium	Ingot Yield (%)
Uranium-5% Fissium[a]	~1000	None	97.3[b]
Uranium Biscuit	2013	None	96.3
Uranium-5% Fissium pins[a,c]	1993	Present[d]	97.4

[a] Added elements as follows (nominal weight per cent): Mo, 2.46; Ru, 1.96; Rh, 0.28; Pd, 0.19; Zr, 0.10; Nb, 0.01.

[b] Average yield obtained in alloy preparation runs performed by the EBR-II Fuel Processing Mock-up Group.

[c] Injection-cast by Metallurgical Division.

[d] Contained ~10 ppm oxygen.

e. Study of Alternate Materials and Designs for EBR-II Melt-refining Furnace
(J. Wolkoff, R. Nowak)

(1) Tests of 1000-MCM (10^6 Circular Mil) Type MI Power Transmission Cable

In the EBR-II processing plant at Idaho, high-frequency (10,000 cycle per sec) power must be transmitted nearly 30 feet from outside the processing cell to the induction coil surrounding the melt-refining crucible. A 28-ft length of the proposed MI cable (mineral-insulated coaxial cable - 10^6 circular mils) has been tested as the power-transmission line. The effect of ground location in the inductor coil on furnace performance was also noted.

The effect of the cable on power consumption compared with the standard short-length power leads was small. An increase in power of from 4.0 kw to 4.5 kw was required to produce an internal crucible temperature of 1400 C. The voltage drop across the 28-ft cable was only 21 volts.

The impedance of the cable was calculated to be 44 microohms. With the MI cable transmission line being used, there was no observable effect in furnace performance produced by changing the point of grounding of the induction coil from the midpoint to one end. It is concluded that the 1000-MCM MI cable is an efficient transmission line for the 10-kc power and that the electrical losses resulting from its use are small.

The steady-state cable temperatures in air were 69 and 64 C for the inner and outer conductors, respectively. Evidently, the compressed magnesium oxide electrical insulation between the inner and outer conductors of the coaxial cable is an effective thermal conductor.

(2) Alternate Insulating Materials and Crucibles

Carbon wool was evaluated as a high-temperature thermal insulator adjacent to the graphite susceptor. Its performance at steady state with a 1400 C crucible temperature is summarized in Table 3, and compared with a previously reported run employing zirconia grain. At the density of wool tested, its performance was approximately equivalent to that of zirconia grain. It is inferior to the silicon carbide and carbon black previously evaluated as thermal insulation. A weight loss of 18 per cent was experienced by the carbon wool. The fiber length was not affected, however.

Fibrous potassium titanate was used to form a grain retainer similar to the rigid Fiberfrax that has been developed in this program. Its performance, summarized in Table 3, showed it to have notable thermal insulation properties. A run with a rigid Fiberfrax retainer is shown for comparison. Although both carbon black and Fiberfrax are very effective insulators, the excellence of the fibrous potassium titanate resulted in the lower power requirement and the higher inner wall grain retainer temperature.

The effectiveness of the fibrous potassium titanate as a thermal insulator is due largely to its ability to block infrared radiation because of the high refractive index of the fibers and their dimensions. The molded grain retainer made from it, however, was inferior in strength to rigid Fiberfrax. Although it possesses the resiliency needed, its strength is not considered adequate at the present time for this duty in the melt-refining furnace.

A slip-cast silica grain retainer was also tested and was found to have cracked during the run. It is better than Amersil as a thermal insulator although it is similar to Amersil in lack of resilience to internal expansion.

Table 3

COMPARISON OF VARIOUS THERMAL INSULATION MODIFICATIONS IN THE MELT-REFINING ASSEMBLY

(Measurements at a pressure of 1 atmosphere of argon)

Insulating Grain	Grain Retainer	Temperature (C)				Power (kw)
		Crucible Wall	Inner Wall Grain Retainer	Outer Wall Grain Retainer	Copper Coil	
Carbon wool, long fiber; 9-μ fiber diameter; density 0.34 g/ml	Rigid Fiberfrax	1405	-	-	438	5.7
25/40 mesh zirconia grain;[a] density 2.1 g/ml	Rigid Fiberfrax	1405	1158	574	473	5.7
Stainless Thermax carbon black;[a] density 0.84 g/ml	Fibrous Potassium Titanate	1405	869	341	314	3.8
Stainless Thermax carbon black;[a] density 0.80 g/ml	Rigid Fiberfrax	1400	612	372	341	4.1
Stainless Thermax carbon black;[b] density 0.88 g/ml; thickness 30% greater than previously used	Rigid Fiberfrax	1400	548	372	345	3.8

[a] Previously reported.

[b] Increased insulation thickness obtained by using a crucible and susceptor with smaller outer diameters than previously used.

A zirconia crucible of smaller outer diameter than now in use was designed with a thinner wall and bottom to improve the performance of the crucibles with respect to breakage during the melt-refining operation. Preliminary tests done by the Design Group in the melt-refining mockup furnaces were encouraging. However, an improvement in the quality of the standard crucible by its manufacturer has de-emphasized the need for crucible improvements through shape modifications.

The new thinner-walled crucible allowed an approximate 30 per cent increase in the thickness of the high-temperature insulating grain. Results of a run under these conditions are summarized as the last

entry in Table 3. A decrease of only about 9 per cent in the power requirement over a standard assembly using the same insulating materials was obtained.

Some of the major objectives of the program have been accomplished. It has been found that either fine-grain silicon carbide or carbon black used as the high-temperature insulation adjacent to the graphite susceptor with a grain retainer of rigid Fiberfrax is superior to the original materials (zirconia grain and Amersil) A combination such as this is compatible at operating temperature and is highly efficient thermally. The power requirement and the inductor coil temperature are substantially lower than with the original materials

2 Liquid Metal Solvents Process Development
(L. Burris, Jr., R. K. Steunenberg)

At the completion of the melt-refining operation, approximately ten per cent of the charge remains behind in the zirconia crucible in the form of a "skull" made up of metal and oxides An auxiliary process is required to recover partially decontaminated uranium from the skull and return it to the melt-refining process While highly efficient fission product removal is not necessary, a substantial amount of each fission product element must be removed in order to maintain the proper fissium composition in the recycled fuel.

Removal of the skull is effected by an argon-oxygen mixture at 700 C, which converts the skull to a free-flowing oxide powder which is easily poured from the crucible The powder resulting from the oxidation step is reduced either by liquid magnesium or by a solution of magnesium in liquid zinc In pure magnesium or in high-magnesium solutions, uranium is precipitated as the metal during reduction Subsequent steps in the process involve uranium-fission product separations based on their different solubilities in liquid metal media, followed by a retorting operation to remove residual magnesium, zinc, or cadmium from the uranium product.

a Processing of Melt-refining Skulls

(1) Oxidation of Melt-refining Skulls
(T R Johnson, J. P. LaPlante, R. L. Christensen)

In the proposed process for the recovery of uranium from EBR-II melt-refining skulls, the first step consists of removing the skull from the melt-refining zirconia crucible The most promising procedure is a high-temperature oxidation which converts the skull constituents to a free-flowing oxide powder. The possibility of volatilizing certain fission oxides in this step has been explored Those fission product elements present in the melt-refining skull which might be expected to form volatile oxides at temperatures below 1200 C include molybdenum, ruthenium, technetium, and tellurium

Recent experiments have shown that the presence of cerium in the skull decreases the volatility of molybdenum oxides, probably through a chemical interaction of the two oxides. Cerium appears to have no significant effect, however, on the behavior of ruthenium during the oxidation.

Two melt-refining skulls, weighing about 30 grams each, were prepared from uranium-6 per cent fissium alloys in zirconia crucibles. Cerium was added to a concentration of 0.6 weight per cent to one of the alloys. The skulls were oxidized in a resistance-heated Vycor furnace tube under relatively severe conditions. A stream of flowing oxygen (1 atm, 800 cc/min, STP) was directed within one inch of the bottom of the crucible. While the nominal furnace temperature was 850 C, the temperature of the burning skull probably exceeded 1300 C. At the end of the four-hour oxidation period, the furnace temperature was raised to 940 C and the pressure within the system was reduced to less than one mm Hg for 30 minutes.

During the first hour of the oxidation, a dense smoke was evolved from the skull which contained no cerium. The smoke deposited as a light yellow powder, which had been identified in previous experiments as molybdenum trioxide. In the case of the skull containing cerium, no evolution of molybdenum trioxide occurred during the oxidation, but it was observed during the evacuation procedure. A black deposit of ruthenium dioxide on the exit gas lines was first noted in both experiments about 30 minutes after the oxidation was started. The deposit grew darker during the remainder of the experiment, indicating a slow volatilization of ruthenium oxide. The volatilized ruthenium was trapped easily on glass wool or Molecular Sieves. Ruthenium appears to be difficult to volatilize during the oxidation step, requiring temperatures above 800 C and a stream of oxygen flowing rapidly past the burning particles.

Preliminary results indicate that technetium behaves much like ruthenium during the oxidation of a skull. Flowing oxygen is required to volatilize technetium from an oxidizing uranium-fissium alloy. It can, however, be volatilized at a lower temperature (700 C) and at lower gas velocities than ruthenium. One-gram samples of fissium alloy containing 0.2 weight per cent technetium and no cerium were oxidized in porcelain combustion boats. Technetium oxides condensed on the cool portions of the furnace tube as maroon and black deposits.

Tellurium is not volatilized during the oxidation of skulls under anticipated process conditions. A 60-gram skull containing about 0 6 weight per cent tellurium was oxidized in a static oxygen-argon atmosphere at 725 C Tellurium tracer prepared by irradiating the metal and separating the iodine and xenon daughters was used. The tellurium

remained in the oxidized material and no evidence of any activity was found outside the crucible. The lack of tellurium volatilization is believed to result from the formation of stable tellurates with cerium.[6] Thus, it appears that significant volatilization of fission products during the skull oxidation can be avoided, thereby eliminating any serious off-gas-handling problem.

(2) Particle Size and Composition of Oxidized Melt-refining Skulls
(R. D. Pierce, T. R. Johnson, L. F. Dorsey)

Three skulls produced in plant-type melt-refining crucibles were oxidized in a 20 per cent oxygen-argon atmosphere. The screen analyses and compositions of these oxidized skulls are presented in Figure 8. These skulls were obtained from cerium-fissium melt-refining runs in the mockup facility.

FIGURE 8
COMPOSITION AND SIZE DISTRIBUTION OF SKULL OXIDES

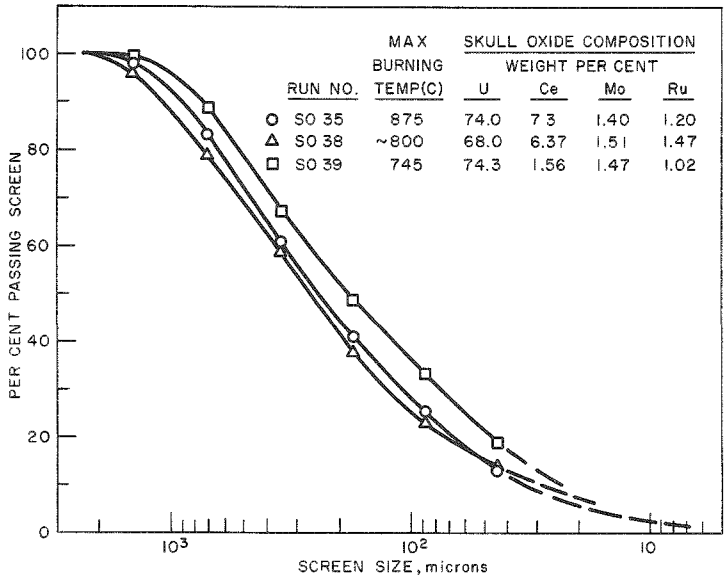

The recovery of uranium from the melt-refining crucibles for these oxidations was greater than 99.5 per cent for Runs SO-35 and SO-38, but only 98.4 per cent for Run SO-39. The uranium residue after Run SO-39 was oxidized, but a small portion of it adhered too tightly to the wall to be dumped without scraping or brushing the wall. This is the first time this behavior has been encountered.

---

[6] Domange, L., Flahaut, J., and Chirazi, A. W., Bull. soc. chem. France, No. 1, 150 (1959).

Some analyses of the screen fractions are presented in Table 4. As in previous runs, cerium was concentrated in the fine skull oxide particles while molybdenum and ruthenium concentrated in the coarser particles. Less total cerium was present in the second run than in the first, which accounts for the generally lower cerium concentrations in the second run.

Table 4

SOME FISSION PRODUCT CONCENTRATIONS IN SKULL OXIDES

	Weight Per Cent		
	Ce	Mo	Ru
Run SO-38			
-14 +25 mesh	3.08	1.87	2.28
-45 +80 mesh	6.4	1.54	1.24
-325 mesh	13.2	0.85	0.52
Run SO-39			
-14 +25 mesh	1.18	2.00	1.35
-45 +80 mesh	1.40	1.71	1.37
-325 mesh	2.60	0.86	0.32

b. Reduction of Uranium Oxides in Liquid Metals

(1) Reduction of Oxidized Skulls in Dilute Magnesium-Zinc Solutions
(R. D. Pierce, L. F. Dorsey)

The reduction of oxidized fissium skulls by solutions of magnesium in zinc is under investigation as a step in one proposed skull-recovery process. In this reduction procedure, the ratio of zinc to uranium in the fissium skull oxide is in excess of that necessary to dissolve all the uranium if it is reduced to metal. These reductions are easily evaluated experimentally by sampling the liquid zinc and analyzing it for dissolved uranium.

During this quarter, the sampling procedures have been critically studied and a successful technique incorporating tantalum sample tubes has been developed. Short tantalum tubes fitted on a tapered steel or tantalum extension rod are introduced into the melts, and samples are forced through No. 60 graphite frits into the tubes by increasing the argon pressure on the melt to about 20 psi. Samples are recovered, after the frits are cut off and examined, by dissolving out the solidified zinc solution with aqua regia. The sample tubes may be fitted with new frits and reused.

In a holding run of three-hour duration, made to check the sampling technique, uranium concentrations remained at the theoretical value within the precision of the analysis. In contrast, uranium analyses in a similar run in which sampling was performed with coated Vycor sampling tubes were generally low and erratic.

FIGURE 9
SKULL OXIDE REDUCTION BY ZINC - 10 WEIGHT PER CENT MAGNESIUM

SOLUTION: ZINC-10 w/o MAGNESIUM
TEMPERATURE: 800 C
CRUCIBLE: 5 IN. TANTALUM WITH BAFFLES
AGITATOR: 3 x 1 IN. TANTALUM
STIRRING SPEED: 400 rpm
SAMPLE TUBES: TANTALUM WITH GRAPHITE FILTERS

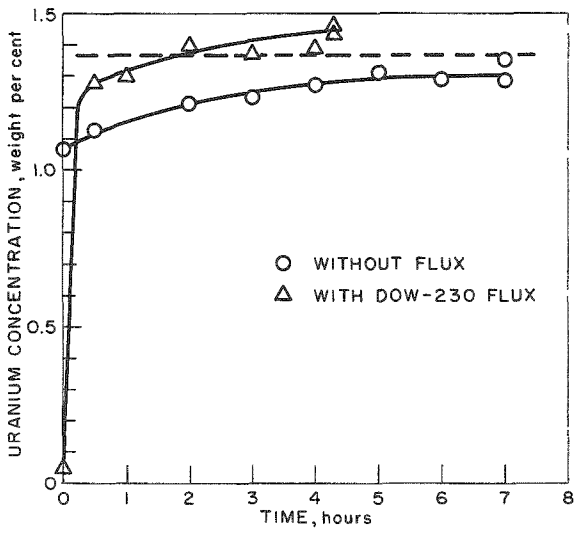

Two subsequent runs to reduce skull oxide were made with zinc containing 10 per cent magnesium. The runs differed only in that the second employed a DOW-230 salt flux (34 per cent magnesium chloride, 9 per cent barium chloride, 55 per cent potassium chloride, 2 per cent calcium fluoride). Essentially quantitative reductions were realized in both runs. Figure 9 shows the increase in uranium concentration during these runs. In both runs, most of the reduction occurred within the first hour. The slight divergence from the theoretical value may indicate only that nonrepresentative portions of skull oxide were taken either for analysis or for the runs. These sampling procedures will be carefully checked.

A possible difficulty in the reduction runs made without flux is believed to be a trapping of uranium oxide in a stagnant magnesium oxide concentrate which accumulates at the surface. This effect can probably be reduced if stirring is begun at temperatures below that required for appreciable reduction. Magnesium oxide clumps do not form when salt flux is used to suspend the magnesium oxide.

(2) Reduction of Uranium Oxides by Liquid Magnesium
(T. R. Johnson, J. C. Hesson, K. R. Tobias, R. L. Christensen)

The feasibility of reducing melt-refining skull oxides by liquid magnesium at 800 C has also been investigated. Since the subsequent fission product separations in the skull recovery process will probably be done in solutions of liquid zinc, the reduction yields were generally determined by dissolving the reduced uranium and unreacted magnesium in zinc and analyzing filtered samples of the solution for uranium.

Prior to the reduction experiments, test runs were made to ascertain whether any chemical reactions between the liquid metal solution and various container materials occurred. Chemical interactions were absent in alumina and tantalum crucibles. In a graphite crucible, interaction between precipitated uranium metal and the graphite was found by X-ray analysis of interfacial areas which showed the presence of uranium carbide. The extent of this reaction appears to be small, however. Difficulty was also caused by reactions of the melt with silica (Vycor) tubes used to sample the melts. The sample tubes were coated with magnesia on the inside and flame-sprayed with alumina on the outside, but these precautions did not entirely prevent reaction. In one case, the material adhering to the outside of the sample tube contained about twice the concentration of uranium in the melt. In recent runs this problem has been overcome by using tantalum sampling tubes.

A number of successful reductions (over 90 per cent) of uranium dioxide and skull oxides have been achieved in liquid magnesium (see Table 5). In these experiments about 30 grams of oxide, 100 grams of magnesium, and one-half to two grams of sodium as a wetting agent were placed in a crucible, heated to 800 C, and stirred for about six hours. The resulting ingot was dissolved in 600 grams of molten zinc, and samples of the melt were withdrawn in tantalum tubes fitted with graphite filter frits for analyses.

Wetting and adequate stirring were found to be important. The presence of a small percentage of sodium appears to improve wetting of both the oxide and the crucible. When wetting of the crucible does not occur, there is greater likelihood that clumps of uncontacted oxide will be found adjacent to the crucible wall.

Two types of stirring were used: a slowly rotated large flat paddle with about the same width as the diameter of the crucible, and a rapidly rotated small propeller having a diameter one-half to one-third the crucible diameter. From the standpoint of ease of removal and replacement, the latter type of stirrer is felt to be more suitable for plant use. However, as shown in Table 5, good reductions were obtained with both types of stirring.

In the case of skull oxide reductions, analyses of the magnesium phase showed nearly quantitative transfer of both cerium and palladium to the magnesium phase.

c. Skull-recovery Process Demonstration Runs
(R. D. Pierce, T. R. Johnson, J. F. Lenc, L. F. Dorsey, M. A. Bowden)

Two demonstration runs of one of the proposed skull-recovery processes were made to pinpoint operational difficulties.

Table 5

SUMMARY OF SMALL-SCALE MAGNESIUM REDUCTIONS OF URANIUM OXIDE

Materials and Conditions:

30 to 40 g UO_2 or Skull oxide
100 g Mg
$\frac{1}{2}$ to 2 g Na

Temp: 775 to 800 C
Time: 6 hours

Per cent reduction determined by dissolution in zinc employing tantalum sampling tubes

Run No.	Type of Oxide	Crucible Material	Stirring Conditions			Per Cent Reduction
			Blade	Baffles	Speed (rpm)	
1	UO_2	Al_2O_3	Small Propeller	Yes	300	<50
2	UO_2	MgO	Large flat	No	100	85
3	UO_2	Ta	Large flat	No	100	97
4	Skull Oxide[a]	Ta	Large flat	No	100	104
5	UO_2	Ta	Small Propeller	Yes	1000	92
PhS-122	Fissium Skull Oxide	Al_2O_3	Small Propeller	Yes	1800-2000	93
PhS-123	Fissium Skull Oxide	Al_2O_3	Small Propeller	Yes	1800-2000	~100

[a] Skull oxide used: U, 78.6 weight per cent; Ce, 6.1 weight per cent

Therefore, it was not expected that either good recovery or purification would be achieved. Emphasis was placed on performing each step in sequence, as diagrammed in Figure 10, even though difficulty might be experienced in any given step. The starting material was crucible skulls from a melt-refining operation, and it was the intent to carry through the process steps to recovery of uranium as metal. The skull used in the first run contained uranium and cerium as metal and oxides, whereas that in the second run contained, in addition to these, the noble metal constituents of fissium - ruthenium, molybdenum, rhodium, palladium, and zirconium. An existing pour furnace was modified as reported in ANL-6183, page 42, to permit transfer of liquid metal phases by pressure siphoning.

FIGURE 10

LIQUID METAL PROCESS FOR RECLAMATION OF MELT REFINING SKULLS

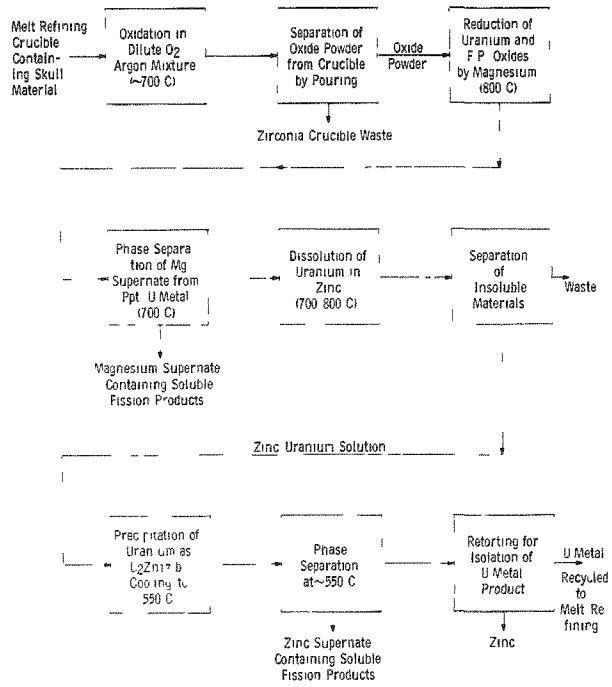

The first process step, oxidation of the skull to recover uranium from the melt-refining crucible, was reported in detail in ANL-6183, page 43. After oxidation, recoveries of 99.4 and 99.6 per cent of the material were achieved by a simple pouring operation in the first and second runs, respectively.

The analytical results are now available for the balance of the steps. The magnesium reductions and washes for the runs were conducted at 760 C in tantalum crucibles. The reductions were nearly complete, as indicated by the absence of uranium oxides as shown by X-ray diffraction analysis. The magnesium supernatant solutions of both runs contained less than one per cent of the uranium and at least 50 per cent of the cerium. About one per cent of the molybdenum and ruthenium were removed in the magnesium in the second demonstration run.

On zinc dissolution at 800 C (during which further reduction may occur), only about 76 and 79 per cent of the uranium was found in solution in the first and second run, respectively, but inasmuch as sampling at that time was performed with Vycor tubes, it is probable that some of the reduced uranium was precipitated by the silica in the tubes. As mentioned previously in this report (page 56), this sampling problem has been overcome by the use of tantalum sampling tubes. The residue remaining in the

tantalum crucible after transfer of the zinc-uranium solution contained 17 and 35 per cent of the uranium originally charged to the two runs. Incomplete and variable transfers were expected because of the exploratory nature of the experiments However, most of the uranium in the residue was contained in the heel solution, which would not be lost in plant operation. Insoluble uranium, precipitated by reactions with impurities or as unreduced oxides, must, however, be avoided at this stage.

The zinc solutions resulting in each run which contained reduced uranium were cooled slowly from 800 to 550 C in the graphite crucible to precipitate uranium-zinc intermetallic. The depleted zinc solutions were removed (by siphoning in the first run and by pouring in the second), leaving beds of intermetallic crystals. The concentrations of uranium in the waste zinc solutions were not determined, but considerable previous experience has shown the concentration of uranium in such solutions to be close to the solubility value, about 0.05 per cent which, in these experiments, would represent a uranium loss of about one to two per cent.

The intermetallic crystals were removed in each run from the graphite crucible and charged to an aluminum oxide-coated graphite crucible for retorting. In the first demonstration run (skull from melt refining of uranium-cerium alloy), 1.4 kg of these intermetallic crystals and residual zinc and magnesium were retorted under initial conditions of 600 C and 6 mm Hg until vaporization of the zinc and magnesium was virtually complete. The still temperature then rose to 900 C and the pressure decreased to less than 1 mm Hg These latter conditions were maintained for 3 hours in the hope of sintering the uranium product The product was finely divided, however and, although it did not adhere to the crucible, only 88 grams of it were removed before the remainder (about 110 grams) ignited

Analyses of the retorted product from this first demonstration run showed a uranium content of about 82 per cent and a magnesium content of approximately 11 per cent. An unsuccessful attempt was made to coalesce, at 1400 C and less than 0 001 mm Hg, the 88 grams of unburned product which had been recovered The magnesium content of this material, after the attempt to coalesce it, remained essentially the same as after retorting, which indicated that the magnesium was initially present as magnesium oxide The presence of magnesium oxide is not surprising, since phase separations were not designed to provide for its removal More attention will be given to this problem in later runs.

In the second demonstration run, the 1.2-kg zinc, magnesium, and uranium-zinc intermetallic cake (skull from melt refining cerium-fissium alloy) was retorted initially at 660 C and less than 2 mm Hg. Prior to retorting, 200 grams of magnesium was added to the cake

(resulting in a charge containing approximately 15 per cent magnesium) in order to precipitate uranium from the uranium-zinc intermetallic during retorting and thereby form a more compact product. The final retorting conditions were the same as those reported for the first demonstration run.

About 144 grams of the retorted product sintered in the crucible bottom and 19 grams deposited on the side wall. The latter material was easily removed but the former stuck to the bottom of the crucible. It is believed that this sticking may have been caused by incomplete retorting, for analyses of portions of the material showed magnesium metal contents of between 0.6 and 2.5 per cent. By mechanical means, 112 grams of the bottom product was removed from the crucible. It was impossible, however, to recover the remaining 32 grams. The product recovered from the crucible bottom and side wall was subsequently coalesced together with 102 grams of additional normal uranium at 1400 to 1500 C and less than 0.001 mm Hg. Melting with additional uranium simulates the return of this material to a melt-refining operation. Approximately 97.5 per cent of the charge coalesced.

The uranium product after retorting contained less than 0.04 per cent magnesium oxide, which accounts for the ability to coalesce the material into the metallic button subsequently. It also indicates that, insofar as magnesium oxide removal is concerned, the pouring operation was considerably more effective than pressure siphoning.

The ability to perform all the process steps in a proper sequence in nonspecialized equipment has been very encouraging. Although separations were usually incomplete, little difficulty was experienced in removal of supernatant liquid metal phases from precipitated uranium (either as metal or as a uranium-zinc intermetallic compound). The phase separation which is likely to prove most difficult is removal of magnesium oxide, although in the second run effective removal was apparently achieved by a pouring operation. However, with either the pouring or siphoning procedure, the magnesium oxide is left behind in the reduction crucible where its buildup can pose an increasing problem.

Because product transfers were incomplete, only qualitative information can be given regarding purification. Removal of palladium and cerium appears to be very good, these elements being removed in the magnesium supernatant solution. Appreciable removal of molybdenum, ruthenium, and zirconium was also achieved, probably by virtue of insolubility in the various metal solvents.

The high reactivity of the retorted uranium product was manifested in the first run by its rapid oxidation on exposure to air. Although in the plant the skull recovery process equipment as finally envisioned would

be located in an argon cell, so that the retorted product would not react with oxygen, the high reactivity of this uranium may permit reaction with the nitrogen impurity expected in the cell atmosphere. Methods of protecting the uranium product, both in experimental work and under the expected plant conditions, must be devised.

d. Retorting of Uranium Concentrates
(J. F. Lenc, M. A. Bowden)

Recovery of uranium in the current dragout process requires final retorting of zinc and magnesium from a two-phase system composed of a zinc-magnesium liquid metal phase and a precipitated uranium-zinc intermetallic phase. The uranium product obtained from this final retorting step must be in a compact form suitable for remote removal and handling. In the preceding two quarterly reports (ANL-6145, page 63 and ANL-6183, page 59), it was reported that a number of successful retorting runs had been made in ceramic or ceramic-coated graphite crucibles. The general experience with tantalum crucibles had been that the uranium product adhered rather firmly to the crucible and was difficult to remove. However, because of the fabricability of tantalum and its relatively good corrosion resistance to zinc, additional work was performed in the last quarter to determine if conditions could be found under which tantalum would be a useful and reliable container material.

The major change in the retorting procedure was that the bulk of the zinc was initially distilled at 525 C instead of at 650 C. In the equipment employed, this also resulted in lowering the distillation rate from about 1.5 kg/hr to about 0.3 kg/hr. Two methods of charge preparation were employed: (1) direct dissolution of uranium in the retorting crucible, and (2) dissolution in a separate graphite crucible and subsequent transfer of an ingot to the retorting crucible. In either case a nominal 2.4-kg charge was prepared by dissolving uranium to a concentration of eight per cent in a dilute (10 per cent or less) magnesium-zinc alloy at 800 C. Five runs were made by the first procedure and six by the second. In the six runs in which the charge had been prepared in graphite, the uranium product was readily removed (Table 6). Inasmuch as product removal from tantalum had previously been difficult, the temperature change was evidently beneficial. However, in the five runs in which the charge was prepared and retorted in the same tantalum crucible, the uranium adhered to the bottom and side wall of the crucible and required mechanical prying for removal. The high temperature and time required for uranium solution may enhance wetting of the tantalum crucible. Wetting also may eventually occur even when the charge is prepared in a separate crucible. The possible introduction of carbon via the charge preparation in graphite crucibles may have been beneficial insofar as eliminating product adherence to the crucible.

Table 6

PERFORMANCE OF TANTALUM AS A CONTAINER MATERIAL FOR RETORTING URANIUM-ZINC SYSTEMS

Run No.	Charge Preparation Crucible: Material	Charge Preparation Crucible: Same Crucible Used as Retorting Crucible	Charge Weight (kg)	Mg Conc (w/o)	U Conc (w/o)	Still Conditions: Temp (C)	Still Conditions: Time (hr)	Still Conditions: Pressure (mm Hg)	Average Rate of Vaporization (kg/hr)	Uranium Recovered (w/o)	Nature of Retorted Product
A-9	Aluminum Oxide[a]	No	3.75	2.5	12.1	650-675 700-880	1.5 3.6	142-2 2-<1	1.88	89.5	Compact bottom cake (74%) - only side wall material adhered to the crucible (26%).
A-19	Tantalum[b]	Yes	9.90	1.0	3.1	600 675 675-890	5.25 1.0 3.75	60-10 17-5 <1	1.40	53.7[c]	Product deposited on bottom and side wall of crucible - not removable.
A-38	Graphite[d]	No	2.23	2.0	9.4	525-550 675-700	5.0 4.0	<1 <1	0.27	~100	Amorphous bottom product - highly pyrophoric - did not adhere to crucible.
A-39	Graphite[d]	No	2.22	2.0	9.5	525-550 600-675 675-900	5.0 2.0 2.0	<1	0.28	86.0	Compact skull-shaped product - easily removed.
A-40	Graphite[d]	No	2.25	10.0	8.9	500-550 700-725 725-860	5.0 2.0 1.5	<1	0.29	98.6	Compact skull-shaped product - easily removed.
A-41	Graphite[d]	No	2.30	10.0	8.7	550-575 625-750 750-950	5.0 2.0 5.5	<1	0.29	~100	Compact skull-shaped product - easily removed.
A-42	Graphite[d]	No	2.35	10.0	8.1	500-540 700-750 750-880	5.0 2.5 2.5	<1	0.29	98.2	Compact skull-shaped product - easily removed.
A-43	Graphite[d]	No	2.87	10.0	10.2	500-600 600-700 700-940	4.0 0.75 3.0	<1	0.38	93.0	Compact skull-shaped product - bottom of skull adhered to crucible - bottom easily removed after second retorting.[e]
A-44	Tantalum[d]	Yes	2.39	~10	8.40	575-600 700-730 850-950	5.0 3.0 2.0	<1	0.27	97.5	Compact skull-shaped product. Adhered to bottom and side wall of crucible.
A-45	Tantalum[d]	Yes	2.35	~10	8.60	575-600 700-825 825-950	5.0 4.0 2.5	<1	0.36	95.0	Compact skull-shaped product. Adhered to bottom and side wall of crucible.
A-46	Tantalum[d]	Yes	2.39	~10	8.47	500-575 525-760 760-860	5.0 4.0 2.5	<1	0.24	97.5	Compact skull-shaped product. Adhered to bottom and side wall of crucible.
A-48	Tantalum[d]	Yes	2.43	~10	8.22	550-600 600-725 800	5.0 4.0 2.0	<1	0.27	98.8	Compact skull-shaped product. Adhered to bottom and side wall of crucible.
A-50	Tantalum[d]	Yes	2.39	~10	8.40	550-600 650-800 850	4.0 4.0 2.0	<1	0.36	96.5	Compact skull-shaped product. Adhered to bottom and side wall of crucible.

[a] Charge prepared by hydriding uranium at 250 C, dehydriding at 325 C, and reacting dehydrided uranium with cadmium below 470 C to form UCd_{11}.

[b] Charge prepared by dissolution of uranium in a cadmium-7 per cent zinc-1 per cent magnesium solution at 650 C.

[c] Based on uranium analysis of product dissolved from a tantalum crucible.

[d] Charge prepared by dissolution of uranium in a dilute (10 per cent or less) magnesium-zinc solution at 800 C, and subsequent crystallization of the uranium as an intermetallic upon cooling.

[e] Second retorting at 700 to 900 C for 2 hours to a pressure less than 1 mm of mercury.

As shown in Table 6, uranium recoveries of 95 per cent and greater were realized in ten of the eleven runs under discussion. Although these are high yields, the fact that they are not quantitative shows that slight entrainment is still occurring. Under the experimental retorting conditions employed, it has not been possible to precipitate the uranium completely prior to retorting. Such will not be the case in plant operation, and quantitative recoveries under plant operating conditions should be achievable.

A compact, skull-shaped product resulted in all the runs except one. In this particular experiment (Run A-38) the still temperature was maintained at 700 C maximum so that an amorphous rather than a sintered product was formed.

The results of the recent work may be summarized as follows:

1) A tendency exists for adherence or sticking of retorted uranium products to tantalum crucibles.

2) Recoveries which are a few per cent short of being quantitative indicate a slight entrainment problem. This is believed to be due to the inability to precipitate completely the uranium. This is a problem inherent in the current experimental procedure but will probably not be a serious problem in plant operation.

Equipment modifications are progressing to permit scale-up of the present type of experimentation to a one-kilogram-uranium level. It is anticipated that investigation on this larger scale will begin in the next quarter.

e. Distillation of Liquid Metals

(1) Large-scale Cadmium Distillation Equipment
(R. Cairns, P. Nelson, R. Fryer, J. Hepperly)

A full-scale distillation station is being constructed to demonstrate metal distillation and retorting operations on a large scale and to demonstrate other associated operations such as metal transfer, liquid-level detection, and freeze-valve operation. Although construction progressed during the last quarter, assembly of components has been unexpectedly delayed since all the piping, freeze values and vapor traps, which were manufactured by an outside contractor, were rejected. Because of inadequate precautions during the pickling operation required by the specification, all items were very severely corroded. The components are being refabricated as quickly as possible, but some difficulty is being encountered in obtaining further quantities of Type 405 stainless steel piping.

(2) Vapor-Liquid Equilibrium Studies
(P. Nelson, R. Zeman,* R. Fryer)

A vapor-liquid equilibrium still for determining activity coefficients in binary solutions of magnesium, cadmium, and zinc has been constructed and is being tested and revised. The revisions were made to improve temperature distribution. A heater is being added to the top of the still to prevent partial condensation of the vapor before it enters the vapor riser leading to the condenser.

f. Materials Evaluation Studies
(P. Nelson, J. Wolkoff, J. DeKany, M. Kyle)

Evaluation of materials for pyrometallurgical equipment is continuing and is being expanded. This program is resulting in the accumulation of extensive data and information on materials and fabrication techniques for equipment for liquid metal processes. The main direction of the present work is the accumulation of specific information on materials for fabricating EBR-II process equipment for dross processing.

(1) Corrosion by Solvent Metals
(M. Kyle, J. Hepperly)

A program is in progress to test the corrosion resistance of refractory metals, graphite, and ceramics to molten metals, particularly to zinc and zinc-magnesium solutions. Corrosion tests are being conducted in tantalum capsules which are continuously rocked in a rocking furnace for 100 hours. The capsules, which contain a coupon to be tested in zinc or zinc-magnesium solutions, are subjected to higher temperatures (850 to 900 C) than are anticipated in process applications in order to accelerate corrosion The following materials are being tested by this method: tantalum, tungsten-tantalum alloys, pyrolytic graphite, molybdenum, single-crystal Al_2O_3, and high-density magnesia. Materials showing promise under these testing conditions will be retested for longer periods of time at processing temperatures.

(2) Solution Stability Experiments
(J. P. DeKany, J. Pavlik)

A series of experiments is being made to determine the stability of uranium in various molten-alloy and container material systems. Of immediate interest are a number of uranium-magnesium-zinc alloys contained in tantalum. The first experiment will determine the solution stability of a 2 per cent uranium-15 per cent magnesium-zinc alloy in a tantalum crucible at 800 C. Other runs in which the activity of uranium will be varied by changing both uranium and magnesium concentrations will also be conducted in tantalum.

*Summer student

(3) Evaluation of Other Materials
(J. Wolkoff, R. E. Nowak)

Two other materials with a potential for applications in the liquid metal program, because of their good corrosion resistance, are tungsten and pyrolytic graphite. As a result of difficulty in fabricating large parts from these materials, coatings on a graphite base are being considered.

A program to purchase and test these and other materials has been initiated. Crucibles of these materials will be subjected to solution-stability tests of the type described above, and tests will also be made to determine the possible use of these coated materials for lining pipes. Thermal cycling tests will be made first to evaluate adherence, and will be followed by holding experiments.

C. Pyrometallurgical Research
(H. M. Feder)

1. Chemistry of Liquid Metal Solvents
(I. Johnson)

The chemistry of liquid metal systems is being investigated to provide basic concepts and data for the logical design of pyrometallurgical separations processes. The separations process under consideration consists of the dissolution of the spent reactor fuel in an appropriate volatile liquid metal, separation of the fission products and other extraneous elements by recrystallizations and/or extractions with immiscible liquids (either fused salts or other liquid metals), and, finally, recovery of the fissile metal(s) by evaporation of the solvent.

a. Solubilities in Liquid Metals

The solubilities of the elements whose separations are being attempted are of prime importance in the design of fuel-reprocessing schemes. The dependence of solubilities on temperature and solvent composition needs to be known. The identity of the solid phase in equilibrium with the saturated solutions is useful when solubility trends are being investigated.

Titanium-Cadmium System
(M. G. Chasanov and P. D. Hunt)

In ANL-6183, page 63, solubility data for titanium in liquid cadmium were reported covering the temperature range from 350 to 650 C. Additional solubility measurements in the lower temperature region have been completed, using the same method, and the composite data are presented in Figure 11.

FIGURE 11
SOLUBILITY OF TITANIUM IN LIQUID CADMIUM

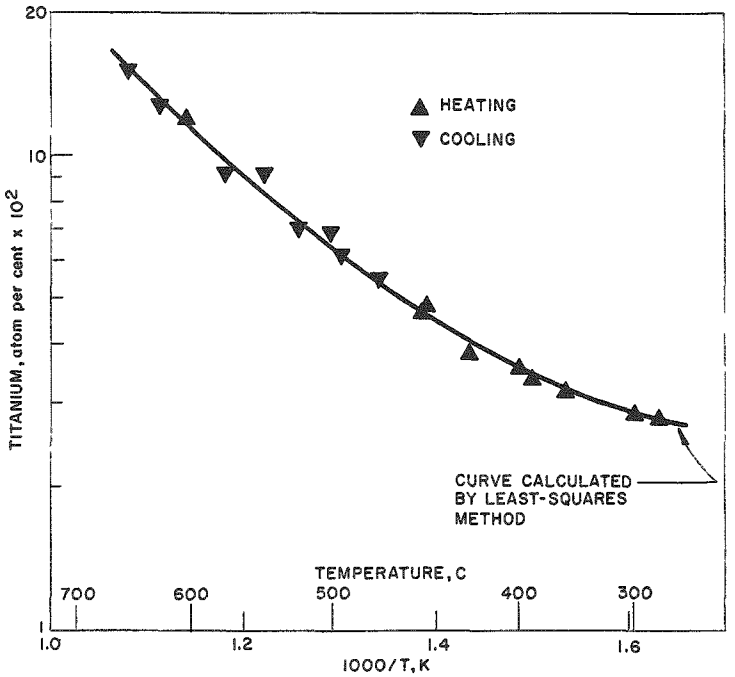

The solubility data over the whole range of temperatures studied may be represented by the empirical equation

$$\log \text{(atom per cent titanium)} = 3.237 - 5333\ T^{-1} + 1.468 \times 10^{6}\ T^{-2} \quad .$$

The standard deviation, σ, was found to be 5.5 per cent. Above 424 C the solubility data may be represented by the linear relation

$$\log \text{(atom per cent titanium)} = 0.9100 - 1620\ T^{-1} \quad ,$$

with a standard deviation, σ, of 5.1 per cent.

The cadmium-richer intermetallic phase "C" reported in ANL-6183, page 65, has a composition which is approximately TiCd. Previously, it was considered that this phase might be Ti_2Cd. The composition TiCd was found by chemical analysis of crystals chemically leached from an ingot and by the preparation of the intermetallic using the stoichiometric amounts plus a slight excess of cadmium to aid crystal growth. The symmetry of this intermetallic is tetragonal.[7] The final computations of the crystal parameters await completion of density determinations on the substance.

---

[7] Schablaske, R. and Tani, B., private communication.

Solubility of Zirconium in Cadmium

(I. Johnson, K. E. Anderson and R. Claypool*)

The solubility of zirconium in liquid cadmium was measured by means of the standard method discussed in ANL-6068, page 66. A zirconium (crystal bar, reactor grade) and cadmium (99.99 per cent pure) melt of about 0.4 per cent zirconium was prepared in an alundum crucible under an argon atmosphere. The melt was stirred with a tantalum paddle and the temperature measured by means of a porcelain-protected thermocouple immersed in the melt. Filtered samples of the equilibrium liquid phase were taken with quartz or pyrex sampling tubes equipped with porous (grade 60) graphite filters, coated on the inside with magnesium oxide. No evidence of reaction between samples and sampling tubes was observed at the temperatures of the runs. Samples of this liquid phase were taken after the system had been held at constant temperature for a minimum of two hours, the last one-half hour without stirring.

The data obtained in this study are given in Table 7 together with data previously obtained by Ader and Pavlik (ANL-5996, page 101).

Table 7

SOLUBILITY OF ZIRCONIUM IN CADMIUM

Temp (C)	Zirconium (wt per cent) This Study	Zirconium (wt per cent) Ader and Pavlik[a]
574	0.33_8	-
545	-	0.30_8
535	0.28_0	-
511	-	0.26_1
502	0.24_5	-
485	-	0.22_8
480	-	0.22_0
461	0.19_6	-
456	-	0.18_9
452	0.18_4	-
417	0.11_7	-
411	-	0.10_8
383	0.076	0.076_2
369	-	0.059_0
350	0.043_5	-
345	-	0.043_2

[a] Ader, M. and Pavlik, J., ANL-5996, p. 101.

*Student Aide, Summer, 1960.

Both sets of data are in agreement, even though the latter data were obtained in an open crucible with a molten salt cover and using a cadmium solution containing 0.1 weight per cent magnesium. Both sets of data are shown in Figure 12. Two distinct lines are shown, corresponding to the solubilities of two different intermetallic phases. The intersection of these lines (at 452 C) corresponds to the peritectic temperature. The solubility line below the peritectic is given by the equation

$$\log \text{(weight per cent zirconium)} = 3.058 - 2750\ T^{-1} \quad ;$$

the solubility line above the peritectic is given by the equation

$$\log \text{(weight per cent zirconium)} = 1.079 - 1314\ T^{-1} \quad .$$

FIGURE 12
SOLUBILITY OF ZIRCONIUM IN CADMIUM

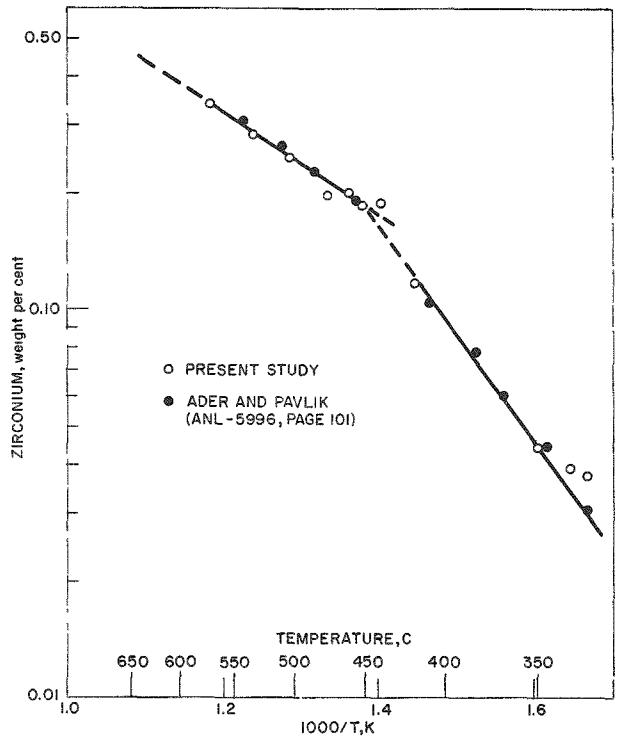

X-ray examination of the intermetallic phase present below the peritectic gave the pattern observed by Pietrokowski[8] for the body-centered tetragonal phase in this system. The phase in equilibrium with the saturated solutions above the peritectic temperature has not been characterized.

---

[8] Pietrokowski, P., Trans. A.I.M.E., 200, 219 (1954).

Solubility of Samarium in Cadmium

(I. Johnson, K. E. Anderson, R. Claypool*)

The solubility of samarium in liquid cadmium has been measured by means of the procedure described above for the zirconium-cadmium system. A melt of samarium metal (99+ per cent, Michigan Chemical Co.) and cadmium (99.99 per cent, American Smelting and Refining Co.) was prepared and sampled in the usual fashion. In the first of two experiments, samples were taken over the temperature range from 355 to 600 C (Experiment A); in the second experiment, samples were taken from 325 to 408 C (Experiment B). The data from these two experiments are given in Table 8 and shown graphically in Figure 13. The data lay on two straight lines which intersect at 420.5 C. The solubility below 420.5 C is given by the equation

$$\log (\text{atom per cent samarium}) = 7.0729 - 4878.2\ T^{-1} \quad ;$$

the solubility above 420 and below 600 may be represented by the equation

$$\log (\text{atom per cent samarium}) = 3.0911 - 2116.1\ T^{-1} \quad .$$

Table 8

SOLUBILITY OF SAMARIUM IN CADMIUM

Experiment A: Samples taken as solution was cooled from 609 to 399 C

Experiment B: Samples taken as solution was cooled from 385.3 to 325.7 C and then heated to get the 330 and 342 C samples.

Experiment A		Experiment B	
Temp (C)	Samarium (w/o)	Temp (C)	Samarium (w/o)
609	6.54	385.3	0.731
563	4.78	367.5	0.348
516	3.38	351.1	0.219
478	2.47	342.0	0.191
433	1.68	330.0	0.127
399	0.834	325.7	0.122

The solid in equilibrium with the melt below 420 C was found by X-ray examination to be the samarium-cadmium intermetallic compound $SmCd_{11}$. The intermetallic phase in equilibrium with the melt above 420 C has not yet been characterized.

*Student Aide, Summer, 1960.

FIGURE 13
SOLUBILITY OF SAMARIUM IN CADMIUM

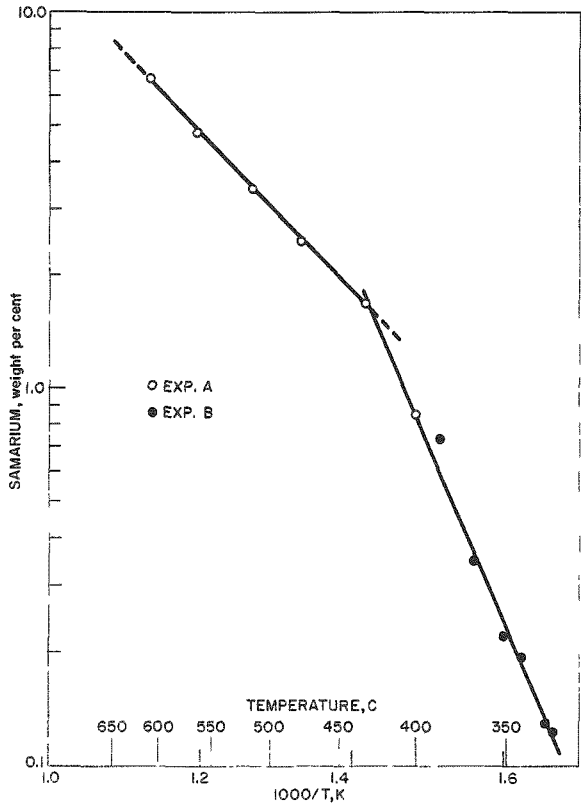

Solubility of Yttrium in Cadmium

(I. Johnson, K. E. Anderson and R. Claypool*)

The solubility of yttrium in liquid cadmium has been measured by means of the same procedure described for the zirconium-cadmium system. Three experiments were done. The data obtained in the first experiment defined the solubility over the range from 326 to 500 C. The yttrium metal used in this experiment was about 97 per cent yttrium; the principal impurities were calcium (one per cent), magnesium (one per cent), and rare earths (0.9 per cent). The yttrium used in the second and third experiments was nuclear-grade material (99.1+ per cent yttrium, Lunex Co.). The second and third experiments covered the lower and upper temperature ranges, respectively. Solubility data obtained in these three experiments are given in Table 9 and shown graphically in Figure 14. The data were represented better by a slightly curved line than by a straight line. The quadratic equation

$$\log (\text{weight per cent yttrium}) = 4.8539 - 4687.5\ T^{-1} + 0.7520 \times 10^{6}\ T^{-2}$$

fits the data to within ±4 per cent.

*Student Aide, Summer, 1960.

Table 9

SOLUBILITY OF YTTRIUM IN CADMIUM

Yttrium charge, weight per cent: Experiment A, 2.0; Experiment B, 0.51; Experiment C, 3.4

Temp (C)	Solubility of Yttrium (w/o)		
	Experiment A	Experiment B	Experiment C
602.0	-	-	3.04
580.7	-	-	2.50
554.8	-	-	1.97
539.0	1.66	-	-
529.3	-	-	1.52
500.0	1.12	-	1.11
478.3	-	-	0.862
463.0	0.742	-	-
455.0	-	-	0.672
431.2	-	-	0.516
423.3	0.440	0.506	-
400.1	-	-	0.356
392.0	-	0.348	-
363.5	-	0.232	-
348.0	0.180	-	-
344.4	-	0.160	-
343.5	-	0.166	-
336.3	-	0.151	-
333.9	-	-	0.152
326.0	0.138	-	-
324.9	-	0.130	-

FIGURE 14
SOLUBILITY OF YTTRIUM IN CADMIUM

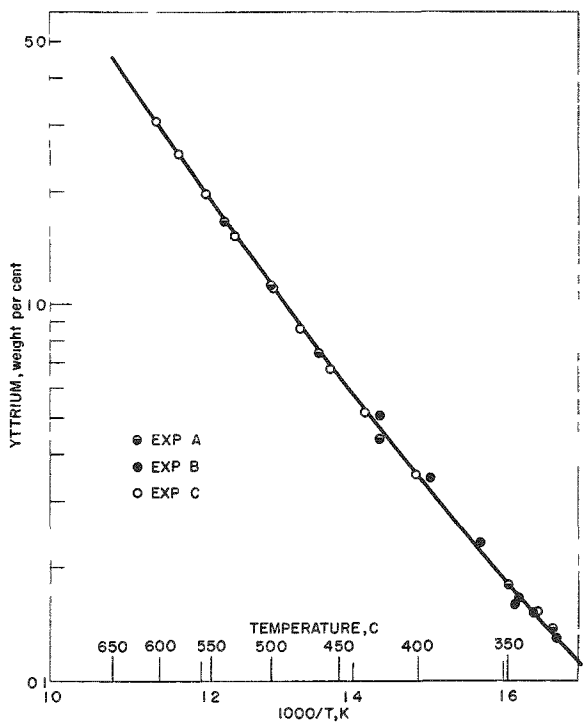

The solid phase in equilibrium with these solutions has not been completely characterized. Preliminary X-ray analysis shows that it is not isostructural with the MCd_{11} rare earth compounds.

b. Liquid-Liquid Distribution Studies
(F. Cafasso and R. Uhle)

Partition of Uranium, Palladium, Cerium, and Strontium between Lead and Zinc

The role of liquid-liquid partition methods in pyrometallurgical processes is being examined in this study. The immiscible liquid metal pairs aluminum-cadmium, lead-zinc and bismuth-zinc are under consideration. Partition data for a number of fissile and fission product elements have been reported for the aluminum-cadmium system (ANL-6183, page 69). Similar measurements for the lead-zinc system are reported below.

Partition coefficients were determined by sampling each phase of a two-phase equilibrium system. Mixtures consisting of lead, zinc, and the solute metal contained in an alumina crucible were stirred by a tantalum paddle for one hour. After a two-hour settling period, samples were taken (by pressurization) with magnesium oxide-coated quartz tubes fitted with graphite filters. All samples of the lower lead phase were obtained by the breakseal method (ANL-6101, page 72). Spectrochemical analyses of both phases showed the silicon content to be below the detectable limits (<0.01 per cent).

Distribution measurements were made for four solutes (uranium, palladium, cerium and strontium) in the range from 728 to 736 C. Distribution coefficients, defined as the ratio of the weight per cent of solute in zinc to the weight per cent of solute in lead, are recorded in Table 10.

Table 10

DISTRIBUTION DATA FOR LEAD-ZINC SYSTEM

	Solubility Data for Lead-Zinc System		Distribution Data for Solutes in Lead-Zinc System			
Average Temperature (C)	Solubility of Lead in Zinc Phase (w/o)	Solubility of Zinc in Lead Phase (w/o)	Solute	Solubility of Solute in Zinc Phase (w/o)	Solubility of Solute in Lead Phase (w/o)	Distribution Coefficient, $K = \frac{\text{w/o Solute in Zinc Phase}}{\text{w/o Solute in Lead Phase}}$
647	8.9	7.8	U	0.27	1.0×10^{-3}	270.0
700	14.1	11.4	U	0.25	3.4×10^{-3}	73.5
728	16.7	14.9	U	0.40	1.3×10^{-2}	30.8
734	21.0	15.1	U	0.23	7.2×10^{-3}	31.9
734	-	-	Ce	1.00	2.7×10^{-1}	3.7
736	-	-	Sr	0.24	1.7	0.14
737	-	-	Pd	2.25	1.5×10^{-2}	150.0

It is apparent from this table that uranium, cerium, and palladium concentrate preferentially in the zinc layer, while strontium concentrates in the lead phase. The tendency for the three solutes to distribute into the zinc layer varies in the following order: palladium > uranium > cerium. The coefficient of palladium is larger than that of uranium by a factor of about five. On the other hand, the coefficient of uranium is approximately eight times larger than that of cerium.

Mutual solubilities of lead and zinc were measured only for the uranium system. These values appear in Table 10.

Temperature Dependence of the Uranium Distribution Coefficient

In attempts to evaluate the utility of a particular solvent system, information about the temperature dependence of the partition of a solute metal would be helpful. For this reason the distribution of uranium between lead and zinc was measured as a function of temperature. Measurements were made at three temperatures 647, 700, 734 C. Two factors, the consolute temperature of the solvent system and the solubility of uranium, limited the temperature range that was investigated. In order to obtain appreciable metal solubility, measurements had to be made at temperatures very close to the consolute temperature (approximately 780 C) of the lead-zinc system.

Values of the logarithm of the distribution coefficient, defined as above, are plotted against the reciprocal of the absolute temperature in Figure 15 and are reported in Table 10.

FIGURE 15
TEMPERATURE DEPENDENCE OF URANIUM DISTRIBUTION
IN THE LEAD-ZINC SYSTEM

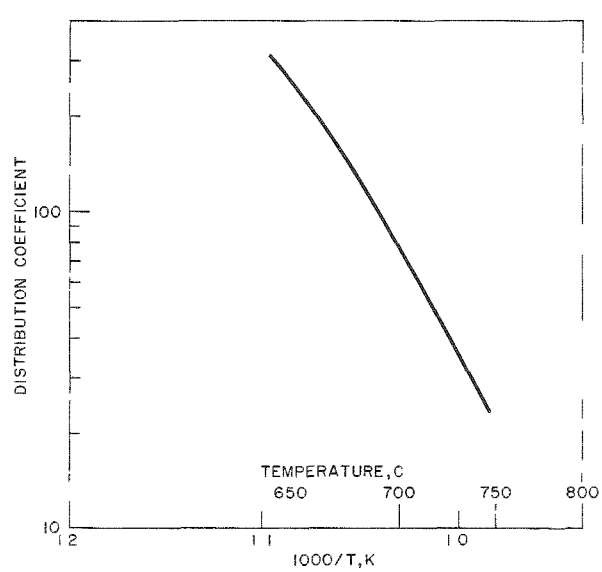

The coefficient changes from a value of 31.9 at 734 C to 270 at 647 C. Over this range, there is a simultaneous change in the mutual solubilities of the solvent metals. From 734 to 647 C, the solubility of lead in zinc falls from 21.0 weight per cent to 8.9 weight per cent. The solubility of zinc in lead changes from 15.1 weight per cent at the higher temperature (734 C) to 7.8 weight per cent at the lower temperature (647 C).

c. Thermodynamic Studies

Thermodynamic functions for key elements in liquid metal solvents and for the important solid intermetallic phases are being measured. Two methods are being used. Galvanic cells have proved to be especially useful for determining activities in liquid solutions and for measuring thermodynamic functions for the most solvent-rich intermetallic phase. On the other hand, for systems containing several well-defined intermetallic phases, measurement of the decomposition pressure by the effusion method is proving to be most useful. The two methods supplement each other.

Thermodynamics of the Uranium-Thallium System
(I. Johnson and R. M. Yonco)

A galvanic cell was assembled to measure the free energy of solution of uranium in a saturated thallium solution and the free energy of formation of the uranium-thallium intermetallic compound UTl_3. The cell construction was similar to previous cells in this series, being of the form

$$U/UCl_3 \cdot KCl\text{-}LiCl \text{ (eutectic)}/U(\text{satd soln in Tl}).$$

The uranium electrode was made by welding a length of high-purity uranium metal to a tungsten wire. The thallium electrode was prepared from high-purity thallium (99.95 per cent thallium, American Smelting and Refining Co.) which was filtered prior to use. Uranium was added to the liquid thallium electrode *in situ* by electrolysis from the uranium electrode. The thallium electrode was about 4.8 per cent uranium.

The data obtained are shown in Figure 16 and may be represented by the linear equation

$$E(\text{volts}) = 0.1933 - 1.735 \times 10^{-4}\, T$$

to within ±0.3 mv.

The half-cell reaction at the uranium electrode (negative) is

$$U(\alpha) \longrightarrow U^{+3} \text{ (molten salt)} + 3e^- \quad .$$

FIGURE 16
EMF AS A FUNCTION OF TEMPERATURE OF THE URANIUM-THALLIUM CELL

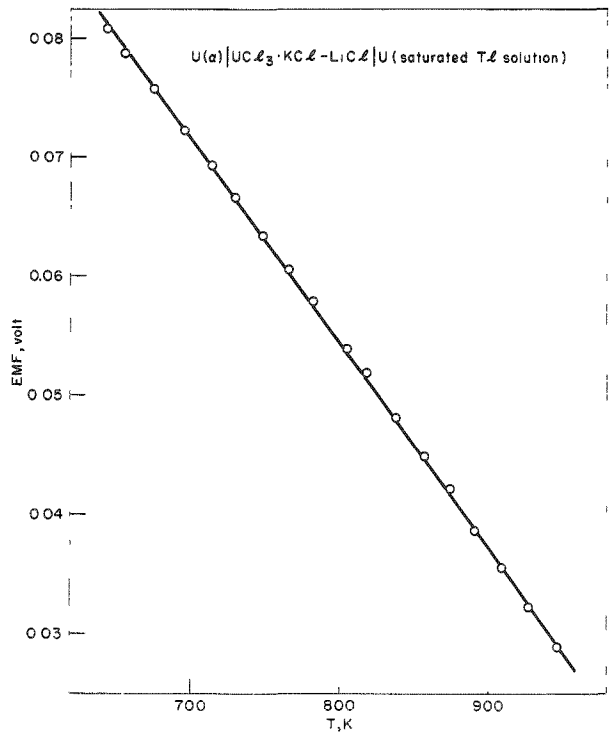

This reaction has been shown to be reversible by Inman et al.[9] The half-cell reaction at the liquid electrode (positive) is

$$U^{+3} + 3e^- \longrightarrow U \text{ (liquid Tl soln).}$$

This reaction has been assumed to be reversible. The analogous reaction in the case of liquid zinc electrodes was shown to involve a three-electron change, and the emf followed the Nernst relation with respect to the uranium concentration in the liquid electrode (ANL-5924, page 134). The cell reaction is, therefore,

$$U(\alpha) \longrightarrow U \text{ (liquid Tl soln).}$$

Since the liquid electrode is saturated with respect to the uranium-thallium intermetallic compound UTl_3, viz.,

$$U \text{ (liquid, Tl soln)} + 3 \text{ Tl (Satd soln)} \rightleftharpoons UTl_3(s) \quad ,$$

---

[9] Inman, D., Hills, G. J., Young, L. and Bockris, J. O'M., Ann. N. Y. Acad. Sci. 79, 810 (1960).

the overall cell reaction may be written as

$$U(\alpha) + 3Tl\ (\text{satd soln}) \longrightarrow UTl_3(s) \quad .$$

Hence,

$$-nFE = \Delta F_f^0 - 3RT \ln a_{Tl}.$$

Since the solubility of uranium in thallium is low at these temperatures,[10] the last term in this equation is negligible (less than four calories) and hence the free energy of formation, ΔF_f^0, for the intermetallic compound UTl_3 is given by the equation

$$\Delta F_f^0 = -13{,}376 + 12{,}008T \quad .$$

At 500 C, the free energy of formation is -4.09 kcal per mole, while the heat of formation is -13.4 kcal.

Thermodynamics of the Cerium-Zinc System
(I. Johnson and R. M. Yonco)

A galvanic cell was assembled to measure the free energy of formation of saturated solutions of cerium in zinc and of the cerium-zinc intermetallic phase $CeZn_{11}$. The cell construction was similar to previous cells in this series, being of the form

$$Ce/CeCl_3 \cdot KCl\text{-}LiCl\ (\text{eutectic})/Ce\ (\text{satd soln in Zn}) \quad .$$

The cerium electrode was prepared by casting cerium metal in vacuum around a tungsten wire. The liquid alloy electrode was prepared by dissolving a cerium-zinc master alloy in pure zinc in the cell.

Since a possibility of reaction between cerium and lithium ion exists, the interpretation of these experiments is of a preliminary nature. In interpreting the results, the overall cell reaction

$$Ce(s) + 11\ Zn(\text{satd soln}) \longrightarrow CeZn_{11}(s)$$

has been assumed.

Hence,

$$-3FE = \Delta F = \Delta F_f^0 - 11\ RT \ln a_{Zn} \quad ,$$

---

[10] Values of 0.12 per cent at 800 C and 0.17 per cent at 900 C are given by Rough, F. A. and Bauer, A. A., Constitution Diagrams of Uranium and Thorium Alloys, Addison-Wesley Press, Inc., Cambridge, Mass. (1959).

where E is the cell voltage; ΔF_f^0 the Gibbs free energy of formation of the intermetallic compound $CeZn_{11}$; and a_{Zn} the activity of zinc in the saturated solution. The saturated solutions are sufficiently dilute to assume that the zinc activity is equal to its mole fraction. The term $11RT \ln a_{Zn}$ varied from -0.07 at the lowest temperature to -166 calories at the highest temperature. The emf of the cell is also related to the activity of cerium a_{Ce} in the saturated solutions by the equation

$$\log a_{Ce} = -3FE/2.3\ RT \quad .$$

The emf was measured over the temperature range from 443 to 742 C. The data are shown in Figure 17. The data may be represented by the quadratic equation

$$E = 1.1168 - 2.9017 \times 10^{-4}T - 2.1221 \times 10^{-7}T^2 \quad .$$

FIGURE 17
EMF AS A FUNCTION OF TEMPERATURE FOR THE CERIUM-ZINC CELL

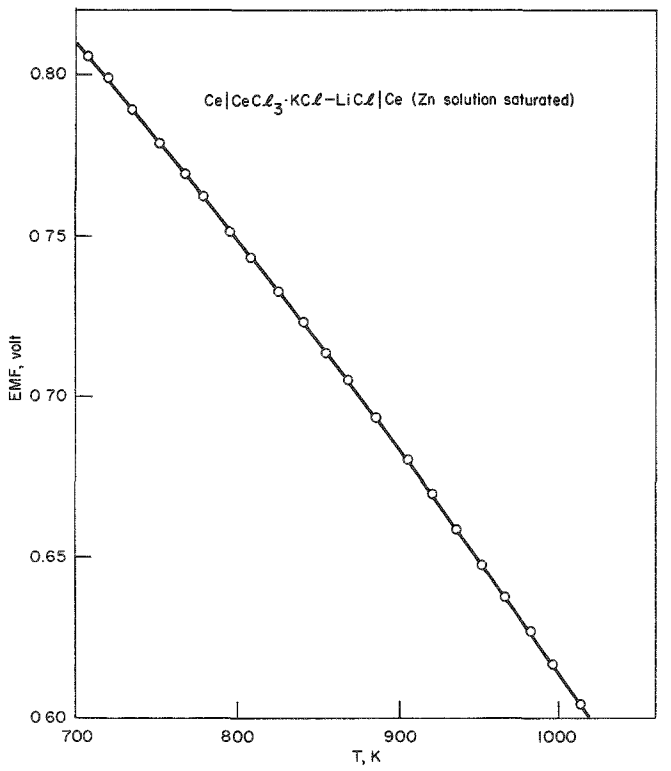

The activity of cerium (pure solid cerium is standard state) in saturated zinc solutions is given by

$$\log a_{Ce} = -16{,}891\ T^{-1} + 4.3887 + 3.2095 \times 10^{-3}\ T \quad .$$

Using Knighton's data (ANL-5730, page 110) for the solubility of cerium in zinc,

$$\log x_{Ce} = 5.2156 - 7449.3\ T^{-1} \quad ,$$

the following equation for the activity coefficient of cerium in saturated zinc solutions is obtained:

$$\log \gamma_{Ce} = -9442\ T^{-1} - 0.8269 + 3.2095 \times 10^{-3}\ T \quad .$$

The free energy of formation, ΔF_f^0, may be computed from the equation

$$\Delta F_f^0 = -79{,}257 + 25.046T + 0.01157\ T^2 \quad .$$

This equation reproduced the observed data to ±23 calories.

2. Calorimetry
(W. N. Hubbard)

Thermodynamic data for many compounds of interest in high-temperature chemistry are unavailable, mainly because of the experimental difficulties involved in making the necessary measurements. A program has been undertaken to help fill this gap.

Part of the program consists of determinations of heats of formation at 25 C by oxygen bomb calorimetry. Because some of the compounds of interest are difficult to burn in oxygen, and, consequently, cannot be studied by oxygen bomb calorimetry, the new technique of fluorine bomb calorimetry has been developed for their study. The accumulation of basic heat of formation data for fluorides is a necessary preliminary adjunct to fluorine bomb calorimetry and is a valuable program on its own merit.

The heats of formation at 25 C from oxygen or fluorine combustion calorimetry will be combined with the changes in enthalpy measured by a high-temperature enthalpy calorimeter to determine thermodynamic properties at high temperatures. A calorimetric system for measurements up to 1500 C has been designed and is now being fabricated. Design concepts for an electron beam furnace to operate up to 2500 C are being tested in the laboratory.

Some of the compounds of interest are borides, aluminides, carbides, silicides, nitrides, sulfides, and selenides of metals such as uranium, zirconium, molybdenum, and tungsten. Some of the compounds are being prepared for the program by Stanford Research Institute. Two compounds (the disulfides of molybdenum and tungsten) have been prepared here.

a. Combustion of Tungsten and Sulfur in Oxygen
(R. L. Nuttall and D. R. Fredrickson)

In a previous report (ANL-6183, page 77) results of measurements of the heat of combustion of tungsten disulfide in oxygen were

reported. To derive the heat of formation of tungsten disulfide from these data, the heats of formation of other reactants and products of the combustion must be known. To minimize the effects of uncertainties associated with some of these values, comparative experiments are being made. In these experiments, tungsten and sulfur, in the mole ratio of 1:2 to correspond to tungsten disulfide, are burned under conditions which are, as nearly as practicable, the same as those which prevailed for the tungsten disulfide combustion. The conditions differed in oxygen pressure, sample support, and method of ignition. A pressure of 30 atmospheres of oxygen was used. The tungsten and sulfur were placed in separate quartz dishes and ignited by cotton threads attached to a platinum ignition wire. Three satisfactory runs have been completed and additional runs are in progress.

b. Trial Combustions of Uranium Nitrides in Oxygen
(E. Rudzitis)

Preliminary studies are being made of the combustions of uranium nitrides in oxygen preparatory to calorimetric determination of their heats of formation. Samples of about three grams of powdered uranium mononitride [actually $UN_{(1.0-1.1)}$] were ignited and were found to burn slowly in five atmospheres of oxygen. Combustion in oxygen at pressures higher than 10 atmospheres resulted in partial sublimation and fusion of the reaction product. At 30 atmospheres, the reaction proceeded violently with fusion, spattering, and partial sublimation of the reaction product. The same behavior was observed while burning uranium dinitride [actually $UN_{(1.8-1.9)}$]. The samples were ignited by an electrically heated spiral of six-mil platinum wire.

The extent of conversion to U_3O_8 was determined by the weight gain resulting from the combustion reaction and also by the weight change after subsequent ignition of the reaction product in air at 800 C. X-ray analysis also helped to identify the end products. When the nitride was placed in a mound in the supporting crucible in the bomb, the X-ray pattern of the central portion of the product showed oxygen deficiency. When the nitride was spread out in a thin layer on a platinum dish, combustion was shown to be complete.

The samples of the uranium nitrides used in this study were supplied by Stanford Research Institute.

c. Trial Combustions of Zirconium Dihydride in Oxygen
(E. Rudzitis)

Trial combustions of zirconium dihydride in oxygen were carried out preparatory to the calorimetric determination of the heat of formation. The samples were the same as those used in studies of the low-temperature thermodynamic properties by the Chemistry Division

One-gram samples of powdered zirconium hydride were ignited by an electrically heated platinum wire and burned in five atmospheres of oxygen. The heat generated in the combustion fused the reaction product. Dilution of the sample with zirconium dioxide resulted in a smooth reaction up to 30 atmospheres of oxygen pressure.

The reaction product was analyzed for unburned hydride by heating in vacuum to 800 C and measuring the amount of hydrogen liberated. The amount of metallic zirconium formed in the combustion was determined by dissolution of the product in 5 N hydrofluoric acid and measurement of the hydrogen liberated. Ignition of the combustion product in air at 900 C yielded a significant weight gain, indicating incompleteness of combustion, i.e., the formation of less than stoichiometric zirconium dioxide.

These preliminary experiments showed that the combustions were about 90 to 95 per cent complete. The incompleteness of the combustion was attributed largely to the formation of less than stoichiometric zirconium dioxide and, to a lesser extent, to the incompleteness of combustion of the zirconium hydride and the formation of metallic zirconium. Further studies are in progress.

d. Combustions of Zirconium in Fluorine
(E. Greenberg)

The value of $-\Delta E_c^0/M$, the energy change per gram of zirconium obtained by calorimetric combustions for the reaction

$$Zr\,(cryst) + 2F_2(g) \longrightarrow ZrF_4(cryst,\ beta) \quad ,$$

has been recalculated. The value previously reported (ANL-6183, page 79) was 4995.8 ± 1.0 cal/g. The value obtained by recalculation is 4995.65 cal/g with a standard deviation of 1.05 cal/g.

From the average value of $\Delta E_c^0/M$, the following thermal data at 25 C were derived: the energy change of the reaction or the energy of formation, $\Delta E_c^0 = \Delta E_f^0 = -455.71$ kcal/mole; the standard heat of formation, $\Delta H_f^0 = -456.89$ kcal/mole [previously reported as -454.5 ± 0.1 kcal/mole (ANL-6183, page 80)]; and the standard free energy of formation, $\Delta F_f^0 = -432.63$ kcal/mole. For calculating ΔF_f^0, the unpublished value of Westrum and Terwilliger, $S^0(298) = 25.03$, was used for the entropy of ZrF_4. The "uncertainty interval," which is equal to twice the overall standard deviation, was found to be 0.25 kcal/mole for the ΔH_f^0 and ΔF_f^0 values.

e. Combustion of Molybdenum in Fluorine
(J. Settle)

The difficulty which had been encountered earlier in this work, namely, the deposition of molybdenum compounds on the walls of the reaction vessel, was largely eliminated by increasing the initial fluorine pressure to 15 atmospheres. At this and higher (20 atm) pressures of fluorine, the molybdenum was nearly completely converted to the volatile molybdenum hexafluoride and, with one exception (Run 1B), no visible deposits were formed on the nickel surface of the bomb (see Table 11).

Table 11

RESULTS OF MOLYBDENUM CONBUSTIONS IN FLUORINE[a]

Combustion No.	Mass Mo Reacted m' (g)	$P^i(F_2)$ (atm)	$\alpha \times 10^4$ (sec^{-1})	$\Delta E_c^0/M$ (cal/g)
26	0.64294	14.0	0.3372	-3869.37
1A	0.51439	15.0	0.3476	-3870.72
2A	0.49686	15.0	0.3291	-3868.02
4A	0.52310	15.0	0.3396	-3870.29
5A	0.50640	15.0	0.3406	-3869.21
6A	0.52098	15.0	0.3334	-3866.43
1B	0.53889	20.0	0.3425	-3869.55
2B	0.53319	21.0	0.3335	-3871.27
			Average =	-3869.36

Standard deviation of the mean = 0.55, or 0.01_3%

[a] These results must be considered preliminary because the calculations have not been checked independently.

After each combustion, a small amount of elemental molybdenum remained. This lack of complete combustion is imposed largely by the method used for sample support and ignition (see Figure 18). The sheet molybdenum was suspended from a relatively massive nickel rod, which also served as the grounded electrode. The ignition wire was threaded through holes drilled in the bottom edge of the sample and attached to the electrodes. Molybdenum wire, 0.005 inch in diameter, was used for both the suspension and ignition wire. Molybdenum sheet, 0.005 inch thick, was used as the main sample. Combustion started at the bottom edge of the sample and proceeded upward, consuming nearly all of the sheet molybdenum as the flame front progressed. In a typical experiment, at an initial fluorine pressure of 15 atmospheres, less than 0.01 gram of unreacted molybdenum was recovered. This consisted of approximately

0.001 gram of wire gripped by the electrode and suspension rod nuts and a few small drops of molybdenum which had melted and dropped onto the cool nickel surface at the bottom of the bomb. These small drops of unburned molybdenum were invariably coated with a thin shell of a nonvolatile compound. This compound was soluble in water and changed from a yellow to a dark blue color on hydrolysis in air. These facts indicated that the molybdenum was in the +5 oxidation state and that the compound was probably molybdenum pentafluoride.

FIGURE 18
SAMPLE SUPPORT METHOD FOR MOLYBDENUM COMBUSTIONS IN FLUORINE

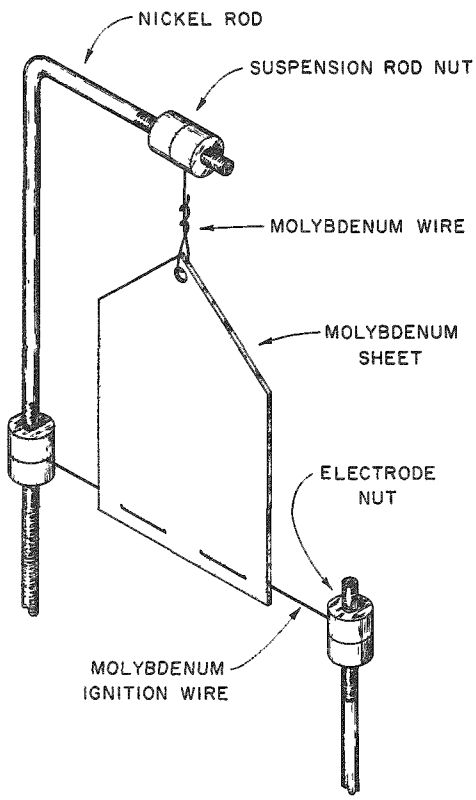

The amount of molybdenum in the deposited nonvolatile molybdenum compound and the amount of elemental molybdenum remaining after combustion was determined for 2 runs. In Run 1B, 1.3 mg of molybdenum compound (0.2 per cent of the amount of molybdenum originally placed in the bomb) and 20 mg of elemental molybdenum were found. In Run 2B, 0.6 mg of nonvolatile molybdenum compound (0.1 per cent of the original amount of molybdenum) and 6.7 mg of elemental molybdenum were found. A slight deposit of nonvolatile compound on the nickel surface immediately around the unburned molybdenum was observed in Run 1B and was attributed to the inordinately large amount of unburned molybdenum in this run.

The possibility of a pre-ignition reaction between molybdenum and fluorine at high pressures was investigated. A molybdenum sample identical to those used in the combustion experiments was placed in the combustion bomb and exposed to fluorine pressures of 15 and 20 atmospheres for periods of one to 16 hours. The weight of the molybdenum sample, determined before and after exposure to fluorine, indicated that no significant reaction occurred under the conditions of the experiment, in which moisture was eliminated by evacuation of the bomb.

Changes in the Ni-1 bomb made it necessary to redetermine the energy equivalent, E (calories), for the calorimetric system. The average value of 3575.06 cal/deg was obtained. The standard deviation of the mean was 0.33 cal/deg or 0.009 per cent.

The data for the molybdenum combustions are presented in Table 11. The mass of sample reacted, m', is the difference between the mass of molybdenum originally placed in the bomb and the mass of unreacted molybdenum recovered after the combustion. The initial fluorine pressure, in atmosphere, is denoted by $P^i(F_2)$, and the heat transfer coefficient by σ. The heat of combustion per gram of molybdenum, $\Delta E_c^0/M$, refers to the reaction

$$Mo(c) + 3F_2(g) \longrightarrow MoF_6(g) \quad ,$$

with reactants and product in their respective standard states. Using the average value of -3869.36 ± 0.55 cal/g for $\Delta E_c^0/M$, a value of -372.44 ± 0.05 kcal/mole is obtained for $\Delta H^0_{f298.15}$, the standard heat of formation of MoF_6(gas). The uncertainty listed is the standard deviation of the mean. An estimate of the overall uncertainty has not yet been made, but it is not expected to exceed the standard deviation of the mean (0.013 per cent) by more than an order of magnitude.

The heat of formation of MoF_6(gas) derived from this investigation is approximately 10 kcal/mole lower than the value of -382.0 kcal/mole appearing in the literature.[11] Because the value of Myers and Brady was obtained by indirect means, it is considered less reliable than the value derived from the direct measurement of the heat of combustion of molybdenum in fluorine.

f Combustions of Boron in Fluorine
(S. Wise)

The study of the combustion of boron in fluorine is being continued. Data obtained to date are presented in Table 12.

---

[11] Myers, O. E. and Brady, A. P., J. Phys. Chem., 64, 591 (1960).

Table 12

COMBUSTION OF BORON IN FLUORINE

Run No.	Weight Boron Burned (mg)	Weight Boron Unburned (mg)	$\Delta E_c^0/M$ (kcal/gm)
1[a]	209.55	1.32	24.790
2	229.92	8.21	25.260
3	206.61	17.08	24.984
4	209.73	2.39	24.847
5	265.31	8.01	25.137
6	252.31	6.45	24.960
7[b]	153.90	0.12	24.753
8	158.49	0.10	24.785
9	108.19	0.13	24.791
10	164.26	0.13	24.728
11	163.75	0.11	24.705
12	165.54	0.14	24.708
13	163.21	2.64	24.713
14[c]	161.76	7.72	24.686
18	165.59	5.90	24.788
19[d]	160.21	9.77	26.889
20	170.12	4.08	27.547
21[e]	170.30	0.11	24.820
22	172.05	0.25	24.846
23	163.35	0.13	24.847
24[f]	158.43	3.96	24.923
25	160.94	0.16	24.888
26	162.30	0.14	24.857
27	160.97	0.27	24.870

[a] In Runs No. 1 through 6, the boron sample was placed on an alumina plate.

[b] In Runs No. 7 through 13, a shell of calcium fluoride was placed between the boron sample and the alumina plate.

[c] In runs No. 14 and 18, the boron sample was placed on commercial calcium fluoride plates. Boron was resifted through a -325 mesh screen between Run 14 and Run 18.

[d] In Runs No. 19 and 20, the boron sample was placed on a calcium fluoride shell supported by a layer of calcium fluoride powder contained in a nickel dish.

[e] In Runs No. 21 through 23, the boron sample was placed on a calcium fluoride shell supported by a commercial calcium fluoride plate.

[f] In Runs No. 24 through 27, the boron sample was placed on a calcium fluoride shell held in a nickel dish.

The sample supports used in the first series of combustions (Nos. 1 through 6) and in the second series of combustions (Nos. 7 through 13) have been described previously (ANL-6183, page 81). The support for the boron in the first series of experiments was an alumina (Morganite) plate. In the second series, the support was modified by placing a shell of fused calcium fluoride between the boron and alumina plate. This modification led to a considerable improvement in the precision of the experiments.

In two runs (Nos. 14 and 18), the samples were supported on a commercial calcium fluoride plate having the same dimensions as the alumina plate used in earlier experiments. The calcium fluoride plate shattered in each run and some of the boron was scattered over the interior surfaces of the bomb.

In Runs 19 and 20, the boron was supported on a calcium fluoride shell which rested on a layer of calcium fluoride powder in a nickel dish. The high results that were obtained are attributed to a possible addition reaction between the calcium fluoride powder and boron trifluoride.

In Runs 21 through 23, the sample support consisted of a shell of calcium fluoride resting on a ceramic plate of calcium fluoride. The completeness of the combustion of boron in these runs was satisfactory. However, the calcium fluoride plates became slightly hygroscopic after exposure to fluorine-boron trifluoride mixtures, indicating that a reaction might have occurred. The fused shell of calcium fluoride remained unaffected. In Runs 24 through 27, the boron was again supported by a calcium fluoride fused shell, but the shell was placed directly on a massive nickel dish. The nickel dish showed a very small weight change (<0.2 mg), indicating little formation of nickel difluoride. The calcium fluoride shell cracked in Run 24 and some boron was scattered in the dish. In the three other runs of this group, the shell remained intact and the completeness of the combustion was satisfactory.

Two main factors must be considered in the evaluation of a given run. The first of these is the completeness of combustion; and the second is the extent of any secondary reactions which might have occurred. Consideration of the first of these factors is made necessary by the fact that, although a satisfactory analytical procedure is available for boron, it is difficult to recover the boron completely when amounts greater than about 0.3 mg remain unburned. When the amount of unburned material is less than 0.3 mg, all of the material is found in a small area on the calcium fluoride shell. When the amount of unburned boron is greater, the boron is found scattered over the surface of the bomb and fused into the supporting alumina or calcium fluoride plates making recovery difficult.

Judged on the basis of these two factors, the series of Runs 7 through 12 and the series of Runs 21 through 27 (with the exception of Run 24) were considered satisfactory.

The discrepancy of about 0.4 per cent between the two series may be due to differences in particle size of the boron samples. The boron sample was sifted through a -325 mesh screen before the first run was made. After Run 14, several spontaneous ignitions of the sample occurred. A resifting of the sample through a -325 mesh screen between Runs 14 and 18 revealed the presence of fine material. The presence of this material may be attributed to the attrition of the boron sample in handling during the time elapsed between Runs 1 and 14 or to incomplete sifting before Run 1. Combustion experiments are now in progress using the same conditions of the series of Runs 7 through 13 with the resifted boron to see whether the new experiments will produce the higher results found in the series of Runs 21 through 27.

g. Development of Combustion Techniques of Magnesium, Aluminum, Zinc, and Cadmium in Fluorine
(E. Rudzitis)

In the investigation of techniques for the combustion of magnesium, aluminum, zinc, and cadmium in fluorine, one of the problems that must be solved is the selection of material for the sample support. It is believed that the ideal support would be the (highest) fluoride of the metal to be burned. However, because of the possibility of decomposition or hydrolysis at elevated temperatures, fabrication of a suitable support of the appropriate metal fluoride presents difficulties. The conditions for sintering magnesium and cadmium fluorides are currently being investigated. Cold-pressing, which may eliminate the problems associated with hydrolysis and decomposition, is also being investigated. A die and punches have been designed to produce cylindrical compacts two inches in diameter, using pressures of approximately 50,000 psi Preliminary combustion experiments using the cold-pressed support plates indicate that the plates are resistant to thermal shock, whereas heat-treated (sintered and molten) support plates tend to crack during the combustion

It was previously found that aluminum and zinc did not burn satisfactorily in fluorine when the wire-to-foil-to-pin technique was used (ANL-6183, page 82). A recent attempt was made to overcome this difficulty by using powdered samples of zinc and aluminum with a "fuse" of magnesium ribbon. This technique yielded practically quantitative combustion at 250 psi fluorine pressure. In a subsequent experiment in which the powdered metal was replaced by 20 to 30 mesh granules, satisfactory combustion was also achieved. (Since the possibility of surface contamination is lessened by their use, granular samples are preferred to powdered samples.)

A successful attempt to reduce the initial fluorine pressure was made by replacing the magnesium "fuse" with a more easily ignitable molybdenum "fuse." Ignition and combustion of granular aluminum were achieved at 100 psi fluorine pressure. In another preliminary experiment, a sample of granular magnesium was successfully burned using a molybdenum "fuse" and 100 psi fluorine pressure. A fluorine pressure of 250 psi was needed in previous combustion of magnesium using the wire-to-foil-to-sample technique (ANL-6183, page 82).

From these preliminary results, it appears that a uniform method of ignition and combustion is possible for some of the metals. This method depends upon the use of an easily ignitable "fuse," such as molybdenum, to ignite a granular metal sample resting on a support of its fluoride. Besides having the obvious advantage of establishing a uniform technique and geometry for a group of metals, this method makes possible the reduction of the ignition fluorine pressure and thereby decreases the possibility of side reactions occurring with surrounding materials.

II. FUEL CYCLE APPLICATIONS OF VOLATILITY AND FLUIDIZATION TECHNIQUES

Several processes, in which advantage is taken of the volatilities of uranium and plutonium hexafluoride and in which fluidization techniques are used, have been proposed for the recovery of uranium and plutonium from irradiated reactor fuels. These include a Direct Fluorination Process and the Fused Fluoride Volatility Process.

The Direct Fluorination Volatility Process is being developed to recover uranium and plutonium from spent uranium oxide, Zircaloy-clad, fuel elements. A proposed processing procedure utilizes the reaction of zirconium with a mixture of hydrogen fluoride and hydrogen chloride for decladding. Plutonium and uranium hexafluorides, which result from the reaction of the oxide fuel with fluorine, may be separated using a combination of the variability of the rates of fluorination of the plutonium and uranium compounds and chemical reactivities of the hexafluorides. Equipment has been constructed and is in operation to study the process steps with multigram amounts (10 to 100 grams) of plutonium.

An investigation of the kinetics and mechanism of the decomposition of plutonium hexafluoride vapor suggests that the reaction is heterogeneous at 161 C.

Investigation of the stoichiometry of the reaction of plutonium hexafluoride with sulfur tetrafluoride has been completed. The resultant products are sulfur hexafluoride and plutonium tetrafluoride. The reaction of sulfur tetrafluoride with plutonium dioxide at 600 C to produce plutonium tetrafluoride was found to be slow. The investigation of the stoichiometry of the reactions of sulfur tetrafluoride with uranium trioxide, uranium dioxide, uranyl fluoride, and U_3O_8 has been completed. Uranium hexafluoride is produced equivalent in amount to uranium in the plus six valence state in these compounds.

Radiation decomposition of plutonium hexafluoride in the presence of uranium hexafluoride, 2.6 per cent per day, was found to be very similar to the value obtained for plutonium hexafluoride alone. Uranium hexafluoride decomposed to the extent of 0.3 per cent per day in the gas mixture.

The solubility of hydrogen chloride in liquid hydrogen fluoride at condenser temperatures would be an important process variable in the decladding step of the Direct Fluorination Volatility process. In terms of weight per cent hydrogen chloride, the solubility of hydrogen chloride in liquid hydrogen fluoride is 0.7 at -38 C and 2.4 at -78 C.

An investigation of the corrosive effect of hydrogen fluoride-hydrogen chloride gas mixtures on A-nickel has been initiated. At 500 C, with a 90 volume per cent hydrogen chloride mixture, after six days, intergranular attack

of 0.4 to 1.0 mil was noted. Under these same conditions the penetration rate was 0.023 mil per day as calculated from the weight change of the test coupons. Due to the short durations of these experiments, the values should be considered preliminary in nature.

Additional studies of metal fluorinations have been concerned with the mechanisms of the nickel-fluorine and nickel-oxygen reactions. The fluorine reaction appears to occur at the nickel fluoride-nickel interface. In the nickel-oxygen reaction, nickel ions migrate through the nickel oxide and the reaction with oxygen occurs at the nickel oxide-nickel interface.

Work has continued on engineering-scale studies of the Direct Fluorination Process applied to dense uranium dioxide pellet fuel. Two decladding runs were made to investigate the effect of close packing of fuel elements on operation of the fluid-bed reactor. One half-inch diameter Zircaloy-2 tubing elements containing uranium dioxide pellets were reacted at 500 C with 10 mole per cent hydrogen chloride-90 mole per cent hydrogen fluoride gas. Fourteen-inch lengths of these 30-mil wall tubing elements were submerged vertically in a calcium fluoride fluidized bed. Decladding was successful in both runs. For a near-maximum packing in which the cross-sectional area of the tubes was 55 per cent of the reactor area, formation of a firm cake raised the pressure differential across the bed and prevented free flowing of the bed at the end of the run. When the number of tubes was reduced to half that used in the above run, essentially no caking or pressure increase was found, and the bed was free flowing. No significant pellet degradation or fines production was observed in these runs.

In a shakedown run in the new forced-air-cooled reactor, pellets were fluorinated at substantially higher rates than previously reported (ANL-6183, page 98). It was found that heat transfer was limited by large temperature differentials from the wall to the bed rather than by the external heat transfer surfaces. Fluorination studies are in progress.

Mockup tests of heat transfer from the surface of fixed packing submerged in a fluid bed were made to determine the effects of bed height and gas velocity. The bed of $\frac{1}{4}$-inch nickel balls and 140 to 200 mesh copper shot gave heat transfer coefficients in the range from 81 to 125 Btu/(hr)(sq ft)(F) for gas rates sufficient to fluidize the finer material. These heat transfer coefficients were five to eight times higher than with the non-fluidized packing alone and 0.6 to 0.9 of those obtained for fluidized material without packing.

Direct Fluorination Processes are also being studied as a means of recovering uranium from highly enriched uranium-zirconium alloy fuels. In general, the processes involve conversion of the element to fluoride salts by means of hydrogen chloride and hydrogen fluoride. In this step

the elements are submerged in a fluidized bed of inert material which serves as the heat transfer medium. The next step, fluorination with elemental fluorine, is expected to volatilize the uranium as the hexafluoride and permit separation. Emphasis during this quarter was shifted from reactions of the metallic fuel with dilute mixtures of hydrogen chloride in hydrogen fluoride to separate reactions with these gases in a two-zone, fluid-bed reactor. The initial reaction is hydrochlorination, forming the volatile zirconium tetrachloride. The volatile material is converted to the solid tetrafluoride by anhydrous hydrogen fluoride which is admitted in the upper section of the reactor. Baffling between the two reaction zones has been found to reduce gas back-mixing considerably (a factor of ten) which resulted in gas mixtures of low reactivity. Eighty five to 94 per cent of a multiplate assembly (1.5 weight per cent uranium-zirconium alloy) was converted to fluorides in about 12 hours by means of this procedure at a temperature of 400 C.

Initial fluorination studies on these reaction products achieved about 85 to 90 per cent removal in two hours at 600 C, in four hours at 550 C, and in eight hours at 500 C. Additional exposure of the fluorinated residues to fluorine at 500 C resulted in increased removal to 96 per cent.

In the Fused Salt Volatility Process for recovery of uranium from zirconium matrix fuels, the alloy fuel elements are dissolved in a molten sodium fluoride-zirconium fluoride mixture at 600 to 700 C with a hydrogen fluoride sparge. A final dissolution was performed in a series of dissolutions of synthetic fuel assemblies to demonstrate operation of the graphite pilot-plant dissolver. A 10-plate Zircaloy-2 fuel element was 90 per cent dissolved in 10 7 hours and 99 per cent dissolved in 13.4 hours. This dissolution rate was slower than previously obtained for pure zirconium and salt without alloy constituents Nickel fluoride, which had been added to the molten salt, was substantially removed from the salt, probably by reduction on the Zircaloy

Examination of the walls of the graphite dissolver showed the expected presence of fused salt in the middle of the lampblack insulating zone. No salt had contacted the outer metal shell About 30 lb of salt were so deposited in the walls

A fused salt charge was allowed to freeze in the dissolver to determine the effect that this would have on dissolver components. This charge was then remelted in the dissolver. Extensive damage to internal graphite downlines and heaters was found. The fuel element support plate (graphite) was eroded. There was no evidence of mechanical damage to the graphite crucible or chemical attack of any graphite components.

In all of the dissolver runs, entrained solids were removed from the dissolver off-gas by a bed packed with $\frac{3}{16}$-inch sodium fluoride pellets followed by grade 60 porous carbon filters. The carbon filters were successful in removing all fines that passed the absorber bed.

The reaction of stainless steel with various gases is being investigated as an initial step in the processing of stainless steel-clad or matrix fuels. Studies carried out in a one-inch horizontal tube furnace showed the initial reaction rates of chlorine and stainless steel, determined by weight loss of the test specimen, were 5.0 mils/hr at 570 C and 9.7 mils/hr at 600 C. The effect of nitrogen dilution was found to be negligible at chlorine concentrations above 50 per cent. A mixture of chlorine and hydrogen fluoride showed a much lower penetration rate than did the chlorine alone. Monel equipment was found to be severely corroded by chlorine. This was caused by leaching of the copper component as cuprous chloride. A single experiment on the reaction of fluorine gas with a 304 stainless steel specimen at 550 C in a fluid-bed reactor gave a low penetration rate, 0.7 mil/hr.

The conversion of uranium hexafluoride to uranium dioxide by reaction with steam and hydrogen in a fluid bed is being studied. A short run at a high temperature (650 C) and high hexafluoride rate, 217 lb/(hr) (sq ft reactor cross section), confirmed that essentially complete conversion (99.99 per cent) to solids is readily achieved, but a second step is required to produce specification-grade (low fluoride) powder by further reaction of the solid with steam and hydrogen. Installation of a three-inch diameter column which will be used for additional studies of the second step is almost complete. Pellet fabrication tests performed by the ANL Ceramics Group achieved about 94.5 to 97 per cent theoretical density for dioxide prepared by this process. One kilogram samples of dioxide powder prepared from uranium hexafluoride by the direct conversion process have been furnished to seven industrial concerns that wish to evaluate the material.

A mass transfer study of the adsorption of water vapor by silica gel is being made to evaluate the characteristics of the new multistage fluidized-bed reactor, as the second phase of a doctoral thesis research problem.

A. Laboratory Investigations of Fluoride Volatility Processes (J. Fischer)

The Direct Fluorination Volatility Process is under development to recover fissionable material from uranium dioxide fuels. Emphasis has been placed on development of the process for a typical Zircaloy-clad oxide fuel. The cladding is removed from the fuel as zirconium tetrafluoride, resulting from the reaction of zirconium with hydrogen fluoride containing 17 weight per cent hydrogen chloride. During the reaction calcium fluoride is used in a fluid-bed reactor to transport heat from the reaction surface of the Zircaloy, maintaining a temperature between 400 and 500 C in the bed.

In the same nickel vessel used for the decladding, uranium and plutonium oxides are then converted to their respective volatile hexafluorides by reaction with fluorine at 500 C in the fluid bed resulting from the decladding operation. Differences in the reactivities of the uranium and plutonium compounds result in an initial fluorination of the uranium and separation of the uranium as the hexafluoride. A plutonium-rich fraction, remaining in the reactor toward the completion of the fluorination step, is then further reacted with fluorine to produce a mixture of uranium hexafluoride and plutonium hexafluoride.

Separation of uranium and plutonium hexafluorides can be achieved by utilizing the reactions of plutonium hexafluoride with such reducing agents as sulfur tetrafluoride or bromine to produce nonvolatile plutonium tetrafluoride. Uranium hexafluoride is not affected by these reagents and may be separated from the plutonium by distillation. A large per cent of the fission products remain, and can be disposed of, in the solid bed of calcium and zirconium fluoride. Development of the process steps is in progress in the laboratory along with pertinent research involving the chemistry of plutonium, uranium, and fluorine compounds.

Work is continuing on metal fluorinations. Further work on the mechanisms of the nickel-fluorine and nickel-oxygen reactions has been completed. In the nickel-fluorine reaction evidence indicates that the reaction occurs at the nickel fluoride-nickel interface. In the nickel-oxygen reaction, nickel ions migrate through the nickel oxide and the reaction with oxygen occurs at the nickel oxide-nickel interface.

1. Fluorine Chemistry and Fluoride Separation Studies
(J. Fischer)

a. Process Development: Plutonium Fluorination and Transport Studies
(L. Trevorrow, G. J. Vogel, L. Anastasia, H. Griffin, J. Riha, G. Redding, T. Gerding and T. D. Baker)

The primary aim of the current program is to demonstrate the steps involving fluorination and transport of plutonium with relatively large quantities (10 to 100 g) of plutonium. A second aim of the program is investigation of the kinetics of fluorination of mixtures of plutonium and uranium oxides, with special attention to the comparison of the rates of fluorination of plutonium and uranium. The possibility that thermal decomposition of plutonium hexafluoride might occur in the outlet lines of the fluorination reactor will be the subject of initial work with large quantities of plutonium hexafluoride. The apparatus for this work has been described in ANL-6145, page 100.

Experimental work in which the behavior of plutonium hexafluoride vapor will be observed under conditions similar to those existing at the outlet of a fluorination reactor has been planned. The temperature in and at the outlet of the fluorination reactor is expected to be about 500 C. The total outlet gas pressure may be tentatively assumed to be 760 mm. Steindler[12] has shown that the reaction of plutonium oxide with fluorine proceeds with an initial rapid fluorination to plutonium tetrafluoride. Therefore, the maximum partial pressure of plutonium hexafluoride in the outlet gas stream can be estimated from the equilibrium constant for the reaction

$$PuF_4(s) + F_2(g) \rightleftharpoons PuF_6(g) \quad .$$

Equilibrium constants for this reaction were discussed in ANL-6101, page 80. At a fluorine pressure of 760 mm, the equilibrium pressure of plutonium hexafluoride at 500 C is about 8 mm. Since equilibrium conditions will not be reached in the fluorination reactor, the partial pressure of plutonium hexafluoride can be assumed to be less than 8 mm in the outlet gas stream. If the ratio of plutonium hexafluoride pressure to fluorine pressure is less than the equilibrium value, there will be no net decomposition of plutonium hexafluoride by the reaction

$$PuF_6(g) \rightleftharpoons PuF_4(s) + F_2(g) \quad .$$

However, the equilibrium constant, $(PuF_6)/(F_2)$, decreases with temperature. Therefore, in traversing the thermal gradient to a condenser, the exit gas will pass through temperature zones where the ratio 8 mm PuF_6/760 mm F_2 will be in excess of the equilibrium ratio. Consequently, a driving force for decomposition will be present. The rate of approach to equilibrium (rate of decomposition) decreases with temperature, and the amount of decomposition is not expected to be significant in the short time required to traverse the thermal gradient.

In the initial large-scale plutonium experiments, a gaseous mixture of plutonium hexafluoride and fluorine was passed through a two-inch diameter pipe to heat the gas to 500 C. The gas mixture exited from the pipe through a length of three-eights-inch diameter tubing to a cold trap. The purpose of the experiments was to determine the extent of recovery of plutonium hexafluoride from the hot zone. The preparation of large quantities of plutonium hexafluoride and experiments testing the transport of plutonium hexafluoride vapor are both currently under way. Data from the early experiments are being analyzed and will be presented in the next quarterly report.

---

[12] Steindler, M. J., Steidl, D. V., and Steunenberg, R. K., Nuclear Science and Engineering, 6, 333 (1959).

The initial separation of uranium from plutonium in the fluoride separations process is to be accomplished by taking advantage of the higher rate of fluorination of uranium oxide. After this initial step, the concentration of plutonium oxide in the uranium oxide matrix is expected to increase to about 4 per cent from a value of 0.4 per cent. The fluorination of this mixture and the recovery of the resulting plutonium hexafluoride is to be studied using at least ten grams of mixed oxides. The equipment to be used in this work has been described in ANL-6145, page 102. This equipment has been tested in preliminary experiments with uranium compounds, and has been shown to be satisfactory for use with plutonium. The preparation of uranium-plutonium mixed oxides for use in this work is currently in progress.

b. Rate of Decomposition of Plutonium Hexafluoride
(L. Trevorrow, W. Shinn)

In the fluoride separations process, plutonium is to be transported as plutonium hexafluoride vapor. Plutonium hexafluoride vapor undergoes thermal decomposition via the reaction

$$PuF_6(g) = PuF_4(s) + F_2(g) \quad .$$

During transport of plutonium hexafluoride, the rate of thermal decomposition should be minimized. The thermal decomposition of plutonium hexafluoride has also been suggested as a means of separating plutonium hexafluoride from uranium hexafluoride. For the separation of plutonium, the rate of thermal decomposition should be maximized. Because of its relation to the fluoride separations process, the rate of thermal decomposition of plutonium hexafluoride has been the subject of laboratory investigation. Experiments are now being performed to determine the effect of pressure on the rate of the decomposition of plutonium hexafluoride. Initial pressures approximately ten times those previously used will be employed in these experiments. It is felt that some of the experiments reported previously were done over too short a reaction time and at pressures which were too low. The results of previous work on the subject were reported in ANL-6183, page 89.

c. Reaction of Plutonium Hexafluoride with Sulfur Tetrafluoride
(M. J. Steindler, D. Steidl)

The investigation of the stoichiometry of the reaction of plutonium hexafluoride with sulfur tetrafluoride, described in ANL-6183, page 94, has been completed. The products of the reaction have been identified and the reaction proceeds as written in the following equation:

$$PuF_6(g) + SF_4(g) \longrightarrow SF_6(g) + PuF_4(s) \quad . \qquad (1)$$

The details of the experiments have been presented in ANL-6183, page 94. A quantity of purified plutonium hexafluoride was condensed at -80 C into a nickel reaction vessel attached to a manifold. The quantity of plutonium hexafluoride transferred to the reaction vessel was determined by weight difference of the supply vessel. An excess of sulfur tetrafluoride, determined by PVT measurements, was then condensed onto the plutonium hexafluoride at -196 C. The vessel was heated to the reaction temperatures shown in Table 13, and after the reaction was complete the gaseous products were distilled off. The amount of plutonium tetrafluoride remaining indicated the completeness of the reaction, as is shown in Table 13.

Table 13

REACTION OF PLUTONIUM HEXAFLUORIDE AND SULFUR TETRAFLUORIDE

(Details of experimental procedure are given in ANL-6183, page 94)

PuF_6 (millimoles)	SF_4 (millimoles)	Temp (C)	Time (hr)	% Reacted: Pressure Measurement	% Reacted: Residue
0.213	0.778	30	1	70	83[a]
0.334	1.207	30	17	102	98[b]
0.327	1.265	70	1.5	-	99[b]
0.330	1.178	70	0.2	100	-
0.477	1.980	30	17	-	83[c]
1.170	3.300	30	17	-[d,e]	-[f]

[a]Based on plutonium analysis of residue in reaction vessel.

[b]Weight of residue in reaction vessel.

[c]Reaction took place partially outside of reaction vessel, in manifold lines.

[d]1.14 millimoles sulfur hexafluoride isolated compared to 1.17 millimoles plutonium hexafluoride used. Sulfur hexafluoride observed molecular weight (vapor density method): 143.4; calc: 146.

[e]Ratio of final pressure to initial sulfur tetrafluoride pressure = 1.0.

[f]F/Pu ratio of solid product by chemical analysis = 4.13.

X-ray diffraction analysis of the solid product (plutonium tetrafluoride) was unsuccessful since the solid was reported to be amorphous or of very small crystallite size. Chemical analysis for fluorine and plutonium was used to obtain a fluorine to plutonium ratio. The value obtained for this ratio was 4.13.

In order to add to the validity of the reaction as shown in Equation 1, it was necessary to identify the gaseous product of the reaction. From the equation of the proposed reaction it can be seen that the total pressure of the sulfur fluoride gases should remain constant. The pressure of the gaseous products of an experiment was measured by means of the Booth-Cromer pressure transmitter and found to be the same as the original pressure of sulfur tetrafluoride. In the same experiment, the sulfur fluoride gases were separated from one another by hydrolyzing the sulfur tetrafluoride in water. This was done by condensing the gases onto ice at -196 C in a nickel test tube and allowing the mixture to warm to 30 C. Sulfur tetrafluoride hydrolyzes while the relatively inert sulfur hexafluoride does not. The hydrolysis reaction, whose rate was followed by pressure drop, appeared to be slow, requiring 24 hours to go to completion. The quantity of sulfur hexafluoride remaining after hydrolysis of the sulfur tetrafluoride was determined. PVT calculations indicated 1.14 millimoles of sulfur hexafluoride present, compared to 1.17 millimoles of plutonium hexafluoride initially used.

A vapor density determination was made on the gaseous residue of the hydrolysis to assure that it was indeed sulfur hexafluoride. This was done by weighing the vessel containing the gas at a known pressure and then weighing the same vessel empty. Results indicated a molecular weight of 143.4, which compares favorably with the calculated molecular weight of 146.0 for sulfur hexafluoride.

It is believed that the reaction as proposed is sufficiently well established by the preceding data, and no further work is planned on this reaction.

d. Reaction of Plutonium Dioxide and Sulfur Tetrafluoride
(M. J. Steindler, D. Steidl)

The reaction between sulfur tetrafluoride and plutonium dioxide was briefly studied. Samples of plutonium dioxide were heated in a stream of gaseous sulfur tetrafluoride and the solid reaction products examined. The results are shown in Table 14.

The conversion of plutonium dioxide to the tetrafluoride is slow, even at 600 C. These data confirm results obtained with uranium compounds which show that sulfur tetrafluoride, although a good fluorinating agent, does not react as an oxidizing agent. Therefore, no plutonium is lost by volatilization as the hexafluoride.

Table 14

REACTION OF SULFUR TETRAFLUORIDE AND PLUTONIUM DIOXIDE

Sulfur tetrafluoride flow rate: 100 ml/min

Time of reaction: 1 hour

PuO_2 (g)	Temp (C)	Weight Change (g)	% Conversion[b]	
			Weight Basis	X-ray
0.6519	375	-0.0096[a]	-	0
0.8076	500	+0.0167	12.7	~15[c]
0.6916	500	+0.0171	15.2	-
0.7992	600	+0.0520	40.1	~35-45[c]

[a]Reaction boat damaged, weight change questionable.

[b]Based on conversion of PuO_2 to PuF_4.

[c]Estimated by comparison with standard samples composed of known mixtures of PuF_4 and PuO_2.

e. Radiation Decomposition of Plutonium Hexafluoride in Mixtures with Uranium Hexafluoride
(M. J. Steindler, D. Steidl)

Plutonium hexafluoride stored in the solid phase decomposes owing to the energy dissipated by alpha decay. The decomposition rate is about two per cent per day in pure plutonium hexafluoride. A 2-gram mixture of 15 weight per cent plutonium hexafluoride in uranium hexafluoride was allowed to stand at 30 C for 19 days. The average decomposition rate of plutonium hexafluoride was determined by analysis of the volatile phase. The rate of plutonium hexafluoride decomposition was 2.6 per cent per day, a value not significantly different from that observed on pure plutonium hexafluoride (unpublished results). The rate observed for uranium hexafluoride was 0.3 per cent per day.

f. Reaction of Sulfur Tetrafluoride with Uranium Oxides
(C. Johnson, J. Stockbar, T. Gerding)

The reaction of sulfur tetrafluoride with uranium trioxide, forming volatile uranium hexafluoride, has been suggested as a basis for a possible fuel recovery process (ANL-6145, page 93). The investigation

of the stoichiometry of this reaction and also reactions of sulfur tetrafluoride with uranyl fluoride, uranium dioxide, and U_3O_8 has been completed and is summarized below.

The apparatus used for this work was as follows: A 1.236-liter nickel vessel heated by a resistance-wound furnace was connected to a service manifold equipped with a supply of sulfur tetrafluoride, a source of vacuum, a thermocouple gage, and a cold trap. Also connected to the manifold were a Booth-Cromer pressure transmitter and an infrared cell. Packless (Hoke 413) diaphragm valves were used throughout the system. The entire manifold was heated to facilitate the movement of uranium hexafluoride in the system. The reaction vessel was equipped with a Teflon-gasketed, flared entry port for the insertion of solids. A calibrated thermocouple positioned in a thermocouple well in the vessel was used for measuring temperatures. The infrared cell was fabricated from nickel and fitted with silver chloride windows. The volume of the system was calibrated to allow quantitative measurements of the gases.

A typical stoichiometry experiment was carried out as follows: The equipment was first evacuated to a pressure of one micron or less. The closed reaction vessel was removed from the manifold and placed in a dry box where a weighed quantity of the solid reactant was added. After replacing the vessel on the manifold and evacuating to a pressure of one micron or less, a measured quantity of sulfur tetrafluoride was added. The vessel was closed and brought to temperature. At the end of the reaction period a sample of gas was taken for infrared analysis. The remainder of the gaseous products were condensed, weighed, and hydrolyzed for chemical analysis. In order to remove any unreacted uranium compound an excess of fluorine was introduced into the heated vessel. The uranium hexafluoride produced was trapped at -80 C, hydrolyzed, and analyzed. Before the vessel could be used for another experiment, it had to be flushed a few times with sulfur tetrafluoride to remove fluorine that had been adsorbed on the interior of the vessel. Heating and evacuation were insufficient to remove adsorbed fluorine. Chemical reaction with sulfur tetrafluoride to form sulfur hexafluoride appeared to insure complete removal of the fluorine.

The stoichiometry of the reaction of sulfur tetrafluoride with uranium trioxide, uranium dioxide, U_3O_8, and uranyl fluoride is given in Equations (1) to (4):

$$UO_3 + 3\ SF_4 \xrightarrow{300\ C} UF_6 + 3\ SOF_2 \qquad (1)$$

$$UO_2 + 2\ SF_4 \xrightarrow{500} UF_4 + 2\ SOF_2 \qquad (2)$$

$$U_3O_8 + 8\ SF_4 \xrightarrow{400} 2\ UF_6 + UF_4 + 8\ SOF_2 \qquad (3)$$

$$UO_2F_2 + 2\ SF_4 \xrightarrow{300} UF_6 + 2\ SOF_2 \quad . \qquad (4)$$

In all cases the only sulfur product found was thionyl fluoride. Examination of the uranium trioxide after momentary contact with sulfur tetrafluoride has definitely established that anhydrous uranyl fluoride is an intermediate in the reaction.

Under experimental conditions of large excesses of sulfur tetrafluoride and temperatures up to 600 C, no reaction occurred between uranium tetrafluoride and sulfur tetrafluoride. Sulfur tetrafluoride is not capable of reacting as an oxidizing agent in these systems.

g. Reaction of Hydrogen Fluoride-Hydrogen Chloride Gas Mixtures with Uranium Dioxide
(C. Johnson and J. Stockbar)

Recent laboratory work has demonstrated the feasibility of using a 90 per cent hydrogen fluoride-10 per cent hydrogen chloride gas mixture as an effective decladding agent for either Zircaloy or zirconium-clad fuel elements. This has also been demonstrated in engineering-scale runs (see page 29). Reported here are experiments on the reaction of this gas mixture with uranium dioxide, both in powder and pellet form.

This experimental work was undertaken primarily to determine the extent of the reaction under the specified conditions. The extent of reaction can be accommodated in the overall process, as both uranium dioxide and uranium tetrafluoride can be fluorinated in the Direct Fluorination Process.

Results, as shown in Table 15, indicate that complete conversion of uranium dioxide to the tetrafluoride was achieved only for uranium dioxide prepared by hydrogen reduction of uranyl nitrate at 900 C. Under the experimental conditions used, uranium dioxide pellets obtained from Manufacturer No. 2 did not react with the 90 per cent hydrogen fluoride-10 per cent hydrogen chloride gas mixture. The uranium dioxide pellets obtained from Manufacturer No. 1 appeared to undergo thermal damage, facilitating further disintegration when the hydrogen fluoride-hydrogen chloride gas mixture was allowed to pass over the pellet. Chemical analysis of the Manufacturer No. 1 pellets indicated 8.5 per cent conversion to the tetrafluoride. The reaction of the gas mixture with arc-fused uranium dioxide powder yielded a 3 per cent conversion to the tetrafluoride.

The densities of No. 2 and No. 1 pellets were determined, giving the following results: No. 2, 11.02 g/cc; No. 1, 10.35 g/cc. The literature value for the crystal density of $UO_{2.00}$ is given as 10.97 g/cc.[13]

---

[13] Katz, J. J. and Rabinowitch, E., The Chemistry of Uranium, National Nuclear Energy Series VIII-S, McGraw-Hill Book Co., New York (1950), p. 261.

Apparently the only difference between the pellets is their densities, although there may be a significant difference in their method of preparation. It can be concluded from these results that the rate of reaction of uranium dioxide with this gas mixture is strongly dependent upon the physical properties of the compound. This problem needs to be investigated with the fuel actually being considered for processing before a sound conclusion can be drawn.

Table 15

REACTION OF 90 PER CENT HYDROGEN FLUORIDE-10 PER CENT HYDROGEN CHLORIDE GAS MIXTURES WITH URANIUM DIOXIDE

Time for Reaction: 1 hr

Reaction Temperature: 400 C

Material	Sample Weight (g) Initial	Sample Weight (g) Final	Remarks
UO_2 Powder	11.0469	12.8142	99.7% conversion to UF_4 indicated by change in weight.
Manufacturer No. 1 Pellet	19.1281	19.1475	Sample completely disintegrated. Chemical analysis gave 2.55% fluorine.
Manufacturer No. 1 Pellet	18.0353	18.0087	Sample completely disintegrated. Analysis gave 2.0% fluorine.
Manufacturer No. 1 Pellet	21.4053	Lost	HCl gas only; sample disintegrated.
Manufacturer No. 1 Pellet	18.7701	17.8174	Helium only, no HF or HCl. Pellet retained shape; some dusting; appeared porous.
Manufacturer No. 2 Pellet	16.3940	16.4043	Apparently no reaction occurred.
Manufacturer No. 3 Arc-fused Powder	23.1748	Lost	Volume of solid increased. Chemical analyses gave 7.6% fluorine.

h. Solubility of Hydrogen Chloride Gas in Liquid Hydrogen Fluoride
(R. L. Jarry, G. Tennenhouse)

The solubility of hydrogen chloride gas in liquid hydrogen fluoride at condenser temperatures would be an important process variable in a hydrogen fluoride recovery step for a reaction system using mixtures of hydrogen fluoride and hydrogen chloride. A potential application would be the decladding of Zircaloy-clad fuel elements by the use of mixtures of hydrogen fluoride and hydrogen chloride (see ANL-6183, page 106).

The experimental apparatus for this investigation was a simple one. It consisted of a set of three 100-ml polyethylene tubes arranged for series flow. The connections between tubes were made with polyethylene tubing using quick-disconnect fittings. The first tube contained fluorolube oil and was used as a bubbler to estimate flow. The second tube, containing the liquid hydrogen fluoride through which the hydrogen chloride was bubbled, was immersed in a constant-temperature bath. The third tube was placed in a water-ice bath to trap any hydrogen fluoride swept through the solubility section. The system was vented to the atmosphere.

The apparatus was first dried by passing nitrogen through the system while gently heating the tubes and connecting lines. The solubility tube was then placed in a constant-temperature bath, and about 30 ml of hydrogen fluoride were condensed in the tube. Hydrogen chloride was then bubbled through the liquid hydrogen fluoride for about 30 minutes. To approach equilibrium from the hydrogen chloride-rich side, excess hydrogen chloride was condensed by lowering the temperature to -174 C. The temperature was then raised to -78 C and hydrogen chloride bubbled through the solution for one hour. At the end of the equilibrium period the dip-tube was raised above the solution and nitrogen was passed through the tube for a few minutes to sweep out hydrogen chloride in the vapor phase. At this point the solubility tube was opened and filled with ice cooled to -78 C. The tube and contents were then allowed to warm to room temperature. The solution was made up to a standard volume, and a total acid titration and Mohr chloride determination were made.

The results obtained are listed below. The value given for -78 C is the average of five determinations, two of which were from the excess hydrogen chloride side. The value at -38 C is the average of two determinations. The deviations listed are the average deviations.

SOLUBILITY OF HYDROGEN CHLORIDE
IN LIQUID HYDROGEN FLUORIDE

Temp (C)	w/o HCl
-38	0.66 ± 0.11
-78	2.34 ± 0.50

These experiments show that if a hydrogen fluoride recovery condenser were to be operated in this temperature range, then approximately 90 per cent of the 17 weight per cent hydrogen chloride in the gas mixture would pass through the condenser.

2. Metal Fluorination Studies
(J. Fischer)

Fundamental studies on metal fluorinations yield information which is useful to the Direct Fluorination Volatility Process. The reactions of fluorine and hydrogen fluoride-hydrogen chloride mixtures with nickel, zirconium, and uranium have been reported (see ANL-6145, page 110; ANL-6183, page 106), and work continues on the study of these reactions.

a. Nickel-Fluorine Reaction
(R. L. Jarry, W. H. Gunther)

In previous reports (ANL-6101, page 89; ANL-6145, page 110) evidence was presented regarding the mechanism of the nickel-fluorine reaction. This evidence indicates that the reaction occurs at the nickel fluoride-metal interface by migration of fluorine through the growing nickel fluoride scale. There is undoubtedly an interchange of fluorine and fluoride positions with a resultant migration of fluorine through the film via crystal defects or vacancies. This conclusion was obtained from both radioactive tracer experiments and a wedge experiment involving impinging fluoride surfaces.

The mechanism of the nickel-fluorine reaction differs from that of the nickel-oxygen reaction. It has been reported[14] for the oxidation reaction that the reaction proceeds at the nickel oxide-oxygen interface. Nickel ions migrate through the nickel oxide with a net movement of nickel to the nickel oxide-oxygen interface, where reaction with the oxygen occurs. Additional confidence in the tracer method for investigating the reaction mechanisms of nickel-gas reactions can be obtained when different results are achieved for the nickel-fluorine and the nickel-oxygen reactions.

It is necessary, in order to use the nickel-oxygen reaction as a check for the radioactive tracer experiments, to predict the ultimate location of the activity in the nickel oxide scale. This was provided by the work of Bardeen and associates.[15] They calculated the expected distribution according to the Wagner theory for a radioactive metal tracer and experimentally confirmed their calculations for the copper-oxygen system. The activity was distributed in the oxide scale, with the concentration diminishing with distance in the scale from the oxide-oxygen interface.*

---

[14] Gulbransen, E. A. and Andrews, K. F., J. Electrochem. Soc., 104, 451 (1957).

[15] Bardeen, J., Brattain, W. H., and Shockley, W., J. Chem. Phys. 14, 714 (1946).

*The expected position of the radioactivity as stated in a previous report, ANL-6101, page 89, for the metal migration case was in error. The position of the activity would be as predicted by Bardeen and coworkers and not at the oxide-metal interface.

This concentration gradient would be quite different from the single position (no gradient) which the activity assumed in the nickel-fluorine system. In the nickel-fluorine system the activity was in the outermost layer of the nickel fluoride scale at the nickel fluoride-fluorine interface.

The nickel oxidations were carried out in the same type of apparatus used for the nickel-fluorine experiments. Nickel-63 was used as the tracer and a one-micron layer of the metal was plated on the nickel specimens. Experiments were run for 40 to 80 hours at temperatures of 950 to 1060 C at an oxygen pressure of one atmosphere. The oxidized coupons were mounted in Bakelite, sectioned, and autoradiographed. For these experiments Autoradiographic Film AR-10 was used. This film has a 10-micron gelatin overlay on the 5-micron emulsion. The additional support furnished by the gelatin layer facilitated removal of the developed emulsion from the specimen.

Examination of the autoradiographs showed a distribution of activity extending 50 to 75 per cent of the distance into the oxide scale as measured from the oxide-oxygen interface. Such an autoradiograph, for a 1.5×10^6-Å thick oxide scale formed at 1060 C, is shown in Figure 19. The line located by the arrow marks the oxide-oxygen interface, and also indicates, by its width, the width of nickel oxide that would represent the original nickel-63 plate.

FIGURE 19

PHOTOMICROGRAPH (280 X) OF AUTORADIOGRAPH OF NICKEL OXIDE SCALE CONTAINING NICKEL-63

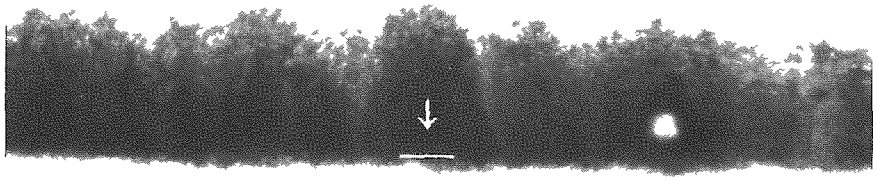

This evidence supports the nickel-migration mechanism for the nickel-oxygen reaction. The reaction producing these thick scales followed a parabolic rate relationship. This was shown by a rate constant of 4×10^{-10} (g/sq cm)^2/sec at 1060 C and 760 mm as compared to a value of 5.5×10^{-10} (g/sq cm)^2/sec reported by Gulbransen and Andrews[14] for this reaction at 1050 C and an oxygen pressure of 76 mm.

The thick nickel oxide scales were adherent. Gulbransen and Andrews[14] have stated that oxide scales greater than 4×10^4 Å in thickness would not remain adherent. The adherence of these thick scales is believed to be in part due to their porosity, which could relieve compressive strain in the growing oxide scale. Figure 20 is a photomicrograph of an oxide scale, 1.4×10^6 Å, in thickness showing this porosity. The porosity is probably due to the coalescences of excess anion vacancies, similar to the formation of voids in the metals undergoing high-temperature oxidation.[16] This phenomenon is reported to be responsible for the formation of hollow oxide cylinders from completely oxidized wire specimens. The presence of voids in both the metal substrate and oxide scale can be seen in Figure 33 of a previous report, ANL-6145, page 111.

FIGURE 20

PHOTOMICROGRAPH (600 X) OF NICKEL OXIDE SCALE SHOWING POROSITY

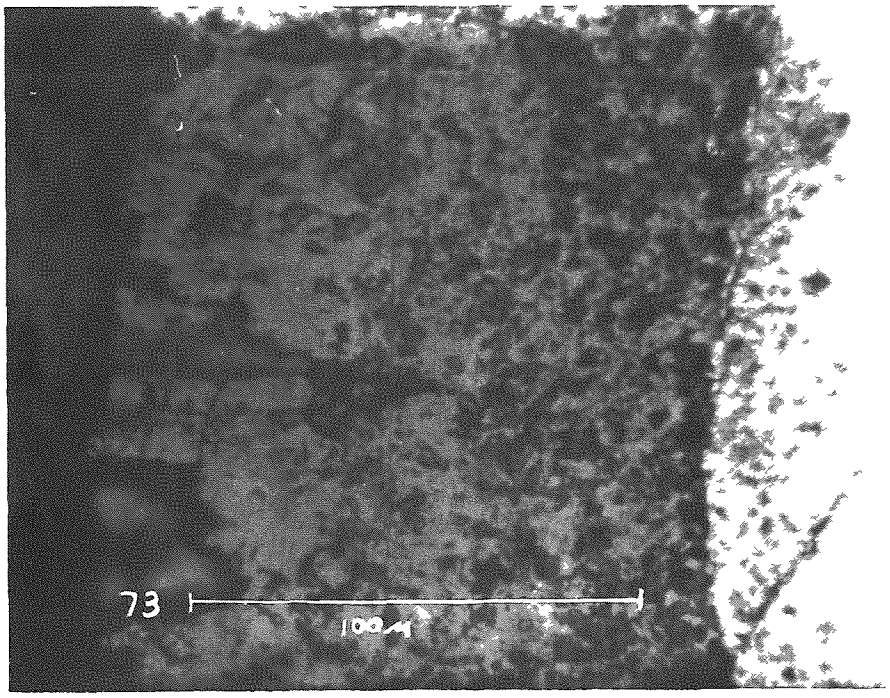

OXIDE-OXYGEN INTERFACE | NICKEL OXIDE | METAL-OXIDE INTERFACE

[16]Vermilyea, D. A., Acta Met., 5, 492 (1957).

b. Corrosion of Nickel by Hydrogen Fluoride-Hydrogen Chloride Gas Mixtures
(R. L. Jarry, G. Tennenhouse)

A potential scheme for processing Zircaloy-clad fuel elements consists of a treatment with hydrogen fluoride-hydrogen chloride to remove the cladding, followed by a direct fluorination step to recover the uranium. Both of these steps would be most conveniently carried out in a single vessel. Nickel is the preferred material of construction for fluorine service; therefore, it was necessary to determine its corrosion resistance to mixtures of hydrogen fluoride-hydrogen chloride.

The apparatus used for this work consisted of a nickel tube reactor, a circulating pump, and a service manifold. Flow was estimated from the physical dimensions of the Rosen recirculating pump (ANL-6183, page 106), the length of stroke, and the number of cycles per minute.

A-nickel coupons, each 1 x 3 x 0.16 cm, were cut from sheet stock and used without further treatment except for a degreasing step in boiling carbon tetrachloride. The coupons were suspended in the reactor from hooks welded to the thermocouple well.

The mixtures of 90 per cent hydrogen fluoride-10 per cent hydrogen chloride were made up in the system, whose volume was five liters, by PVT measurements. The gases were admitted to the reactor after it had been brought to temperature. Pressure was allowed to drop in some experiments as the reaction proceeded, while in others it was made up to the original pressure after each decrease of 100 mm.

Results obtained at reaction temperatures of 450 and 500 C are shown in Table 16.

Table 16

THE CORROSION OF A-NICKEL BY A GAS MIXTURE OF 90 VOLUME PER CENT HYDROGEN FLUORIDE AND 10 VOLUME PER CENT HYDROGEN CHLORIDE

(See above for a description of apparatus and procedure)

Flow: 150 ml/min

Coupons: A-nickel, 1 x 3 x 0.16 cm

Experiment No.	Temp (C)	Pressure (mm)	Time (days)	Penetration[a] Rate (mil/day)
I	450	740[b]	3	3×10^{-3}
II	500	750[b]	3	9×10^{-3}
III	500	750	6	23×10^{-3}

[a]Calculated from the change in weight of the coupon assuming the film was nickel fluoride.

[b]Final pressure approx 360 mm.

Coupons from Run III were mounted and sectioned normal to the surface. The specimens were than etched and examined under the microscope. Intergranular attack was noted, extending 0.4 to 1.0 mil into the metal. The penetration figures given are based on a half-thickness of 30 mils and the geometric surface area.

These preliminary results indicate that, on the basis of penetration rates, nickel is a suitable construction material up to 500 C. However, the extent of intergranular attack, which is several orders of magnitude greater than the penetration, should be investigated further.

B. Engineering-scale Investigations of Fluoride Volatility Processes (A. A. Jonke)

Direct Fluorination Processes for the recovery of uranium from clad uranium or alloy fuels are under development. These processes (outlined in ANL-6183, pages 87 and 101) involve the use of exothermic gas-solid reactions and fluidized beds of inert media to provide heat transfer. Process application is intended for typical fuels such as enriched uranium alloyed with Zircaloy in the form of plate assemblies, and rods composed of uranium dioxide clad in Zircaloy or stainless steel.

A direct fluorination recovery process for uranium dioxide reactor fuels is of interest because of increased use of this fuel in nuclear reactors. The dense pelleted fuel material has been shown to be capable of fluorination at practical rates. Pilot plant-scale work has been directed toward means of controlling the reaction and removing the large amount of heat involved. The use of an inert fluidized material to cover and fill the void spaces of a nonfluidized packed bed of pellets has some of the advantages of fluidization for solid-gas reactions, particularly for the removal of heat.

In a previous report (ANL-6145, page 105) data were presented on fluorination rates, fines production, and fluorination efficiencies as functions of pellet bed height and inlet fluorine concentration (up to 30 per cent) at a single temperature of 500 C. In deeper pellet beds (to 9 inches), more uranium intermediates were formed, resulting chiefly in fines but also producing some solid cake. At 20 per cent fluorine, fines production at 400 C was at least as great as at 500 C; however, deeper beds of inert fluidized material retained most of the fines within the bed (ANL-6183, page 99).

Work is continuing toward optimization of process control for deeper pellet beds. In the present period, initial fluorinations were carried out in a new forced-air-cooled reactor. Preliminary results indicate internal heat transfer from the bed to the reactor wall is the limiting factor in temperature control for fluorine gas rates of 0.25 ft/sec and higher.

A series of heat transfer tests in a mockup system was made. Representative average heat transfer coefficients, from heated, nonfluidized pellets in a packed bed to fluidized material in the voids, were found to be over five times that for the packing without a fluid bed. These data confirm the potential advantage of fluidization for reaction control and are helpful in predicting practically achievable heat transfer rates. These rates depend also on caking tendencies, on the range of variation of heat transfer coefficients for individual pellets in a bed, and on the effective overall heat transfer from the center of the bed to the reactor walls.

In the overall fuel recovery process, a decladding operation is required prior to pellet fluorination. Decladding of pellets in Zircaloy-2 tubing with a hydrogen chloride-hydrogen fluoride gas mixture was demonstrated in two initial runs. Caking of the fluid bed in this operation was found for tubes packed to nearly maximum closeness in the reactor, but caking was not appreciable for tube packing of one-half the maximum. The pellets themselves showed very little attack in this operation.

The Direct Fluorination Process may be applied to recovery of uranium from fuels consisting of enriched uranium alloyed with Zircaloy. The process involves conversion of the metal to fluoride salts, followed by fluorination of the salts to volatilize uranium. A two-zone reaction scheme for the first step is being investigated. This scheme involves contact of the uranium-zirconium alloy with anhydrous hydrogen chloride diluted with nitrogen in the lower portion of the reactor, and conversion of the volatile zirconium tetrachloride to the solid tetrafluoride in the upper zone by contact with hydrogen fluoride.

Dissolution of zirconium-uranium alloys in molten fluoride salt with a hydrogen fluoride sparge is being considered as an initial step in a fluoride volatility process. A final dissolution in a series of dissolutions of synthetic fuel assemblies was performed to demonstrate operation of the graphite pilot-plant dissolver.

1. Direct Fluorination Process for Oxide Fuels
(W. J. Mecham)

a. Decladding Runs
(J. D. Gabor, J. Wehrle)

Since Zircaloy-2 cladding is used for some uranium oxide fuels, it is of interest to demonstrate a decladding process that can be readily combined with subsequent fluorination steps. Two runs were made, using the hydrogen chloride-hydrogen fluoride process. Work has also been done in the laboratory on the corrosion of nickel by hydrogen fluoride-hydrogen chloride gas mixtures (see page 107).

Tubing elements were simulated by inserting reactor-grade uranium dioxide pellets (1/2 inch x 1/2 inch right cylinders) into 29-inch lengths of reactor-grade Zircaloy-2 tubing. The pellets fit the tubing very closely and were secured by crimping the ends of the tubing. The Zircaloy tubing had a 30-mil wall.

The elements were loaded vertically in the three-inch diameter reactor and were completely submerged below the surface of a bed of 60 to 140 mesh calcium fluoride. Fourteen elements were charged in the first run and seven in the second. The conditions and results are summarized in Table 17. In both runs a 10 mole per cent hydrogen chloride-90 mole per cent hydrogen fluoride gas mixture was used to react with the cladding and provide fluidization. The superficial gas velocity was 0.5 feet/second at process temperature and one atm. The reactions were continued for five hours at 500 C.

Table 17

GAS-PHASE DECLADDING OF ZIRCALOY-CLAD ELEMENTS

General Conditions:

Run time: 5 hours
Run temp: 500 C
Gas velocity: 0.5 ft/sec at 500 C and 1 atm
Inlet gas composition: 10% HCl-90% HF
Total Material Charged:

Material	Run No. UOF-15	Run No. UOF-17
Zirconium tubing, g	1100	550
Uranium dioxide pellets, g	6200	3100
Calcium fluoride, g	1400	1940
Total Charge, g	8700	5590

Tubular Elements:

UO_2 pellets in 30-mil wall Zircaloy-2 tubing
Tubing length: 14 inches
Tubing diameter: 0.560-inch OD

Configuration:

Tubing elements vertical in 3-inch ID reactor and completely submerged 1 to 3 inches below the surface of a bed of 60 to 140 mesh calcium fluoride.

	Run No. UOF-15	Run No. UOF-17
Number of tubing elements:	14	7
Cross-sectional area of reactor occupied by fuel elements, %	55	28
Entrained fines collected on filter, g	62	4.0
Increase in pressure drop for gas flow through reactor, psi	0.8 to 13.6	0.8 to 1.3
Final bed condition:	caked	free-flowing

In both runs the fluorination of the Zircaloy was complete except for a few fragile sections of tubes. The decladding was considered complete inasmuch as no cladding remained that would inhibit subsequent pellet fluorination. The pellets remained essentially intact in both runs. For the close-packed case, in which the total cross-sectional area of the elements was 55 per cent of the reactor cross-sectional area, caking of the fluid bed occurred. However, when tubing elements were packed only one-half as closely as before, no appreciable caking was evident. In subsequent experiments a complete cycle of decladding and fluorination will be included.

b. Fluorination Shakedown Run in the New Reactor
(J. D. Gabor, J. Wehrle, A. Rashinskas, J. Gates, H. Dykema,* G. Gaerte**)

A new forced-air-cooled three-inch reactor was installed and put into service. The reactor was charged with a nine-inch bed of pellets (1/2-inch size) submerged in a 34-inch bed of 60 to 100 mesh magnesium fluoride. Fluorine gas rates of 0.25 to 0.50 feet/second with various nitrogen dilutions and temperatures of 400 to 500 C were tried in a shakedown run. Heat generation rates of up to about three times the previous maximum values were encountered. While the reaction was always under regulation by means of fluorine flow control, steady-state conditions under the above ranges of process variables were not established in this initial test. Temperature profiles of the bed and wall of the reactor showed large temperature gradients from the bed to the wall; it thus appeared that heat transfer was limited by these temperature gradients. Somewhat more conservative fluorination rates will be employed in further experiments now in progress.

c. Heat Transfer Study
(B. Bydal)†

The simplicity of dry fluorination of metal and oxides is sometimes difficult to achieve in practice because the highly exothermic reactions offer problems of temperature control. A promising general way to improve heat transfer for solid-gas reactions is by means of fluidization. In some cases, such as the fluorination of uranium dioxide pellets, it is not feasible to fluidize the solid reactant directly, but the fluidization of an inert material in the voids of a pellet bed can be used to improve heat transfer from the pellet surfaces. The degree of improved heat transfer depends on the nonfluidized reacting material and its configuration, as well as the usual fluid-bed variables.

---

*Student Aide from University of Illinois.

**Student Aide from Purdue University.

†Summer Research Associate from the University of Minnesota.

A summer program was carried out in which measurements were made of heat transfer from the heated surfaces of simulated pellets to a fluid bed surrounding the pellets. Tests were made for single and multiple pellet-sized heaters, for heaters in a fluidized medium alone, for heaters in a pellet bed alone, and for heaters in combined pellet-fluidized systems of various heights, such as could be encountered in process fluorinations. Since the objective of these tests was the study of the heat transfer mechanism, mockup materials of metal were used because their properties were well-known and because of the durability of metal.

The independent variables investigated included heat flux, temperature difference, and heater surface temperature. Pressure drop and heat transfer coefficients as a function of gas velocity were used to compare the various bed configurations.

Earlier work (ANL-6101, page 115) described preliminary fluidization studies of packed-fluidized systems, but without measurement of heat transfer.

(1) Equipment and Procedure

The fluidization column used was a brass tube, 2.88 inches in inside diameter and with an overall length of 46.5 inches. The bottom 18.5 inches was water cooled. Nonfluidized bed materials were $\frac{1}{4}$- to $\frac{5}{16}$-inch nickel balls and brass pellets of $\frac{1}{2}$-inch diameter and $\frac{3}{4}$-inch long. The cartridge-type, electric resistance heaters were of approximately the size and heat output of uranium dioxide pellets used in fluorination runs. The fluidized material was 140 to 200 mesh copper shot. Air was the fluidizing gas. Heater temperatures were obtained by thermocouples soldered or welded to the metal jackets of the heaters. Fluid-bed temperatures were obtained by thermocouple junctions positioned so that they contacted only the gas and the fluidized material, but not the stationary packing.

(2) Heat Transfer to a Fluidized Bed without Packing Material

In these experiments the objective was to obtain baseline data for the fluidized bed without pellet packing for comparison with later experiments. The fluidization behavior of the copper shot has been examined for several bed heights by measuring the pressure drop across the bed as a function of superficial linear gas velocity, both in the presence and absence of the cartridge heater.

The single $\frac{1}{2}$-inch diameter, $1\frac{1}{2}$-inch long heater was mounted on a vertical axis in about the center of the fluid bed. No difference in fluidization behavior due to the presence of the heater was noted except for a very slight decrease (about 10 per cent) in the minimum fluidization point.

The heat transfer coefficient for this configuration is shown in Figure 21 as a function of gas velocity. The heat transfer coefficient rose from 11 Btu/(hr)(sq ft)(F) for the static bed condition below a gas velocity of 0.21 ft/sec to about 110 at 1.25 ft/sec. The various bed heights showed no important effect on the heat transfer coefficient. Changes in heater power and variations of the vertical position of the heater within the bed also had little effect.

FIGURE 21
HEAT TRANSFER FROM A SMALL CYLINDER TO A FLUIDIZED BED. EFFECT OF GAS VELOCITY ON HEAT TRANSFER COEFFICIENT, h

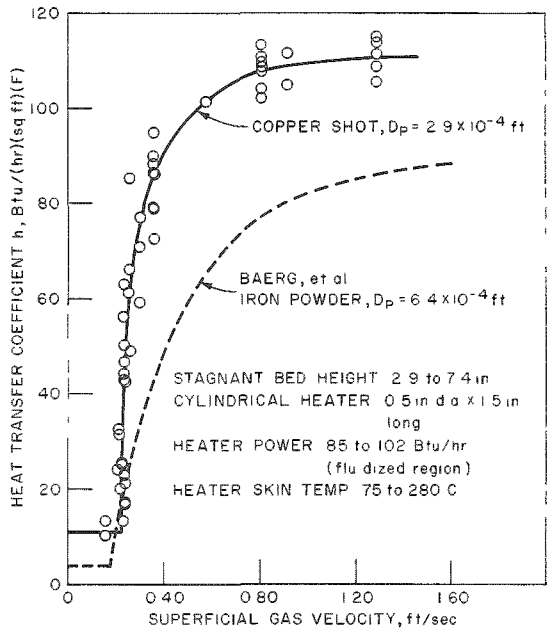

Also shown for comparison are the data of Baerg et al.[17] Baerg's equipment and results are generally similar to ANL equipment and results, although he used iron powder of a large size. The differences in the curves are believed due to different particle size and the fact that Baerg's heater was an axial tube at the midpoint, an arrangement which contributes less turbulence in fluidization.

(3) Heat Transfer to a Fluidized Bed Containing Packing and a Single Heater

In these tests the objective was to determine the performance of a single heater surrounded by packing and with fluidization in the voids of packing. The heater and its position were generally the same as in the preceding series of runs. The depth of the packing ($\frac{1}{4}$- to $\frac{5}{16}$-inch nickel balls) ranged from nine to sixteen inches. The fluidizable solid (copper shot) was loaded to depths ranging from 65 to 80 per cent of

[17] Baerg, A. et al., Can J. Res. F, 28, 287-308 (1950).

the packed bed depth. With increasing gas velocity the fluid bed expanded to the top of and above the packed section. The pressure-drop curves for this configuration showed generally the same behavior as without packing, except that the minimum fluidization points occurred at lower superficial gas velocities (40 to 50 per cent less) owing to the large percentage of the cross section occupied by the packing.

The effect of superficial gas velocity on the heat transfer coefficient, h, for this series of runs is shown in Figure 22. The three different bed heights show the same values of h for the static bed condition, but with increasing fluidizing gas rate an initial divergence of the three curves occurred, followed by what appears to be a tendency for convergence at still higher gas rates. The effect seems to be real and it is probably due to differences in circulation or turbulence in the fluidized medium within the packed bed. Thus the heat transfer coefficient appears to vary by ±20 per cent, depending on the arrangement of the packing around the heater. It does not seem likely that the coefficient is dependent on bed depth. The observed decrease in h above a certain gas velocity may be due to a decrease in density of the fluid bed caused by high gas flow through interstices in the packing.

FIGURE 22
HEAT TRANSFER FROM A SMALL CYLINDER TO A FLUIDIZED SOLID IN BEDS CONTAINING NONFLUIDIZED PACKING

STATIONARY PACKING NICKEL BALLS 1/4 to 5/16 in
FLUIDIZABLE SOLID COPPER SHOT 140 to 200 MESH
HEATER SKIN TEMP APPROX 120 C

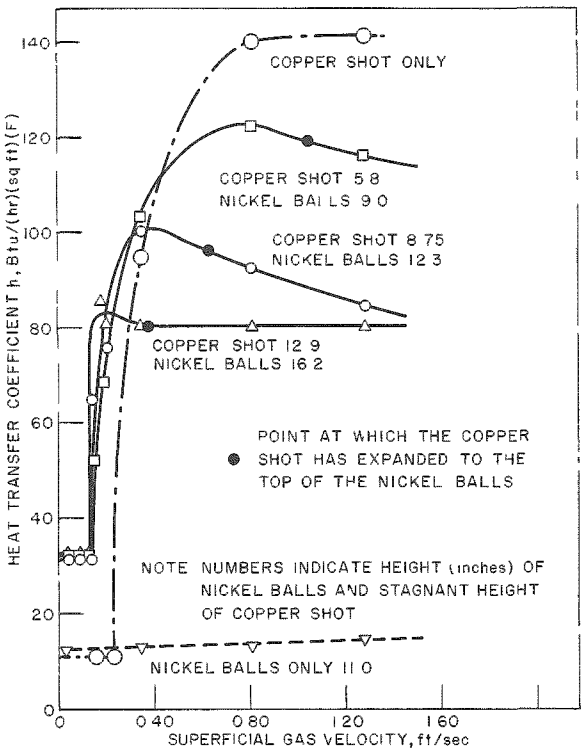

For reference, the heat transfer coefficients in this system are also shown for (a) the case of fluidization without packing and (b) the case of packing without the presence of fluidized material in the voids. The packing causes some decrease in the value of h, but the coefficients are at least fivefold higher than in the absence of fluidizable material.

The heat transfer coefficient for fluidization without packing is higher in this series than in the preceding series. No definite reason can be given, but this effect may be due to increased turbulence produced by the heater mounting used in this case. The effects of heat flux from 40 to 65 watts, temperature difference from 50 to 150 C, and heater skin temperature from 80 to 200 C on the heat transfer coefficient were measured and found to be small.

(4) Heat Transfer to the Fluidized Bed Containing Packing and Multiple Heaters Simulating Pellets

The objective of this series of runs was to obtain a configuration closer to process conditions. Nine pellet-sized heaters were included in a packed bed of solid brass pellets. These components and the general bed configuration are shown in Figure 23.

FIGURE 23

CONFIGURATION USED IN HEAT TRANSFER STUDIES IN PACKED FLUIDIZED BED

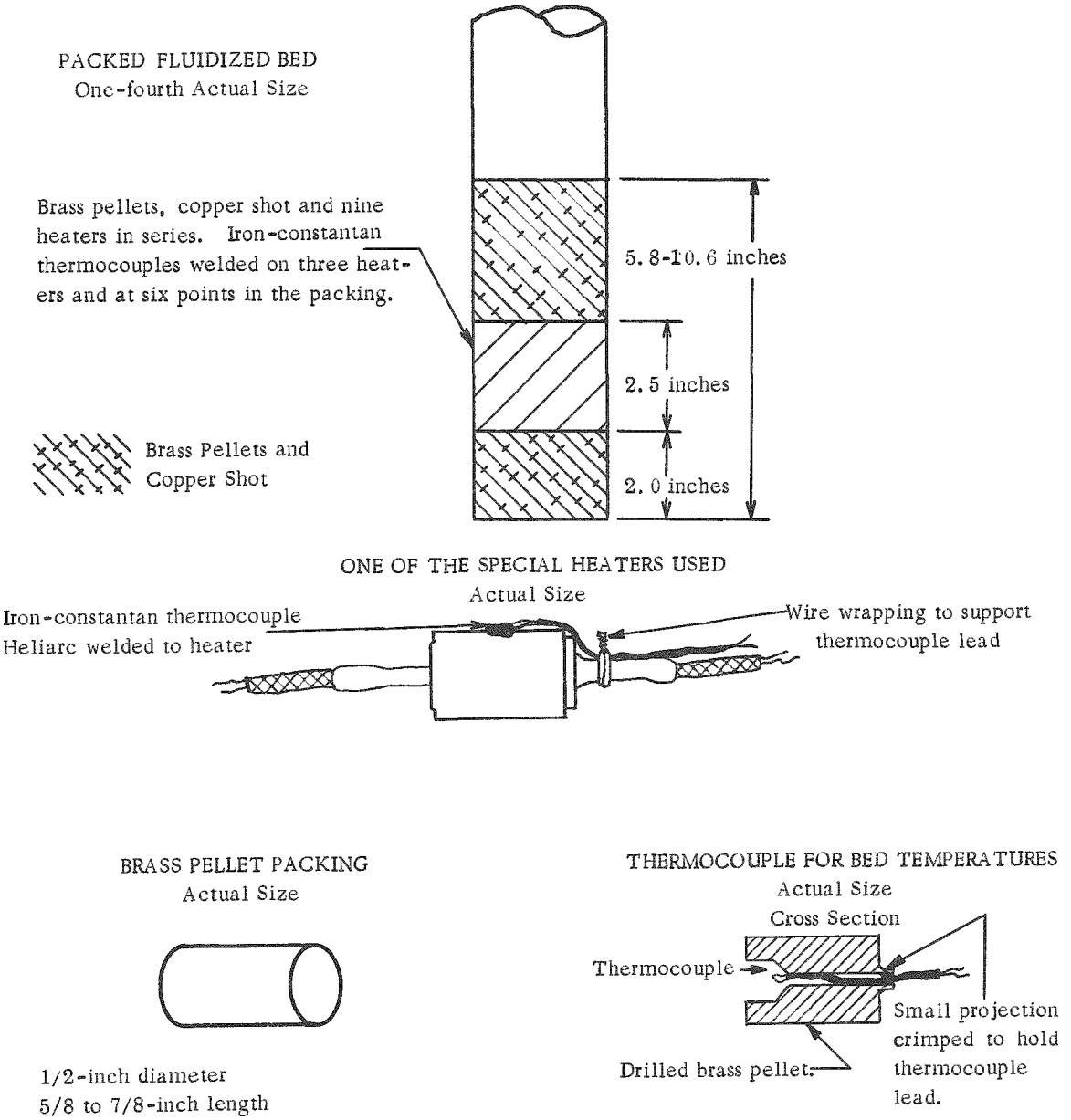

Five different bed heights were used. In one series the static level of the fluidizable material was at the top of the pellet packing. In another series the effect of various relative heights of fluidized material with respect to the pellet bed was also investigated. Power to each of the heaters in a run was the same; overall power levels were varied to maintain approximately equal surface temperatures over the full range of gas velocities. The heating rate of each pellet heater was 85 to 102 Btu/hour in the fluidized region. This is of the same order of magnitude as may be encountered in the fluorination of a uranium dioxide pellet.

The average heat transfer coefficients, shown in Figure 24, were calculated as a single value based on the average temperature difference measured for three of the heaters. The coefficients show a smooth curve from 23 Btu/(hr)(sq ft)(F) at the onset of fluidization to a plateau at about 80. Without fluidizable material the heat transfer coefficient was nearly constant at 10 Btu/(hr)(sq ft)(F). The average heat transfer coefficients for various relative heights of fluidized material are nearly identical with those for equal heights of fluid bed and packing, indicating no effect of the different bed configuration on the average values.

FIGURE 24
HEAT TRANSFER TO A FLUIDIZED BED
CONTAINING PACKING AND
MULTIPLE HEATERS

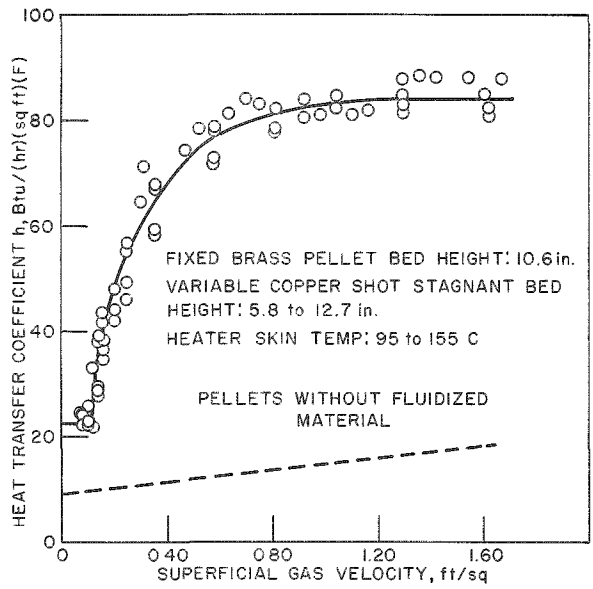

In order to indicate the variations of heat transfer for individual pellet heaters in the same bed, individual heat transfer coefficients, h, are plotted in Figure 25 for the run with the largest copper shot static bed height. Here is observed the divergence and peaking of h for one of the heaters similar to that noted for a fluidized bed containing packing and a single heater (see Figure 22). This effect is obscured in the

calculation of heat transfer coefficients from average temperatures. Evidently the variations in individual heat transfer coefficients in these configurations can be quite large, probably depending on differences of turbulence and circulation of the fluidized material.

FIGURE 25
INDIVIDUAL HEAT TRANSFER COEFFICIENTS FOR THREE PELLET HEATERS IN THE SAME FLUID BED

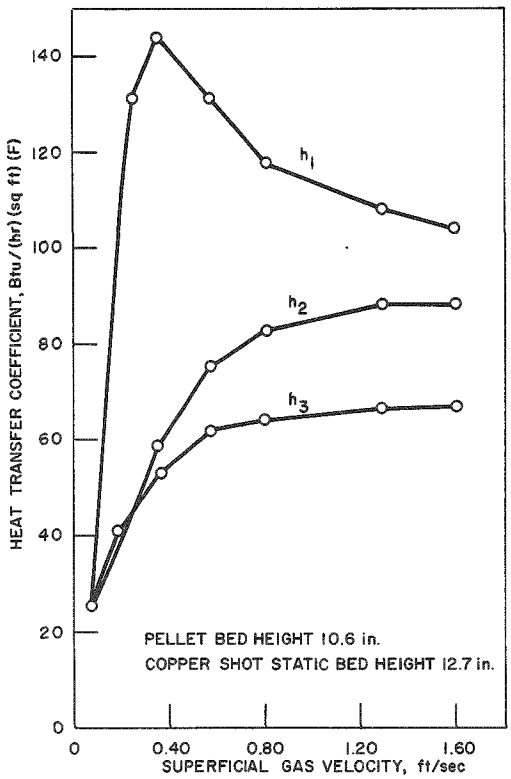

2. Direct Fluorination Process for Uranium-Zirconium Alloys (N. Levitz)

Direct Fluorination Processes for the recovery of uranium from clad uranium or alloy fuels are under development. In the case of uranium-Zircaloy alloys, previous work on the first step, conversion of the metal to fluoride salts, was demonstrated by the reaction of dilute gaseous mixtures of hydrogen chloride in hydrogen fluoride with the alloy immersed in a fluidized bed. About 95 per cent of a 10-plate assembly (~2 kg) of 1.5 weight per cent uranium-zirconium alloy had reacted in 12 hours using 10 volume per cent hydrogen chloride in hydrogen fluoride at 450 C (see ANL-6183, page 104). Efforts during this quarter were concentrated on a two-reaction zone scheme, hydrochlorination followed by hydrofluorination, in a single two-zone fluidized-bed reactor. Fluorination studies for removal of uranium from the resulting powders have been initiated.

a. Hydrochlorination-hydrofluorination Studies in a Two-zone Reactor (J. Barghusen, J. Kincinas, D. Armstrong*)

Work on the two-reaction zone scheme for processing uranium-zirconium alloy fuels was continued in the six-inch diameter fluid-bed reactor. The primary reaction (hydrochlorination) is carried out in the lower zone of the fluidized bed at temperatures above the sublimation point of the zirconium tetrachloride (331 C). In the upper zone, separated from the lower zone by a baffle, hydrogen fluoride is admitted to react with the volatile zirconium tetrachloride, forming the solid tetrafluoride. Also the uranium trichloride is probably converted to the tetrafluoride.

*Cooperative student from Northwestern University, Evanston, Illinois

Previous work, where no baffle was used, indicated that back-mixing of the hydrogen fluoride may have occurred, resulting in gas mixture of low chemical reactivity (see ANL-6183, page 105 and Figure 25, page 111). Before resuming process work, the effect of baffles on back-mixing was studied.

Gas Back-mixing in a Baffled Fluidized Bed

Two types of baffles were tested, a punched plate ($\frac{1}{8}$-inch diameter holes, staggered spacing, $\frac{3}{16}$-inch centers, 40 per cent open) and a 60° cone with a 1.5-inch diameter opening. Both baffles were of stainless steel and were installed horizontally at approximately the center of the fluidized bed. The test procedure consisted of fluidizing the bed with a hydrogen chloride-nitrogen mixture, admitting hydrogen fluoride gas above the baffle plate, and then by sampling and analysis determining the concentration of hydrogen fluoride at some distance below the baffle. The punched plate was installed 10 inches above the primary gas distributor plate; the hydrogen fluoride was admitted at 12 inches above the gas distributor plate. For the cone baffle, the cone inlet and hydrogen fluoride inlet were at 12 and 23.5 inches, respectively, above the gas distributor plate. The hydrogen fluoride inlet was at the wall (periphery) and the gas samples were taken at a point diametrically opposite and about five inches below the baffles.

The inlet gas was a mixture of 20 volume per cent hydrogen chloride in nitrogen at a total flow rate of 2.4 scfm. Two hydrogen fluoride flow rates were employed, 0.24 and 1.21 scfm. Duplicate gas samples were taken for each trial.

The data (see Table 18) clearly indicate that substantial reduction of back-mixing may be achieved with either type of baffle. The ratio of hydrogen fluoride in the sample to that at the inlet was lower by a factor of about 10 for each of the experiments with baffles than for the case in which no baffle was used. This was true for both hydrogen fluoride rates. Typical values were 24 volume per cent in the inlet and 0.58 volume per cent in the sample.

On the basis of these results, it was decided to use the cone baffle; it offered simplicity in design, having only a single opening.

Reaction Studies on Uranium-Zirconium Alloy Assemblies

Three multiple-plate assemblies (1.5 weight per cent uranium-zirconium alloy) have been reacted to date in the baffled, two-reaction zone fluid-bed reactor. The fuel charges, weighing 1533, 2063 and 3360 g, were immersed in 18 kg of 60 to 325 mesh calcium fluoride (27-inch static bed depth). Mixtures of hydrogen chloride in nitrogen ranging from 19 to 89 volume per cent were used as the primary reactant.

Table 18

EFFECT OF BAFFLES ON BACK-MIXING IN A FLUIDIZED BED

Equipment:	6-inch diameter reactor
Bed Material:	18 kg of 60 to 325 mesh calcium fluoride
Temperature:	380 C
Fluidizing Gas:	20 v/o HCl in nitrogen at 2.4 scfm
Superficial Gas Velocity:	0.45 ft/sec at sampling port (6 inches above reactor bottom)
Secondary Gas (above baffle):	HF

Baffle Type	HF Feed Rate (cu ft/min) at 380 C	At inlet (v/o) = C_0	At Sample Port (v/o) = C	Concentration Ratio, C/C_0
No Baffle	1.45	37.3	9.30	0.25
	0.42	14.7	4.55	0.31
Punched Plate	1.15	32.1	0.78	0.024
	0.32	11.6	0.58	0.050
Cone	1.26	34.1	0.58	0.025
	0.29	10.6	0.33	0.031

Hydrogen fluoride, the secondary reactant, was admitted in the upper zone in mole ratios of 0.5 to 1.6 moles of fluoride per mole of chloride. The bed temperature ranged from 360 to 425 C and run duration from 1.75 to 6.3 hours. The inlet superficial gas velocity was 0.36 ft/sec. The final bed from each run was used as the starting bed for the subsequent run. Two or three runs were made on a single metal charge while investigating temperature and hydrogen chloride concentration effects.

The major objectives of these experiments were to determine the feasibility of the two-reaction zone scheme and to produce a fluidizable powder for use in fluorination studies in which uranium removal and recovery were to be demonstrated. Data are presented as the amount of metal reacted (weight loss) per hour per unit of metal charged or percentage weight loss per hour. Since in each case the unit area of charge and operating conditions were changed after the initial reaction period and the fuel elements were degraded, it was difficult to measure a true area and determine comparative reaction rates.

Approximately 85 to 94 per cent of the elements reacted in periods of about 12 hours. The greatest amount of metal reacted when 60 volume per cent hydrogen chloride at 400 C (see Run 20, Table 19) was used. Increasing the temperature to 425 C resulted in a diminished amount reacted and caked material was found on the element. The higher temperature would normally be expected to give a higher reaction rate, but the rate of heat removal by the bed apparently was insufficient to prevent sintering. A high amount of metal reacted/hr (15%/hr) was also achieved by lowering the temperature to 360 C and increasing the hydrogen chloride concentration to nearly 90 volume per cent.

Sieve analyses of the starting and final beds showed a slight increase in -200 mesh particles. Evidently, some of the zirconium tetrafluoride produced in the upper zone appears in the fluidized bed as a fine powder. The bulk of the zirconium tetrafluoride appears to deposit on the bed particles (calcium fluoride). The conversion of zirconium tetrachloride to the tetrafluoride is believed to be complete, since no evidence of zirconium compounds has been observed in the off-gas piping or scrubber system. A small amount of chloride was detected in the fine solids collected on the off-gas filters, but the amount is considered to be insignificant. Chemical analyses of the final bed solids in the upper and lower zones showed the composition to be uniform, indicating that considerable mixing of solids occurs between the two zones.

In this series of runs the zirconium fluoride concentration of the bed increased to about 40 per cent, the remainder being primarily calcium fluoride from the starting bed. The uranium concentration of the bed reached a value of 0.22 per cent. For semicontinuous operation the uranium concentrate at steady state should reach a value of about 0.8 per cent for a fuel alloy containing 1.5 per cent uranium.

Future studies will include the effects of using refractory-grade alundum in place of calcium fluoride as the starting bed and chlorine in place of hydrogen chloride. Alundum is being considered because calcium fluoride appears to be more friable and may result in particle degradation.

b. Fluorination of Uranium-Zirconium Fluorides Obtained from Hydrochlorination-hydrofluorination of Uranium-zirconium Fuel Alloys
(E. Carls, L. Marek, R. Schlaug*)

A series of exploratory experiments has begun on the fluorination and removal of uranium from the reaction products obtained from the two-reaction scheme (hydrochlorination followed by hydrofluorination) being used on uranium-zirconium fuel alloys.

---

*Student Aide from Case Institute of Technology.

Table 19

SUMMARY OF HYDROCHLORINATION-HYDROFLUORINATION RUNS FOR THE TWO-ZONE PROCESS

Equipment: Six-inch diameter Inconel reactor
Specimen: 1.5 w/o U-Zr, ten-plate subassembly
Bed: 18 kg of 60 to 325 mesh calcium fluoride
Baffle: Stainless steel cone with 1.5-inch diameter opening
Inlet Superficial Gas Velocity: 0.36 ft/sec
HF/HCl mole ratio: 0.5 to 1.0

Run No.	HCl Concentration (v/o)	Bed Temperature (C)	Mole Ratio HF/HCl	Run Duration (hr)	Fuel Element Weight		Percentage Weight Loss per hour[b]
					Initial (g)	Final (g)	
18	19	390	1.6	4.5	1533[a]	1230	2.9
25	60	380	0.9	6.3	1485	485	10.7
19	60	390	1.0	3.5	1230	617	14.2
20	60	400	1.0	4.0	617	144	19.2
21	60	425	1.0	6.0	2063[a]	1077	8.0
24	86	360	0.5	1.8	2000	1485	14.3
23	89	360	0.6	4.7	1077	250	16.4
22	88	385	0.6	4.8	3360[a]	2000	8.4

[a]A new charge of metal was used in these runs. Remaining runs were made with the residual unreacted metal as the charge.

[b]The initial unit area of the charge varies from run to run.

The procedure for the runs involved charging approximately 500 grams of material to the two-inch diameter nickel reactor and fluidizing with nitrogen during the heatup period. The nitrogen was replaced with fluorine at temperatures ranging from 100 to 300 C. The unit was then brought up to the desired operating temperatures and held there for the specified times.

Samples of the final beds were ground to minus 200 mesh and analyzed by means of X-ray spectrographic techniques. Wet chemical analyses were used to confirm the accuracy of the X-ray spectrographic results in some cases.

The goal of the fluorination step is to achieve a minimum of 99 per cent removal of the uranium from fuel alloys having an overall uranium concentration of 1.0 weight per cent. This means an acceptable uranium concentration in the residual solids is 0.01 weight per cent, neglecting the calcium fluoride diluent. The initial materials that have been fluorinated contained only up to 0.22 per cent uranium and up to about 40 per cent zirconium tetrafluoride, the remainder being calcium fluoride.

The results (Table 20 and Figure 26) show fluorination temperature and time to be important.

Table 20

RESULTS OF FLUORINATION EXPERIMENTS ON SOLIDS FROM HYDROCHLORINATION-HYDROFLUORINATION OF URANIUM-ZIRCONIUM ALLOYS

Equipment: 2-inch diameter nickel fluorinator
Weight of Charge: 500 g[a]
Fluidizing Velocity: 0.6 to 0.7 ft/sec at column conditions
Concentration of Gas: 100%
Amount of F_2: 16 to 22 scf/hr

Temperature (C)	Duration at Temp (hr)	Starting Uranium Content (w/o total bed)	Residual Uranium Content (w/o)	Cumulative Uranium Removed (%)
400	1	0.06	0.047	19
600[b]	1	-	0.010	83
600	2	0.06	0.009	84
600	2	0.22	0.048	78
500	4	0.15	0.046	69
500[a]	4	-	0.017	89
500[a]	4	-	0.006	96
550	4	0.15	0.016	89
550[a]	4	-	0.015	90
600[a]	1.4	-	0.010	93

[a]CaF_2 content of the fluid bed ranged from 78 to 94 weight per cent of the total charge.

[b]Refluorination of the residue from the preceding run.

FIGURE 26
URANIUM REMOVAL DURING FLUORINATION OF ZIRCONIUM-URANIUM FLUORIDES

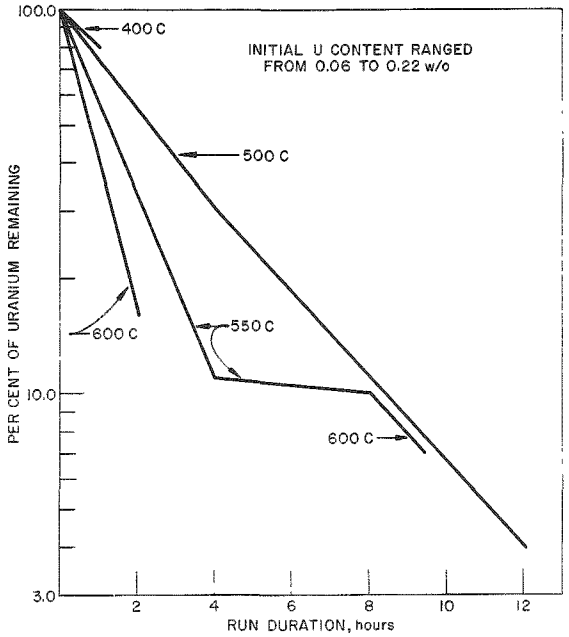

The temperature effect is obvious from the plot of data shown in Figure 26, that is, increased temperature gives greater initial rates of uranium removal. The effect of time is illustrated by the set of runs made at 500 C, where repeated four-hour fluorinations continued to show uranium removal, up to 96 per cent after 12 hours. The residual uranium content of this material was only 0.006 per cent. However, at 550 C a plateau was noted, in which the rate of uranium removal leveled off during the second four-hour period. A slight additional removal, to 93 per cent, was effected by a 1.5-hour fluorination of this residue at 600 C. The rate of uranium removal at 600 C was high, about 84 per cent in two hours. However, it is not yet known whether the removal would continue at this rate for longer fluorination periods. Similar removal (~84 per cent) was achieved at 600 C with material of two different starting uranium concentrations, 0.06 and 0.30 per cent, indicating no concentration effect in this range.

The peculiar behavior observed in the runs made at 550 C needs some clarification. Fluorination experiments are, therefore, planned in laboratory-scale equipment to determine the effects of time and temperature more completely.

3. Direct Fluorination Process for Stainless Steel-clad or Matrix Fuels
(N. Levitz)

The reactions of stainless steel with gases such as chlorine, fluorine, hydrogen fluoride, or chlorine-hydrogen fluoride mixtures are being investigated as a means of decladding stainless steel-clad fuel or as an initial step in the processing of stainless steel matrix fuels.

a. Reaction of Stainless Steel with Chlorine and Hydrogen Fluoride
(J. T. Holmes, D. Raue)

Tseitlin[18,19,20,21,22,23] and Brown[24] presented corrosion data for 18-8 (chromium-nickel) stainless steel, which indicate that a de-cladding reaction having a penetration rate of about 10 mils/hr might be carried out in the vicinity of 600 C with dry undiluted chlorine gas. Brown also indicated that a much higher temperature would be required to achieve the same reaction rate with hydrogen chloride gas.

A one-inch diameter horizontal-tube-reactor was installed and used to study further the variables of the chlorination reaction. The reaction rates were calculated from the weight loss of 0.5-inch segments of $\frac{5}{8}$-inch diameter 304 stainless steel tubing. The flow of chlorine and nitrogen was 2.0 g-mole/hr for each gas. The surface condition of the metal specimen was "as received." Figure 27 shows the dependence of the average reaction rate on time. The initial rates were 5.0 mil/hr at 570 C and 9.7 mil/hr at 600 C, slightly higher than the rate-temperature data of Tseitlin and Brown. The effect of dilution with nitrogen was investigated and found to have a negligible effect for chlorine concentrations above 50 mole per cent. Below 50 mole per cent chlorine, the chlorination rate was reduced.

FIGURE 27
REACTION OF 304 STAINLESS STEEL WITH
50 MOLE PER CENT CHLORINE IN NITROGEN

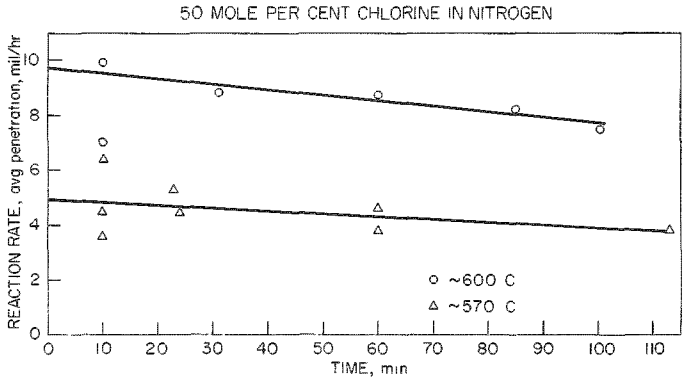

[18]Tseitlin, Kh. L., J. Appl. Chem. (USSR), 27, 887 (1954).

[19]Tseitlin, Kh. L., J. Appl. Chem. (USSR), 28, 467 (1955).

[20]Tseitlin, Kh. L., J. Appl. Chem. (USSR), 29, 253 (1956).

[21]Tseitlin, Kh. L., J. Appl. Chem. (USSR), 29, 1281 (1956).

[22]Tseitlin, Kh. L., J. Appl. Chem. (USSR), 29, 1793 (1956).

[23]Tseitlin, Kh. L., J. Appl. Chem. (USSR), 31, 1832 (1958).

[24]Brown, M. H., DeLong, W. B., and Auld, J. R., Ind. Eng. Chem. 39 839 (1947).

The horizontal-tube-reactor chlorination experiments showed that the ferric chloride was volatilized, but that the chromium and nickel chlorides remained as a powder on the metal surface. This reaction, carried out in a fluidized bed of inert particles (for heat dissipation), might be expected to proceed at a rate equivalent to the initial reaction rate measured in the horizontal tube reactor. Fresh metal surface would be continually exposed if there were sufficient abrasive action from the bed particles to remove the nonvolatile chloride powder.

A single experiment at 565 C with mixed gases, 28 mole per cent chlorine, 41 mole per cent hydrogen fluoride, and 31 mole per cent nitrogen, gave a rate of 1.7 mils/hr. The formation of nonvolatile fluorides apparently inhibited the reaction.

Initial experiments on the chlorination of 304 stainless steel at about 550 C in a 1.5-inch diameter fluid-bed reactor were inconclusive. The Monel preheater and reactor were severely corroded because of leaching of the copper from the Monel as cuprous chloride. In some runs the cuprous chloride reacted with the stainless steel to form metallic copper, which inhibited further chlorination of the base metal. (A free energy calculation showed that metallic copper could be deposited on stainless steel in an atmosphere of cuprous chloride and chlorine.) All Monel parts of the fluid-bed reactor system are presently being replaced with nickel. The corrosion rate of nickel in chlorine is expected to be about 20 mils/month at 600 C.[19,24]

Since volatile ferric chloride and uranium pentachloride would be formed when a stainless steel fuel is reacted with chlorine at about 600 C, a two-zone, baffled, fluid-bed reactor might be used, in which chlorination is carried out in the lower zone, and hydrofluorination in the upper zone to convert the volatile chlorides to nonvolatile fluorides. This scheme would be the same as that used in the zirconium alloy process work (see page 117). The uranium could then be removed as the volatile hexafluoride by reacting the solids formed in the hydrofluorination step with fluorine. Work is planned to study the two-step, chlorination-hydrofluorination process on simulated stainless steel fuels in the 1.5-inch fluid-bed reactor using calcium fluoride or alundum as the inert bed material.

b. Reaction of Stainless Steel with Fluorine
(E. Carls)

A four-hour exposure of 304 stainless steel to fluorine was carried out at 550 C in a three-inch fluid-bed reactor. The reaction rate, calculated from a weight loss measurement (after scale removal) was about 0.7 mil/hr. The fluoride scale was not removed by the abrasive

action of the calcium fluoride bed particles. This rate is lower than expected, since Myers[25] measured a rate of about one mil/hr for Type 347 stainless steel in fluorine at 400 C.

4. Fused Salt Processing of Zirconium Matrix Fuels
(W. J. Mecham)

In the fused salt process for recovery of uranium matrix fuel, the alloy is dissolved in the fused salt at 600 to 700 C with a hydrogen fluoride sparge, and then the uranium in the salt is volatilized as the hexafluoride in a fluorine sparge. A pilot plant-scale graphite-lined dissolver-hydrofluorinator has been developed for the first step to avoid corrosion incurred in metal systems. Dissolution of a synthetic element of Zircaloy-2 in salt containing equilibrium amounts of alloying constituents (tin, iron, chromium, nickel, and uranium) fluorides proceeded at a rate one-half as fast as for pure zirconium in sodium fluoride-zirconium fluoride salt containing only uranium. Of the various alloy constituents present in the salt as fluorides, only the concentration of nickel was reduced by the dissolution. Substantial salt carryover in the dissolver off-gas was encountered during these runs, the major portion being retained in the sodium fluoride pellet bed and all of the remainder on the porous carbon filters. No chemical attack of salt on graphite components was revealed in an examination following disassembly. In a freezing and remelting test, extensive damage to graphite downlines was incurred. Such damage could be minimized or eliminated by suitable design and operation procedures. The amount of salt holdup in the lampblack layer between the graphite lining and the nickel shell was determined.

a. Graphite Dissolver Tests
(R. W. Kessie, J. Gates, R. Kinzler, W. Murphy, A. Rashinskas)

Zircaloy Dissolution

A synthetic Zircaloy-2 fuel element was dissolved (Run A-11) in the graphite dissolver under conditions similar to runs previously reported (ANL-6145, page 120 and ANL-6183, page 115), but with the salt spiked with all alloy constituents in equilibrium concentrations. The dissolution was 90 per cent completed in 10.7 hours and 99 per cent completed in 13.4 hours. The reaction was one-half as fast as with pure zirconium in salt without alloying elements under the same conditions, namely, 700 C, 40 mole per cent zirconium fluoride in the salt, and with a hydrogen fluoride sparge of approximately 60 lb/hr. In the previous run with pure zirconium-clad uranium-zirconium alloy, dissolution was 90 per cent completed in 4.95 hours and 99 per cent completed in 6.75 hours. A sketch of the Zircaloy fuel element is shown in Figure 28. It is very similar in

[25]Myers, W. R., and DeLong, W. B., Chem. Eng. Prog., 44, 359 (1948).

dimensions to the zirconium-clad zirconium-uranium alloy elements used in previous runs. No operational difficulties were encountered and no maintenance shutdowns were required. All instrumentation functioned perfectly in both runs. The course of the dissolution is shown by the record of total off-gas shown in Figure 29. This off-gas includes the argon purge maintained throughout the run.

FIGURE 28
SYNTHETIC ZIRCALOY FUEL ELEMENT
RUN A-11

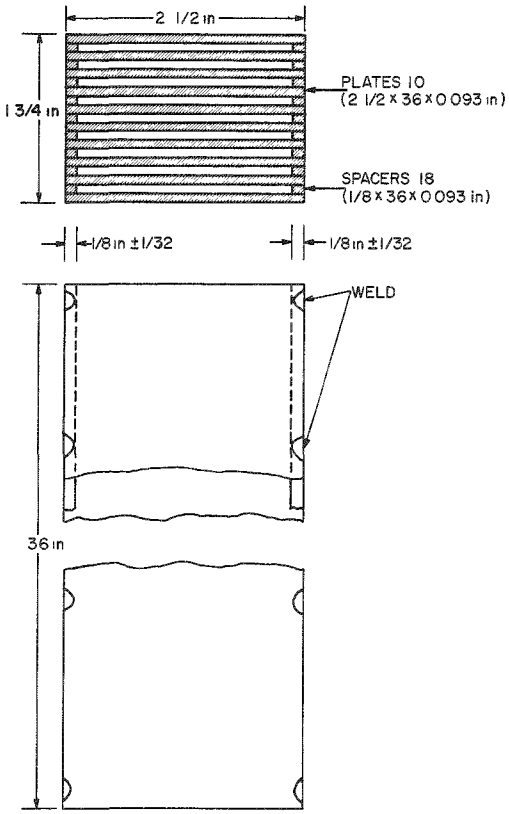

FIGURE 29
DISSOLUTION OF ZIRCALOY ELEMENT IN FUSED SALT:
OFF-GAS RECORD, RUN A-11

Dissolution Conditions
Temperature: 700 C
Salt Composition: 40 mol per cent ZrF_2-60 mol per cent NaF (with minor amounts of uranium, tin, iron, nickel, chromium fluorides)
HF Sparge Rate: Approx. 60 lb/hr

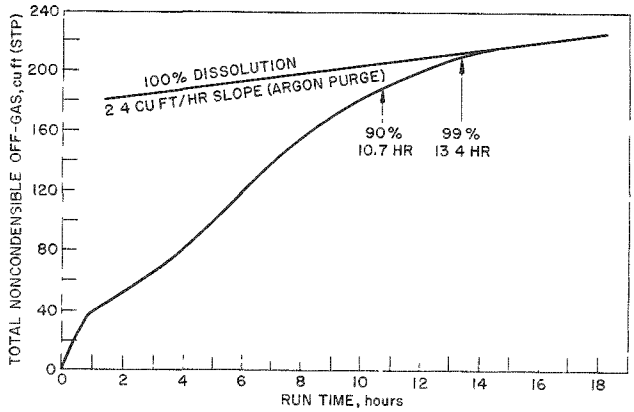

The concentration of the alloy constituents as fluorides in the fused salt under equilibrium conditions is the same as in the alloy. These are as follows, relative to zirconium in the fused salt: uranium, 1.0 per cent; tin, 1.6 per cent; iron, 0.12 per cent; chromium, 0.10 per cent; and nickel, 0.05 per cent. These materials were added to the salt charge as anhydrous fluorides. All concentrations were below the solubility limits in the salt. The total salt charge was 498 lb, with a zirconium content of 41.7 weight per cent. The element was completely submerged.

Salt samples before and after dissolution were analyzed by an X-ray spectral method to determine concentration changes in any of the above salt constituents. No change was noted except for nickel, which was substantially removed from the molten salt phase. It thus appears that nickel fluoride is reduced to metal by Zircaloy. Probably

continued sparging with hydrogen fluoride (after complete dissolution of the fuel element) would redissolve the nickel, although this was not investigated. It is possible that a metallic nickel deposit on the element surfaces contributed to the lower dissolution rate in Run A-11, since previous runs did not contain nickel fluoride in the fused salt.

Salt Holdup

The amount of salt holdup in the dissolver was determined during disassembly and inspection following completion of the dissolution runs. Salt holdup was found, as expected, in two zones: (1) salt remaining inside the graphite crucible at the bottom as a result of the bottom of the transfer line being slightly above the crucible bottom; and (2) salt frozen in the lampblack layer in the annulus outside the graphite crucible.

In the case of the salt residue after transfer, 31.2 lb of material remained. The use of a salt wash could dilute and remove uranium or fission products in this residue when necessary.

The salt in the lampblack insulating layer around the graphite crucible is a consequence of the porosity of the graphite. The dissolver utilized a frozen-wall principle of fused salt containment. By surrounding the graphite crucible with a $1\frac{1}{2}$-inch layer of tamped lampblack insulation, any penetrating fused salt would solidify before contacting the outer metal shell, which was cooled by normal air convection. In this way vapor containment was provided by the metal shell which was protected from salt corrosion by the lampblack layer. A sketch was shown in ANL-5858, page 25.

Upon examination of the dissolver after 2200 hours of exposure to molten salt, the frozen salt in the lampblack annulus showed the distribution given in Figure 30. Salt in the vertical sections was confined to a zone nearly exactly in the center of the annulus, with no visible salt in contact with either the graphite crucible or the metal shell. The same condition was found at the bottom annulus, with the exception that the solid salt layer passed over the top of the graphite support posts and filled the space between the support posts and the bottom of the crucible.

The dissolver crucible and shell is assembled from separate upper and lower sections. The salt layer in the annulus was thin in the wall of the top section; the thickness ranged from about $\frac{1}{16}$ inch to $\frac{3}{16}$ inch maximum. The salt layer was very fragile, being supported by packed lampblack on each side. It could not be determined whether the layer was fully continuous; it probably was not since it was not self-supporting even in small sections.

FIGURE 30

FROZEN SALT IN THE DISSOLVER LAMPBLACK LAYER

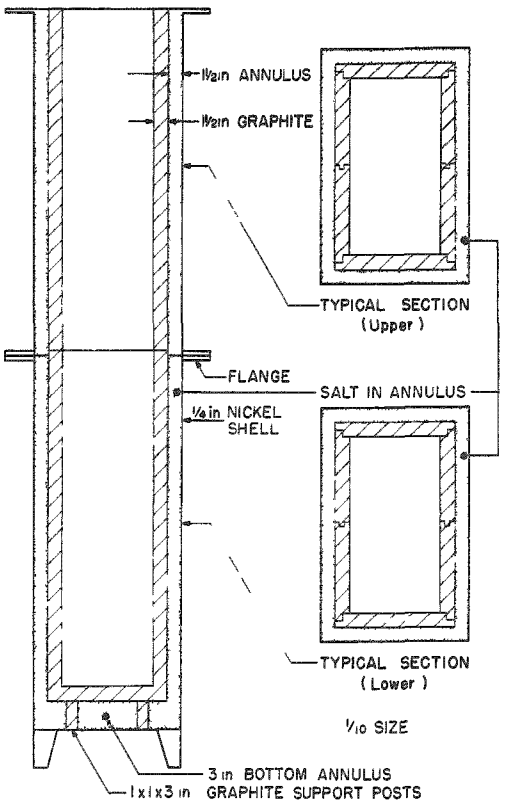

In the lower wall section, the salt was thicker, from about $\frac{3}{16}$ inch near the top to about $\frac{3}{8}$ inch for most of the lower part. These thicknesses apply to maximum values for a given side elevation.

In both the upper and lower sections, the salt in the annulus was found only in the two large side panels, and was thickest at the region of the longitudinal mortised joint at the center of the graphite slab. Near the bottom of the lower section, the salt layer extended around the corner into the end zone. At the bottom three inches of the lower section the salt layer was continuous around sides and ends. The thickness was about $\frac{3}{8}$ inch. The total amount of salt in the lampblack was approximately 30 lb.

The mechanism responsible for this distribution of salt in the lampblack layer is the following: The graphite slab was maintained at 700 C, well above the salt melting point. The temperature of the outside steel shell was measured at about 100 C. These surfaces bounded the lampblack layer. Therefore, the temperature gradient between these two would fall to the freezing point (ca 510 C) near the middle of the lampblack layer. During operation, salt vapor or liquid could move through the inner half of the lampblack layer, up to the freezing zone. Since the salt layer was found above the liquid level, and the inner, salt-free lampblack layer was found below the dissolver bottom, the chief method of salt transport in the lampblack layer may have been as vapor rather than as liquid. Further consideration of this point will be given following results of salt analysis. Since uranium tetrafluoride would not be transported in the vapor phase, the presence or absence of uranium may determine whether the transfer occurred as vapor or liquid. The dissolver crucible was made of ATL graphite. More nearly impervious grades of graphite are now available; their use should considerably reduce salt penetration.

Internal Damage to Graphite Components in Salt Remelt Test

Because of a volume change of approximately 25 per cent in the freezing and melting of sodium fluoride-zirconium fluoride salt, large stresses can be encountered in a vessel during remelt operation, depending on the vessel design and mode of heat transfer. While the most serious failure is a breaching of the container, experience with metal systems has shown that downline damage has been the most common difficulty. Remelt tests are particularly destructive to graphite, which is more brittle than metal. This test simulates the condition encountered in an emergency power failure of long duration. The heat capacity of the salt would preclude extensive freezing in power failures of short duration.

Following Run A-11, the salt in the graphite dissolver was allowed to freeze and cool to nearly room temperature, after which it was remelted and the salt transferred out. In order to remelt the salt it was necessary to adjust the position of the central electrodes in both heaters, and to make the transfer it was necessary to replace the salt exit line. After disassembly, the total damage was determined to be that shown in Figure 31.

FIGURE 31

INTERNAL DAMAGE TO GRAPHITE COMPONENTS IN SALT REMELT TEST

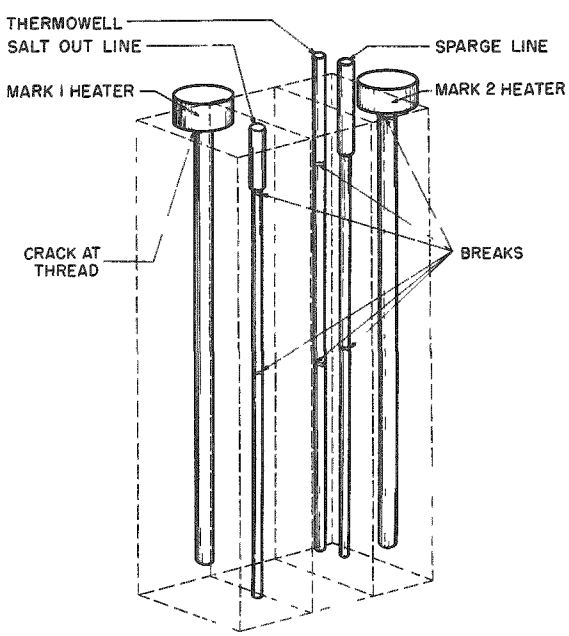

All downlines were broken in at least one place, and one of the heater shells had broken at the top. These components had $\frac{1}{4}$-inch walls with outer diameter ranging from 1 to $2\frac{3}{4}$-inches. It appears that such downlines, while resistant to vigorous salt sparging, are not capable of withstanding the freezing operation.

The heater rod adjustment previously mentioned was necessary to eliminate electrical shorting between rod and shell at the upper part of the rod. In the case of the Mark 2 heater this was most serious, since the broken shell leaned against the rod. In the case of the Mark 1 heater, a less serious short was involved from bowing of the center rod due to thermal expansion before the bottom had been freed from frozen salt.

The center rod of the Mark 1 heater was intact, but the center rod of the Mark 2 heater was broken at the bottom. This break probably was caused by a twisting force due to the heater shell fracture. Design changes which would make the damage less serious are (1) to provide emergency power systems to prevent freezing, (2) make the downlines easily replaceable, and (3) incorporation of downlines in the wall.

Effect of Salt and Electrical Current on Graphite Components

No effect on graphite of salt exposure up to 800 C was evident. Only the heater center rods exceed this temperature. In the case of the Mark 2 heater, which was an improved design in which salt was completely excluded from the central rod, no significant attack was apparent. In the Mark 1 heater, dimensional attack up to about $\frac{1}{8}$ inch was evident in the zone which contacted salt. Rod temperatures were probably above 1200 C. Possibly this graphite attack accompanies salt vaporization and arcing. Signs of arcing were observed where broken components shorted the normal electrical circuit, but this was not an important effect No arc attack was observable at the bottom slip joint of each heater rod, through which high currents (up to 800 amp) normally pass

The only other point of significant attack of graphite was the fuel element support plate, which also served as gas distributor. This was in the form of a cone machined in a block of graphite with a one-inch bottom hole for gas discharge. Deep grooves of rectangular section corresponding to the fuel element dimensions were cut into the graphite by erosion under the weight of the agitated fuel element. These grooves were of the order of two times the plate thickness and up to two inches deep. If this erosion rate continued, another 10 dissolutions would have completely penetrated the block. Graphite was used for the block material to facilitate machining. Probably the use of a harder material, such as carbon or better, molybdenum, would eliminate this problem.

Solids Carry-over and Entrapment in Off-gas Components

Off-gas from the dissolver passes through the following components in turn:

1. The 6-inch slug chute (approximately 2 feet in length)
2. The $1\frac{1}{2}$-inch exit pipe (approximately 4 feet in length)
3. The sodium fluoride-packed absorber (16-inch diameter, 18 inches high)
4. The porous carbon filters (5 units in parallel)
5. The hydrogen fluoride condenser.

The buildup of a hard salt cake at the entrance to the slug chute has been described previously. This required reaming out with the fuel element charger following each dissolution.

The $1\frac{1}{2}$-inch exit pipe has previously produced plugs of both powdery and hard-caked material. In the last two runs (10 and 11) no plug appeared, but a hard cake of up to $\frac{1}{4}$-inch had formed on the inside walls. Such a deposit requires periodic reaming, and the present design makes provision for this operation.

The sodium fluoride pellet bed had plugged previously at the bed inlet, and prior to Runs 10 and 11 the bed was replaced. A 10-mesh stainless steel screen, the full diameter of the vessel, was used to support the new bed. A 6-inch layer of $\frac{1}{2}$-inch stainless steel Raschig rings was laid on the bottom, followed by another screen and the sodium fluoride pellet charge of $9\frac{1}{2}$ inches. A screen was also used on top of the pellets. Following Run 11, the bed was removed from the top and screened to determine the fines pickup. The bottom two screens had disintegrated. The total fines collected in Runs 10 and 11 amounted to 8.1 lb. A preliminary size analysis by screening showed 30 per cent of these fines smaller than 60 mesh.

The porous carbon filters (National Carbon Co., Grade 60) had an effective porosity of 48 per cent with an average pore diameter of 33 microns. No appreciable increase in pressure drop across the filters was encountered in the entire series of runs, and therefore the filters were not cleaned before this final inspection. It was found that a soft cake, about $\frac{1}{8}$-inch thick, had deposited evenly on the filters. A total of 311 g collected over the period of 11 runs was removed from the filter chamber. About 80 per cent of this material had remained on the filter as a cake. A preliminary optical microscopic examination showed most of the particles to be below one micron.

Sampling and analysis of the hydrogen fluoride condensate received showed a very small amount of salt carry-over into the condenser, that is, about one gram in 11 runs.

From these data it appears that a $9\frac{1}{2}$-inch deep absorber bed with $\frac{3}{16}$-inch sodium fluoride pellet packing removes over 90 per cent of the fines produced in process operations, and that a 33-micron porosity filter, when precoated, removes even the smallest particles with high efficiency.

C. Conversion of Uranium Hexafluoride to Uranium Dioxide

(I. Knudsen, H. Hootman,* N. Levitz, M. Jones)

A fluid-bed process for the preparation of uranium dioxide from uranium hexafluoride is being studied for application to the production of ceramic-grade fuel. Two reaction procedures have been shown to be feasible: simultaneous pyrohydrolysis and reduction of uranium hexafluoride

---

*Resident Student Associate from Michigan College of Mining and Technology.

with steam and hydrogen in a single step, or the separate reactions using two steps. The newly formed material deposits as a dense coating on the particles of the bed. Conversion to solids has been about 99.99 per cent complete in both cases. Uranium hexafluoride rates up to 104 and 205 lb uranium/(hr)(sq ft reactor cross section) for the one-step and two-step procedures, respectively, have been used to date. The process appears promising in view of the high sintered densities, 94 to 97 per cent of theoretical, obtained in the pellet fabrication tests reported last quarter (ANL-6183, page 118). Work is now being concentrated on the two-step procedure because it offers greater flexibility in choice of reactor conditions and process control. Installation of a second three-inch diameter unit for further studies of the reduction step is almost complete. The equipment will be flexible enough to permit both fluid-bed and fixed- or moving-bed operation.

While making preparations for extended runs with the two-step procedure, an additional experiment on the simultaneous reaction process was conducted to determine the combined effects of high temperature, 650 C, and a high uranium hexafluoride rate, 125 g/min, equivalent to 217 lb/(hr) (sq ft reactor cross section). About 75 per cent excess steam and hydrogen were used at a mole ratio of 2 to 1. Approximately 1.3 bed equivalents were made in the 1.9-hour run. Because of the high feed rate, the final product had, as expected, a relatively high fluoride content, namely, 5.08 per cent. Analyses showed a uranium dioxide content of about 40 per cent the remainder being uranyl fluoride and U_3O_8. Based on past experience, a cleanup step, in which the powder was exposed to hydrogen and steam, would readily produce a powder of specification grade.

Reduction of Uranium Hexafluoride

Several attempts to carry out the hydrogen reduction of uranium hexafluoride to produce uranium tetrafluoride in a fluidized bed (see ANL-6183, page 122) were unsuccessful. Caking of the bed occurred shortly after introduction of uranium hexafluorides in tests at 500 C and 600 C, and was accompanied by loss of the hexafluoride in the off-gas. A run in which the starting bed was made up from green salt prepared by hydrofluorination of refined uranium dioxide (as in the previous successful run) ran smoothly for about one hour at feed rates up to 140 g/min before interruption by plugging of the off-gas line by uranium hexafluoride reaction products. No evidence of suspected uranium fluoride intermediates which may have caused these difficulties was found either by chemical or X-ray diffraction analyses. Further tests of this reaction have been postponed until completion of the pyrohydrolysis-reduction studies.

Pellet Fabrication Experiments

Samples of dioxide prepared by both the simultaneous reaction procedure and by the two-step process were ground to -325 mesh and pelleted and sintered.* Table 21 summarizes the powder properties, sintering conditions, and results. No binder was added to the powder and the sintering was done in dry hydrogen. Higher densities were obtained with the oxide prepared by the simultaneous reaction route, 96.7 per cent of theoretical as compared to 94.7 per cent for the two-step process. The powder which gave the better results was characterized by a higher fluoride content (540 ppm as compared to 70), somewhat higher surface area (3.4 sq m/g as compared to 2.9), and a slightly higher bulk density (4.5 g/cc as compared to 4.0), but it can only be conjectured that these contributed to any extent. These results are even more favorable than those reported last quarter, since the pelleting pressures were much less severe and a simpler overall procedure was used.

Table 21

RESULTS OF PELLET FABRICATION EXPERIMENTS ON URANIUM DIOXIDE PREPARED BY FLUID-BED CONVERSION OF URANIUM HEXAFLUORIDE

Material:
-325 mesh uranium dioxide
Pellet Size:
1/2 in. diam x 1/2 in. high
Pelleting Pressures:
8000 psi pre-press followed by 25 tsi isostatic
Sintering Procedure:
Heat to 1200 C overnight; increase temperature rapidly to 1700 C and hold for 2 hours; turn off heat and cool overnight

Run No.	Chemical Analysis before Sintering (w/o)			Surface Area by Methylene Blue Adsorption	Sintered Pellet Density
	(F)	(U^{+4})	(U^{+6})	(sq m/g)	(% Theor)
46 (simultaneous reaction procedure)	0.007	84.7	3.1	2.9	94.1 to 94.7
54 (two-step procedure)	0.054	86.8	1.8	3.4	96.6 to 96.9

*Work done by ANL Ceramics Group under J. Handwerk.

D. Multistage Fluidization
(K. Williamson, Jr.)

The second phase of the multistage fluidization column work, a mass transfer study of the effect of operating variables on the adsorption of water vapor by silica gel, is in progress. Determination of Murphree stage efficiences, the ratio of actual change in the average vapor composition accomplished by a stage to the change that would occur if the vapor stream reached equilibrium with the stage, will permit the calculation of a modified mass transfer coefficient by established procedures.[26]

---

[26]Treybal, R. E., Mass Transfer Operations, McGraw-Hill Book Co., Inc., New York, N. Y. (1955), p. 225.

III. REACTOR SAFETY

The oxidation, ignition, and combustion processes of uranium, zirconium, plutonium, and thorium are being studied to provide information to aid in minimizing the hazards associated with handling these metals.

In the continued study of the ignition of uranium it has been confirmed that an aggregate or array of pieces ignites at a considerably lower temperature than an individual piece of the same specific area. The condition of decreased heat loss from an interior piece surrounded by other pieces which are also generating heat by reaction may be the explanation of some of the uranium fires which have occurred.

The results of sample geometry studies on the ignition behavior of uranium powder show that constant ignition temperature values are obtained for a given particle size powder when the powder exceeds a critical height, independent of the container diameter. With fine spherical uranium powder (-200 + 230 mesh), the critical height was estimated to be approximately 1 to 2 millimeters based on geometry studies; intermediate powder (-80 + 100 mesh), approximately 3 millimeters; and coarse powder (-18 + 20 mesh), approximately 7 millimeters. Using experimental ignition temperatures and corresponding critical height values, one can estimate the effective thermal conductivities of uranium powder beds based on the Frank-Kamenetskii theory of thermal explosions. The calculated effective thermal conductivities were found to be in agreement with values expected for powders. Extrapolated critical height and effective thermal conductivity values can be used to estimate ignition temperatures over a wide range of specific area powders on the basis of Frank-Kamenetskii theory.

The use of nickel sulfate or zinc chloride solutions to decrease the pyrophoricity of uranium powder has been attempted. No evidence of increasing the ignition temperature of spherical or irregular 200 mesh powder or 0.13-mm (5-mil) foil was observed from burning-curve experiments after treatment with either solution.

Continued studies of the effects of halogenated hydrocarbons on the burning propagation of uranium and zirconium foils indicate the possibility of preventing continued combustion of individual zirconium foils or turnings thicker than 0.05 mm (2 mils). This may include the entire practical range of thicknesses of turnings. Preliminary studies of the effects of various gas contaminants on the burning propagation rates of a plutonium alloy indicate that dibromomethane (CH_2Br_2) and bromochloromethane (CH_2BrCl) are markedly effective in decreasing the burning rate.

A self-consistent mechanism for the isothermal oxidation of uranium has been devised; this explains most of the observations, such as linear rate, pressure dependence, and absence of higher oxides. The rate controlling step in the oxidation occurs on the exterior surface of the oxide and

may be ionization, dissociation, or surface diffusion. The increased rate of the second stage is attributed to the increased exterior surface area due to nodule growth and development.

The experimental program to determine rates of reaction of molten reactor fuel and cladding metals with water is continuing. The principal laboratory-scale method involves the rapid melting and dispersion of metal wires in a water or steam environment by a surge current from a bank of condensers. Construction of a high-pressure reaction cell has been completed. A series of runs with 60-mil zirconium wires was carried out in the new apparatus. The runs were made at initial metal temperatures in the region of the melting point. Solid zirconium at temperatures near the melting point reacted to the extent of four to five per cent with room temperature water (vapor pressure ca 0.5 psia). At saturated vapor pressures of from five to 230 psia, eight to nine per cent reaction occurred. Liquid metal at the melting point gave about eight per cent reaction with room temperature water, whereas 30 per cent reaction was observed at pressures from 16 to 140 psia.

The results indicate that the overall reaction depends strongly on the pressure of water vapor up to some point between 0.5 and 5 psia. A further increase in pressure causes no additional reaction. This limit suggests that the reaction becomes controlled by the transport of water vapor through a film of hydrogen generated by reaction. This latter process would be expected to be relatively independent of pressure.

A series of in-pile experiments was conducted in TREAT with oxide-core pins, cermet-core pins, and uranium wires. Each transient with the oxide-core pins resulted in rupturing and melting of the Zircaloy-2 jacket. The extent of metal-water reaction increased from 4.1 to 14.1 per cent as the reactor bursts became more energetic. It was concluded tentatively from the results of runs with the oxide-core, metal-clad pins that the Zircaloy-2 jacket was more readily ruptured and melted than the stainless steel jacket. It was also noted, by comparing runs with clad and unclad cermet-core pins, that dispersion of the fuel into particles is favored by the use of a jacket. An experiment with a fully enriched uranium wire, 34 mils in diameter, gave 28.3 per cent reaction with complete conversion of the metal into particles. Tests on a "radiation resistant" unbonded strain gage pressure transducer showed that the pickup did respond to the transient radiation and that the radiation signal was decreased by using an AC carrier system rather than DC.

A. Metal Oxidation and Ignition Kinetics
(J. G. Schnizlein)

1. Ignition Studies by the Burning-curve Method

The burning-curve procedure has been used extensively to provide reproducible data on the ignition characteristics of uranium. The sample, mounted on a thermocouple, is heated at a uniform rate of temperature increase (usually 10 deg per min) in a flowing oxidizing atmosphere. As the rate of reaction increases, the sample self-heats and finally ignites. A graphical intersection method is used to determine ignition temperature. The difference between furnace and sample temperature gives an indication of the rate of reaction over a wide temperature range. The burning-curve method has been used to define the effects of varied specific area, alloy additives, and gas composition on ignition temperature and maximum burning temperature (see ANL-5974, pages 10 through 39).

a. The Effect of Aggregation on the Ignition Temperature of Uranium
(J. G. Schnizlein, J. D. Bingle)

In the study of the ignition characteristics of uranium by the burning-curve method, the most important variable leading to lower ignition temperatures of single samples has been the specific area (surface area per gram) of the sample. Linear relationships have been found between the reciprocal absolute temperature of ignition as determined by burning curves in both air and oxygen, and the logarithm of the specific area of the sample (see Figure 32). These relationships were determined with individual samples of various sizes and shapes, e.g., cubes, slices, foils, and wires. In spite of the differing heat-loss characteristics of the variously shaped samples, the only deviation from linearity in the relationships was apparently caused by metallurgical variables.

However, the ignition-temperature measurements of smooth, spherical, uranium powders have shown that there is a decided lowering of ignition temperature as the amount of sample (of constant specific area) is increased up to a certain critical point (see, for example, ANL-6183, page 130). This has been attributed to the heat loss from the sample. A single particle, understandably, will lose proportionally much more heat to the surroundings than an aggregate or an array of particles. Figure 32 also includes ignition temperatures of the various sizes of spherical powders with sufficient mass to achieve relatively constant values (see Section 1c below).

In an extension of the burning-curve method it seemed appropriate to examine aggregates of the more massive uranium specimens used in establishing the specific area relationships described above. A pile of cubes might well be expected to ignite at a lower temperature than one

individual cube. It will be remembered (see ANL-5974, page 27) that simply shredding a piece of 0.03-mm uranium foil resulted in a 20-degree lowering of the ignition temperature of that foil.

FIGURE 32
RELATIONSHIP BETWEEN SAMPLE SPECIFIC AREA AND IGNITION TEMPERATURE FOR URANIUM IN AIR AND IN OXYGEN

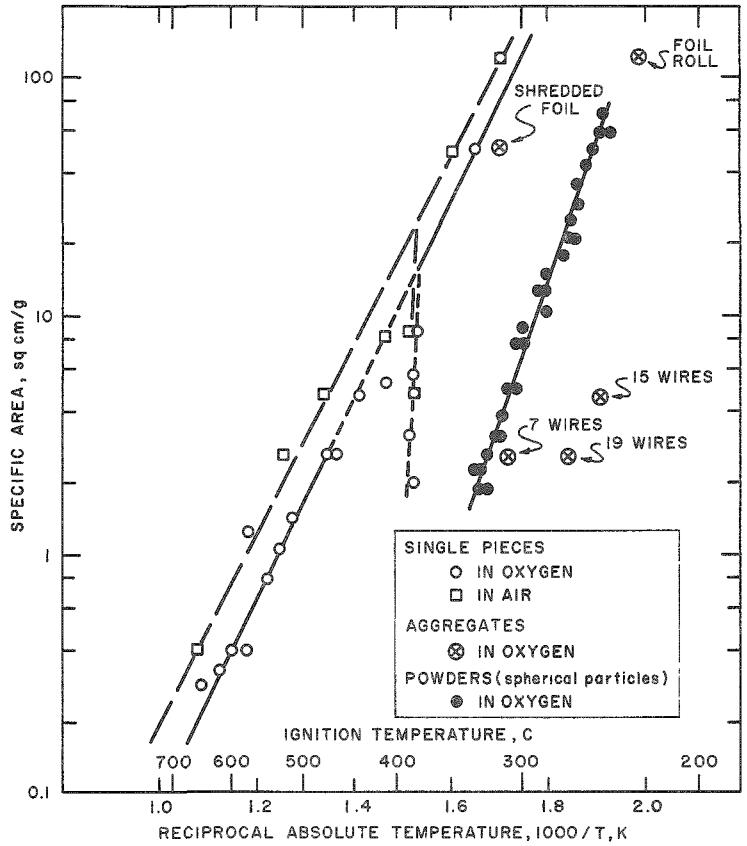

Several experiments have been carried out in oxygen using aggregates to test this hypothesis. Bundles of two sizes of uranium wires and a tightly rolled cylinder of 0.01-mm uranium foil were each subjected to burning-curve ignitions. The results of these runs are compared with the values obtained for individual specimens in Table 22 and are also indicated on Figure 34, page 144 (see ANL-6101, page 129 for detailed discussion of individual specimen data). It can be seen that a marked reduction in ignition temperatures can be achieved when sample aggregates are used; lower values are achieved than with the powders of equivalent specific area. It is believed that, under certain circumstances, the ignition temperatures of such aggregates might easily be even lower, because of unfavorable heat loss conditions. This may be a reasonable explanation for some uranium fires that have occurred.

Table 22

COMPARISON OF IGNITION TEMPERATURES OF INDIVIDUAL SPECIMENS AND AGGREGATES FOR URANIUM IN OXYGEN

Sample	Ignition Temperature[a] (C)
0.47-mm diameter wire	
one wire	435
bound bundle of 15 wires	250
0.83-mm diameter wire	
one wire	460
bound bundle of 7 wires	310
bound bundle of 19 wires	270
0.01-mm thick foil	
one piece	315
bound cylinder (~8 thicknesses) of foil	230

[a] Determined by the burning-curve method in 1200 cc/min flowing oxygen.

Another experiment of a similar nature was carried out with the irregular uranium powder obtained from the Sylvania-Corning Nuclear Corporation. It will be recalled (see ANL-6101, page 130) that this powder gave an ignition temperature in oxygen of 140 C in the unsieved condition (density of 5.5 g/cc). However, by compacting this powder in a dry box by means of a hand pill press, pellets were made with a density of approximately 7.8 g/cc; these yielded an ignition temperature of 120 C under the same conditions in a graphite crucible. This experiment emphasizes the complexity of heat-loss considerations for powders and other aggregates.

Experiments in air will be made to provide information which may be of greater applicability to the practical problem. There is, however, good reason to believe that runs in air will yield substantially the same ignition temperatures as those in oxygen. It is unlikely that reactions leading to ignition are extensive or rapid enough to generate a diffusion barrier of nitrogen between the oxygen of the air and the metal.

b. The Effect of Halogenated Hydrocarbons and Metal Salts on Ignition
(L. Leibowitz, J. D. Bingle, L. W. Mishler)

It has been observed (ANL-6145, pages 137 and 142) that the presence in air of certain halogenated hydrocarbons, e.g., ethyl bromide, dibromomethane, difluorodibromomethane, chlorobromomethane, and carbon tetrachloride, causes a significant decrease of burning-propagation rate with both uranium and zirconium foil strips. These substances also cause a marked decrease of the burning-curve ignition temperature of uranium; however, recent measurements of shielded ignition temperatures of both uranium and zirconium show no such decrease (see Table 23 for uranium data).

Table 23

THE EFFECT OF HALOGENATED HYDROCARBONS ON THE BURNING PROPERTIES OF URANIUM FOILS IN AIR
(SMF-5 uranium foil strips, 0.13 x 3.0 x 70 mm)

	Burning Propagation Rate (cm/sec)	Ignition Temperature (C)	
		Burning-curve Technique	Shielded Technique[a]
Polished metal run in pure air	0.56	400	330
Polished metal run in air-3% CH_2Br_2	0.37	275	335
Polished metal run in air-5% CF_2Br_2	0.35	290	-
Metal pretreated in argon-5% CF_2Br_2 at 300 C and subsequently run in pure air	-	420	-

[a] Sample temperature when air is introduced. This temperature is, therefore, low by the amount of self-heating which the sample undergoes prior to ignition.

Because of the possible existence of a reaction between uranium and the halogenated hydrocarbons, some experiments were conducted to examine the effect on uranium ignition of pretreatment with difluorodibromomethane. Specimens of uranium foil were heated at about 300 C for 30 minutes in an atmosphere of 5 per cent difluorodibromomethane

in argon. Burning-curve ignition tests were then carried out in pure air. The pertinent ignition temperature data are also included in Table 23. It is noteworthy that this pretreatment gave only a slight increase in ignition temperature. The effect of pretreatment is apparently quite different from that of having the halogenated hydrocarbon present during ignition.

These apparently conflicting results, namely, that halogenated hydrocarbons lower the propagation rate, lower the burning-curve ignition temperature, and have no effect on the shielded ignition temperature, simply illustrate that these tests do not measure the same thing.

Additional work, both experimental and theoretical, is needed to clarify the means by which these agents affect ignition and burning. The practical utility of these agents in the control of metal fires must also be investigated further.

It has been reported[27,28] that, if uranium powder is treated with a zinc chloride or nickel sulfate solution, its pyrophoricity is reduced. A number of attempts to verify this report have been made.

Samples of 0.13-mm thick uranium foil and both spherical and irregular -200 + 230 mesh uranium powders were vigorously agitated for thirty minutes at room temperature in 200-gram per liter zinc chloride solution of adjusted pH 3 to 4. The samples were washed with water, dried, and subjected to burning-curve ignition heats in oxygen. No increase in ignition temperature was observed.

Since the specific method of the original workers was not available, a treatment similar to the zinc chloride method was used with nickel sulfate. Samples were placed in 200-gram per liter, pH 2 nickel sulfate solutions and left undisturbed for one hour. Other metal specimens were placed in solutions of the same concentration and agitated for thirty minutes. These samples were washed, dried, and subjected to burning-curve ignition tests in oxygen. In no case was a significant change in ignition temperature observed. If further information indicates that the treatments were incorrectly applied or that the burning-curve ignition test in oxygen is inappropriate, additional tests may be done.

---

[27] Accary, A. and Blum, P., Nuclear Power (British) 5, 122 (1960) (Reference to French patent PV 700823).

[28] Dubuisson, J., Houyvet, A., LeBoulbin, E., Lucas, R., and Moranville, C., Rev. Met. 56 55 (1959).

c. Ignition of Uranium Powder
(M. Tetenbaum, L. W. Mishler, G. Klepac*)

The effect of sample geometry on the ignition behavior in oxygen of a coarse (low specific area) spherical uranium powder (-18 +20 mesh),** and an intermediate fraction (-80 +100 mesh) was investigated during this period. Previous studies (see ANL-6183, page 132) with fine spherical uranium powder (-200 +230 mesh) showed that the minimum height required to yield constant values of ignition temperature was approximately 1 to 2 mm. This height has been termed the critical height and was found to be practically independent of container diameter.

The results with coarse and intermediate fractions are shown in Figures 33 and 34. From the data plotted in these figures, the critical height for -18 +20 mesh spherical uranium powder was estimated to be approximately 7 mm, and for -80 +100 mesh, approximately 3 mm. The variation of critical height with particle diameter or effective thermal conductivities of the packed bed is in the expected direction (see Section 1d). The somewhat higher ignition temperatures obtained with crucibles of smaller diameter (see Figure 33) can be attributed to radial heat losses.

FIGURE 33

EFFECT OF SAMPLE HEIGHT ON THE IGNITION TEMPERATURE OF -18 +20 MESH SPHERICAL URANIUM POWDER

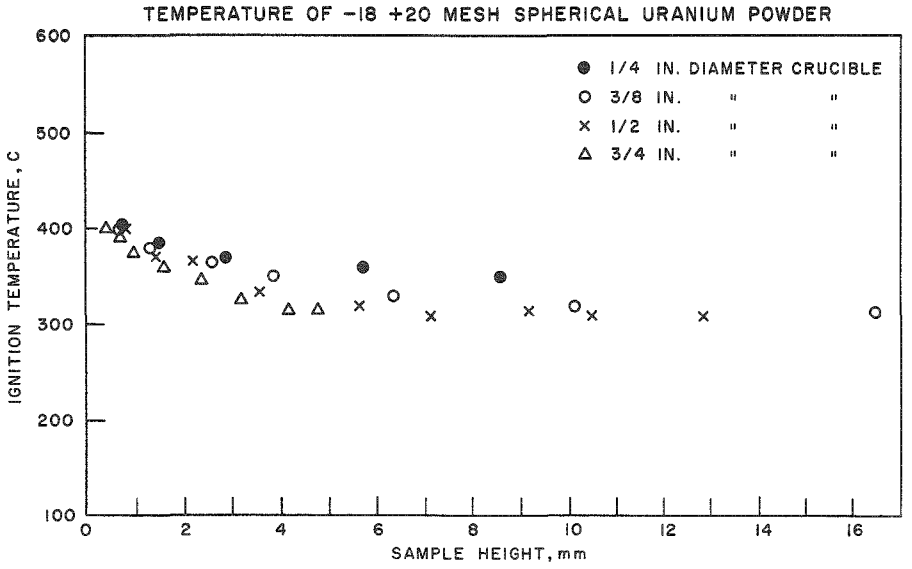

* Summer employee

** Particle diameters based on sieve opening of screens retaining particles, i.e., -18 +20 mesh, d = 840 microns; -80 +100 mesh, d = 149 microns; -210 +230 mesh, d = 62 microns.

FIGURE 34
EFFECT OF SAMPLE HEIGHT ON THE IGNITION TEMPERATURE OF −80 +100 MESH SPHERICAL URANIUM POWDER

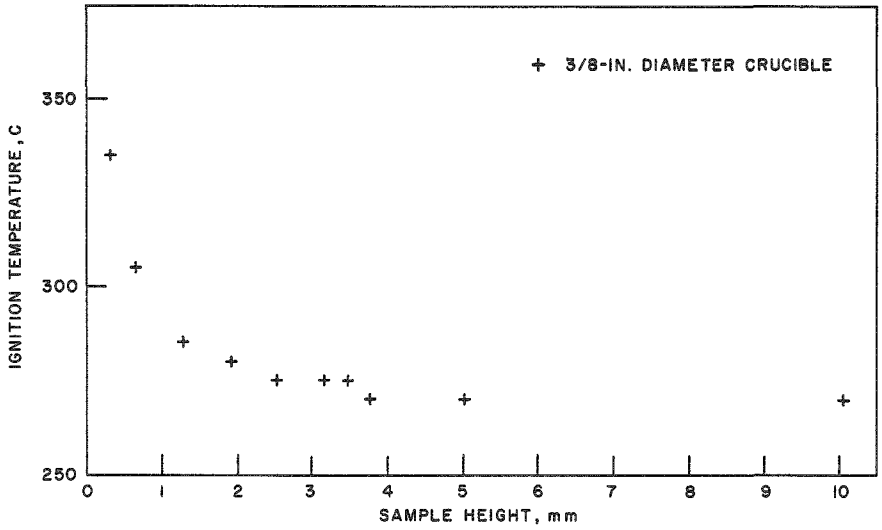

Study of the ignition behavior of uranium powder has continued during this quarter with investigations over a wide range of specific area fractions. The results to date (in oxygen) with sieved and subsieve spherical uranium fractions (including data previously reported in ANL-6183, page 134) are shown in Figure 35. The ignition temperature values shown in Figure 35 represent constant ignition values (as shown by sample geometry studies), independent of sample size for each specific area (calculated from particle diameter) powder. The apparent energy of activation derived from a least-squares treatment of the data was found to be 26.9 $\pm$ 3.2 kcal/mole, assuming linear oxidation kinetics. [Note: The first-stage linear rate activation energy obtained from the isothermal oxidation of uranium metal in pure oxygen was 18.7 kcal/mole (see ANL-5974, page 51).]

The subsieve spherical fractions were separated by the Armour Research Foundation using toluene as the elutriating agent. The size distributions, by number, are shown in Table 24. The median diameters of samples 2, 3, 5, and 6 were 12.5, 20, 33, and 37 microns, respectively. The sphericity of the particles was verified microscopically.

From Figure 35 it is seen that the subsieve fractions yield ignition temperatures approximately 15 to 25 degrees C higher than the values expected from extrapolation of the least-squares line obtained with sieved fractions. It is possible that the subsieve powders were partially oxidized during the separation procedure. These powders will be examined further.

FIGURE 35

EFFECT OF SPECIFIC AREA OF SPHERICAL URANIUM POWDERS ON EXPERIMENTAL IGNITION TEMPERATURES

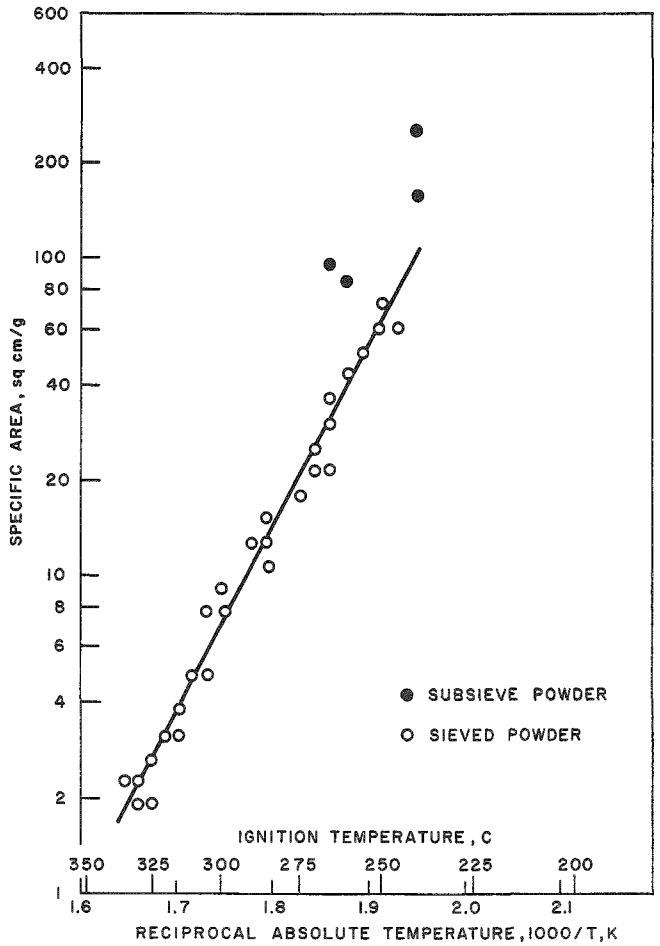

Table 24

SIZE DISTRIBUTION OF SUBSIEVE SPHERICAL URANIUM POWDER

Diameter d (microns)	Per cent by number of particles smaller than diameter d			
	Sample 2	Sample 3	Sample 5	Sample 6
6.0	0.98			
8.0	2.3			
10.0	12.4			
12.5	39.4			
15.0	76.5			
16.3	-	5.6	-	0.4
20.0	100	-	-	-
21.8		70.6	0.9	1.2
27.0		98.5	6.9	3.7
34.0		100	59.5	10.3
41.0			100	87.5
54.0				99.5
68.0				100

Ignition temperatures were also obtained on subsieve irregular powder separated at Armour Research Foundation. The size distributions, by number, are shown in Table 25. The median diameters of samples 1 through 4 were 6.2, 15.8, 22.5, and 28.0 microns, respectively. The four samples of irregular uranium powder gave ignition temperature values of approximately 150 C. By extrapolating the data obtained with spherical powder to this temperature (see Figure 35, extrapolation not shown) we find that the specific area of these subsieve irregular powders should be of the order of 27,000 sq cm/gram. An area determination of sample one using the BET method with ethylene as adsorbate (measurement performed by Armour Research Foundation) gave a value of 10,500 sq cm/gram. This corresponds to an ignition temperature of ~160 C (extrapolated value from Figure 35). The lower ignition temperature obtained experimentally can be attributed to the strong effect of the particles higher specific area present in the subsieve samples on ignition temperature (see ANL-6183, page 130).

Table 25

SIZE DISTRIBUTION OF SUBSIEVE IRREGULAR URANIUM POWDER
(Separated at Armour Research Foundation)

Diameter d (microns)	Per cent by number of particles smaller than diameter d			
	Sample 1	Sample 2	Sample 3	Sample 4
2.7	13.6	1.7		
5.4	36.3	3.0	0.4	
10.9	78.5	5.6	3.1	
16.3	99.3	49.0	7.3	1.2
21.8	100	89.6	42.0	6.7
27.2		99.5	82.5	46.6
34.0		100	99.5	89.5
40.8			100	97.5
54.4				100

The smallest particle diameter measured in these subsieve samples was 2.7 microns. This corresponds to a specific area of only 1175 sq cm/gram based on spherical geometry. The roughness factor for these powders might be crudely estimated to be 10 to 20.

d. Application of Frank-Kamenetskii Theory to Powder Ignition
(M. Tetenbaum)

Attempts were made to use the thermal theory of explosions originally proposed by Semenoff[29] and developed by Frank-Kamenetskii[30] to estimate ignition parameters of uranium powders. The treatment of Frank-Kamenetskii was originally applied to gas mixtures in vessels. Briefly, the critical condition for ignition is given by

$$\lambda \nabla^2 T = -QnK \quad , \tag{1}$$

where T is the sample temperature, λ the thermal conductivity, Q the heat of reaction, n the concentration, K the rate constant, and ∇^2 the Laplacian operator. For a first-order reaction with energy of activation E, and for $K = Ae^{-E/RT}$,

$$\nabla^2 T = \frac{-Q}{\lambda} nAe^{-E/RT} \quad . \tag{2}$$

According to Frank-Kemenetskii, Equation 2 permits a solution which is everywhere finite when δ, a dimensionless constant, is less than a fixed value. For δ greater than this value, no steady state exists, and such a condition may result in explosion. This critical condition is given by

$$\delta = \frac{Q}{\lambda} \frac{E}{RT_0^2} r^2 nAe^{-E/RT_0} \quad , \tag{3}$$

where T_0 is the temperature of the walls of the vessel and r is the significant geometric dimension of the vessel. The critical values of δ obtained by Frank-Kamenetskii, and also by Chambré,[31] are 0.88 for an infinite plane-parallel sided vessel, 2.0 for a cylindrical vessel of length much greater than its radius, and 3.32 for a spherical vessel.

The application of Frank-Kamenetskii theory to metal powder systems is apparently not treated in the literature. Frank-Kamenetskii discusses briefly and qualitatively the application of his theory to the combustion of carbon in fluidized beds, and for some strongly heterogeneous catalytic processes, such as the contact oxidation of alcohols to aldehydes or ketones. The treatment discussed below in some detail for

---

[29] Semenoff, N., Z. Physik. Chem. 42, 571 (1928).

[30] Frank-Kamenetskii, D. A., Acta. Physiochim. USSR 10, 365 (1939).

[31] Chambré, P., J. Chem. Phys. 20, 1795 (1952).

uranium powder ignition, therefore, may represent a novel approach to the general problem of metal powder ignition on the basis of Frank-Kamenetskii theory.

As an example, the ignition temperature of -18 +20 mesh spherical uranium powder will be estimated. For the concentration term in Equation 3, we shall use the surface area of the particles per unit volume of packed bed. Therefore, n = 42.2 sq cm/cc for a bulk density of 11.2 g/cc. The first-stage linear rate constants (ANL-5974, page 51) are E = 18700 cal/mole and A = 5.17 g/(sq cm)(sec). Other terms are Q = 8100 cal/g oxygen, R = 1.99 cal/(mole)(deg), and n = 42.2 sq cm/cc. The significant geometric dimension of the powder sample was estimated from sample geometry measurements (see above) which showed that the minimum height of -18 +20 mesh spherical uranium powder required for constant ignition temperature was approximately 7 millimeters. Therefore r = 0.35 cm. The effective thermal conductivity value of $\lambda = 8.7 \times 10^{-4}$ cal/(cm)(sec)(C) obtained by Kimura[32] with 350 to 450-micron lead powder, may be used, since the thermal conductivity of lead is almost identical to that of uranium. Inserting these values in Equation 3 for $\delta = 0.88$, and solving for the ignition temperature, yields T_0 (calc) = 316 C. The experimental value is 310 C.

It would be instructive, however, to calculate by means of Frank-Kamenetskii theory the effective thermal conductivity of the uranium powders using measured critical heights and ignition temperatures, and to compare the calculated conductivities with experimental and theoretical packed bed values based on heat transfer considerations. The results obtained are shown below

Mesh	Critical Height, mm	Calculated Effective Thermal Conductivity, cal/(cm)(sec)(C)
-200 +230 (fine)	1.5	9.1×10^{-5}
-80 +100 (intermediate)	3	2.4×10^{-4}
-18 + 20 (coarse)	7	6.7×10^{-4}

The calculated values appear to be consistent with the effective thermal conductivity values expected for powders, and for the variation of power conductivity with particle size. As noted above, the thermal conductivity of lead is almost identical to that of uranium. Also, the measurements of the effective thermal conductivity of spherical lead powder (350 to 450 microns) by Kimura[32] gave a value of 8.71×10^{-4} cal/(cm)(sec)(C). Measurements by Schumann and Voss[33] on 2500-micron lead powder resulted in an effective thermal conductivity value of 1.0×10^{-3} cal/(cm)(sec)(C).

[32]Kimura, M., Chem. Eng. (Japan), 21, 472 (1957).

[33]Schumann, T. E. W., and Voss, V., Fuel 13, 249 (1934).

The theoretical equations derived by Kunii and Smith[34] were used to estimate the effective thermal conductivity of uranium powder. Their analysis show that the effective thermal conductivity of a packed bed is a function of the properties of the solid and fluid phases, the void fractions and, if thermal radiation is important, the emissivity, mean temperature, and diameter of the solid particles. Using their equations for the case of uranium powder (void fraction = 0.42), an effective thermal conductivity value of 1.2×10^{-3} cal/(cm)(sec)(C) was calculated. A similar value was obtained using the semi-empirical relationship developed by Deissler and Einn.[35]

These values compare favorably with the conductivity values obtained with coarse spherical uranium powder on the basis of ignition temperature data and the Frank-Kamenetskii theory of thermal explosions.

Using the above concepts, it is possible to estimate ignition temperatures for a variety of specific area powders using the Frank-Kamenetskii theory. The critical heights of very fine and very coarse uranium powder were calculated using limiting ignition temperature values for these powders, and estimated effective thermal conductivities. For example, with -270 +325 mesh spherical uranium powder, the constant ignition temperature values measured were 245 C. Estimating an effective thermal conductivity value of $\sim 10^{-4}$ cal/(cm)(sec)(C) (the conductivity value for oxygen gas in the pores at 245 C), one can calculate a critical height value of 1.5 mm. With a very coarse powder, -10 +12 mesh spherical uranium for example, an effective thermal conductivity value of 10^{-3} cal/(cm)(sec)(C) is assumed, based on the measurements of Schumann and Voss on 2500-micron lead powder. [The calculated value of 1.2×10^{-3} cal/(cm)(sec)(C) based on the equations of Kunii and Smith could also have been used.] Using the constant ignition temperature value of 330 C obtained with -10 +12 mesh spherical uranium powder, a critical height of 9.5 mm was calculated. From a plot of specific area versus the above calculated critical height and estimated thermal conductivity values, one can calculate ignition temperatures for a variety of specific area powders using Frank-Kamenetskii theory of thermal explosions. The results are shown in Table 26. The values in parentheses in column 4 are the experimental critical heights derived from sample geometry measurements. The ignition temperatures calculated for various mesh size uranium powders using the Frank-Kamenetskii theory show good agreement with the experimental results. The above treatment should hold for ignition behavior in air, since it is anticipated that experimental ignition temperature values will be the same in air and oxygen atmospheres.

---

[34] Kunii, D., and Smith, J. M., A.I.Ch.E. Journal 6, 71 (1960).

[35] Deissler, R. G., and Einn, C. S., Natl. Advisory Comm. Aeronaut., RM E52605 (1952).

Table 26

THEORETICAL IGNITION TEMPERATURES OF URANIUM BASED ON FRANK-KAMENETSKII THEORY OF THERMAL EXPLOSIONS

Mesh	Specific Area of Particle (sq cm/g)	Estimated Thermal Conductivity [cal/(cm)(sec)(C)]	Interpolated Critical Height[a] (mm)	Ignition Temperature (C)	
				Calculated	Experimental
-200 +230	51.2	1.2×10^{-4}	1.8 (1.5)	253	255
-120 +140	30.2	1.7×10^{-4}	2.4	263	260
-80 +100	21.3	2.2×10^{-4}	2.9 (3.0)	270	270
-40 +45	9.06	3.7×10^{-4}	4.3	290	295
-18 +20	3.78	6.4×10^{-4}	6.8 (7.0)	310	310
-12 +14	2.25	8.9×10^{-4}	8.8	325	320

[a] Experimental values in parentheses.

2. Burning-propagation Studies

The burning-propagation rate is the rate of advance of a combustion zone along a metal foil or wire. It has been a useful and reproducible quantity for investigating the nature of metal burning as well as for judging the influence of various factors in the combustion process.

A motion picture record is made of the advance of combustion along a metal strip. The metal is ignited at one end by an electrically heated platinum wire. Linear propagation rates are readily obtained from these motion pictures. The effect of sample size and geometry, gas composition, pressure, and ambient temperature are being examined for zirconium, uranium, and plutonium.

It has been found that decreasing the thickness of foil strips will markedly increase the burning-propagation rate and that addition of small quantities (about 5 per cent by volume) of various halogenated hydrocarbons to air will significantly lower the burning-propagation rate.

a. Burning Propagation at Elevated Ambient Temperatures (L. Leibowitz, L. W. Mishler)

All the work carried out thus far on burning propagation has been with the surrounding atmosphere at room temperature, the only source of heat being the metal combustion itself. Since in many practical cases there may be considerable heating of the atmosphere, it seemed of interest to explore, on a laboratory scale, the effect of this additional variable. Quite massive samples of uranium, for example, have actually burned in heated atmospheres, although present information, based on propagation data with the surroundings at room temperature, indicate that

this is unlikely. The way in which external heat alters the burning characteristics of metals is important in practical cases and of considerable theoretical significance.

An apparatus suitable for measurement of burning-propagation velocities at elevated ambient temperature has been constructed and tested for satisfactory operation. This consists simply of a glass tube covered with a furnace which contains openings for photographing the event. Provision is made for sample mounting, ignition, and control of gas flow. For the experiments at elevated temperatures, the foil strips are protected during heatup by a stream of argon (1500 cc/min) purified by passage over hot copper turnings and Molecular Sieves. This purified argon contains less than 0.02 per cent of both oxygen and water. The furnace temperature is raised to the desired value while argon is flowing. At this point air at the desired flow rate is introduced and, after a certain time (the delay time), the sample is ignited.

Before reliable measurements of the heating effect could be made, it was necessary to test several experimental variables and to check the agreement of burning-propagation rates obtained using the new cell with the rates previously reported. Gas flow rate, gas flow direction, and delay time were examined for two different zirconium and two different uranium foils and were found to have no effect on measured propagation rates within the ranges tested (20 and 60-second delay times, and 0.65 to 3.03-cm/sec linear flow velocities). Measurements made with the foils and the surrounding air at 150 C showed no effect on either 0.02-mm thick zirconium foil or 0.13-mm thick uranium foil. These preliminary results are summarized in Table 27. This study will be continued at higher ambient temperatures.

Table 27

BURNING-PROPAGATION RATES AT ELEVATED AMBIENT TEMPERATURES

Ambient Temperature (C)		Burning-propagation Rate (cm/sec)
Uranium 0.13 x 3.0-mm foil strips		
24[a]	previous value (5-run average)	0.56 ± 0.02
24[a]	6-run average	0.52 ± 0.03
150	8-run average	0.57 ± 0.03
Zirconium 0.02 x 5.0-mm foil strips		
24[a]	previous value (1 run)	1.5
24[a]	7-run average	1.4 ± 0.2
150	8-run average	1.5 ± 0.2

[a] Average room temperature.

b. The Effect of Halogenated Hydrocarbons on Burning Propagation

(L. Leibowitz, J. D. Bingle, D. F. Fischer)

It has been observed that the presence in air of various halogenated hydrocarbons will significantly lower the burning-propagation rate of uranium and zirconium foil strips (ANL-6145, pages 137 and 142). Similar experiments using plutonium are reported here along with additional experiments with zirconium.

Pure zirconium foils, 0.13-mm thick, would not sustain burning in air containing either 5 per cent chlorobromomethane or 5 per cent chlorodifluoromethane (Freon-22). Even the 14.9 atom per cent titanium-zirconium alloy which normally burns rapidly in air would not sustain burning in air containing 5 per cent chlorodifluoromethane, and showed a significantly reduced propagation rate, burning temperature, and burning-zone length in air containing 5 per cent chlorobromomethane.

Several additional runs have been carried out with thinner zirconium foils to determine more exactly what rate changes may be expected and also what thickness of foil can actually be kept from burning by these compounds. All the data available are given in Table 28. These tests indicate that burning of zirconium foils as thin as 0.05 mm (2 mils) can be prevented by the presence of about 3 per cent dibromomethane.

Table 28

THE EFFECT OF VARIOUS GAS CONTAMINANTS ON THE BURNING-PROPAGATION RATE IN AIR OF ZIRCONIUM AND PLUTONIUM FOILS

		Burning Propagation Rate, cm/sec for Indicated Foil Samples						
Contaminant	Concentration (volume %)	Zr (0.13 x 0.6 mm)	Zr (0.05 x 0.85 mm)	Zr (0.02 x 0.9 mm)	Zr (0.007 x 1.0 mm)	2.12 a/o Ti-Zr Alloy (0.13 x 0.6 mm)	14.9 a/o Ti-Zr Alloy (0.12 x 0.6 mm)	2 a/o Al-Pu Alloy (0.25 x 1 mm)
None		0.46 (1.3)[a]	1.07 (2.3)	3.23 (2.0)	19.5	0.84 (2.6)	1.06 (3.7)	0.45
He	5.0	0.48 (1.2)				0.85 (2.2)		0.49
He	10.0		1.01 (2.1)					0.45
O_3	1.0	0.57 (1.2)						
H_2O	3.1	0.54 (1.4)				0.81 (2.6)		0.44
CO_2	5.0	0.43 (1.1)						0.44
CH_2Br_2	3.2		N.P.[b]					N.P.
CF_2Br_2	3.3				10.9			
CF_2Br_2	6.3			0.76 (0.8)	9.3			
CF_2Br_2	8.9			0.84 (0.8)	7.9			
CH_2BrCl	5.2	N.P.				N.P.	0.71 (1.7)	0.26[c]
CH_2BrCl	11.8							N.P.[d]
CHF_2Cl	5.0	N.P.		1.98 (1.4)		N.P.	N.P.	0.52
CHF_2Cl	10.0							0.52

[a] Numbers in parenthesis are burning zone length, cm.

[b] N.P. - Propagation was not sustained.

[c] The burning propagation progressed for approximately one cm when the sample started to break and bend.

[d] In one case, upon disassembly of the apparatus it was observed that a surface reaction had occurred over the entire foil, despite the fact that the photographic record (for 30 sec after ignition) showed that the ignited end had cooled and ceased to burn perceptibly.

Preliminary experiments have been made to study the effect of various gas contaminants on the burning-propagation rate of plutonium in air. For this work a 2 atom per cent aluminum-plutonium alloy foil (0.25 mm thick) is being used since pure plutonium foils are not yet available. The data obtained thus far are also included in Table 28. As is evident from the table, no reductions in rate were seen with helium, water vapor, carbon dioxide, or chlorodifluoromethane (Freon-22). However, for the other two compounds tested, dibromomethane and chlorobromomethane, marked influences on propagation rate were found.

Dibromomethane was the most effective contaminant. Four burning-propagation experiments were attempted in which burning was not sustained. After ignition in the chlorobromomethane tests, the burning had progressed approximately one cm when the sample broke and bent and the propagation ceased. In uncontaminated air, burning will usually propagate the entire length of the sample even if breaking or bending should occur. In the two experiments attempted, the burning-propagation rates over the portion of sample that did burn were 0.23 and 0.29 cm/sec.

Work in this area is continuing to clarify the mechanism of the effects involved and to provide information which may help in the selection of compounds for tests on a larger scale.

3. The Kinetics of Uranium Oxidation
(L. Leibowitz)

Measurements of the rate of oxidation of electropolished uranium have been made in oxygen in the temperature range from 125 to 250 C and at pressures from 20 to 800 mm. This information has already been reported (ANL-5974, pages 39 to 86) and it has been proposed that the course of the reaction is best described by two linear rates (see Figure 36). Linear metal-oxidation kinetics generally are considered to indicate continuous cracking of the oxide film, yielding a diffusion barrier of constant thickness leading to initially parabolic oxidation kinetics followed by a linear rate law.[36]

Considerations of the oxide species formed, the dependence of rate on oxygen pressure, the effect of polishing method on the kinetics, absence of an adequate fit above about 200 C of the initial phases of the oxidation to parabolic kinetics, and the independence of the course of the process on interruption (ANL-6183, page 140), make the cracking hypothesis an unlikely one.

---

[36] Haycock, E. W., J. Electrochem. Soc. 106, 771 (1959).

FIGURE 36

RATE-DETERMINING DATA FOR A TYPICAL URANIUM OXIDATION RUN (150 C and 50 mm oxygen pressure)

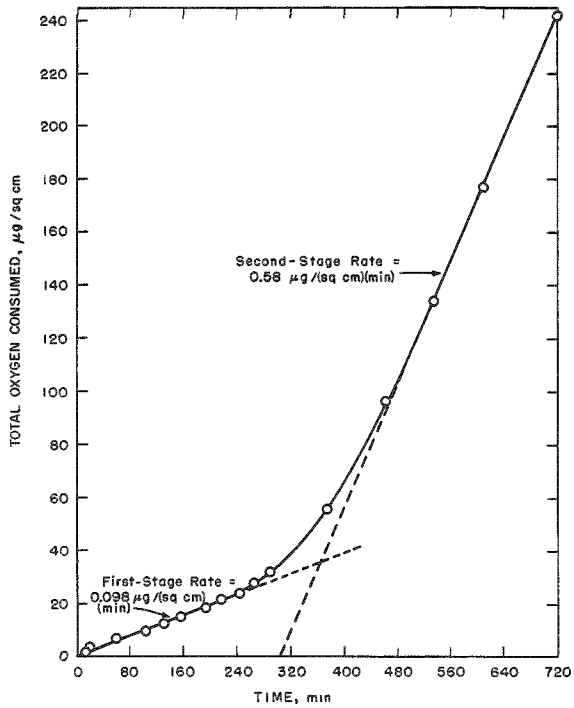

An alternative proposal to explain linear oxidation kinetics is that the rate-controlling step is at the oxide surface. In this case a linear oxidation would be observed from the start, provided the true oxide surface area remained constant. Microscopic studies of the metal surface during the course of the oxidation have indeed shown a marked roughening to occur at the same time as the onset of the second stage (ANL-6101, page 138). Quantitative discussion of this point is not possible because of the absence of surface area measurements.

If the overall rate of oxidation is controlled by the rate of a process occurring in the outer oxide surface, then we would expect

$$v = kC_a \quad ,$$

where v is the oxidation rate, C_a the concentration of adsorbed oxygen, and k the rate constant. For an energetically heterogeneous surface Halsey[37] has shown that

$$\theta = C\chi_m \left[\left(\frac{P}{P^0}\right)^{\left\{RT/\chi_m (1-rT)\right\}}\right] \quad ,$$

[37] Halsey, G. D., Advances in Catalysis, Vol. IV, Academic Press, Inc., New York (1952). p. 259.

where θ is the fractional coverage, P the pressure, T the temperature, R the gas constant, and P^0, χ_m, C, and r are constants related to the entropy and surface energy of the adsorption. Assuming θ to be proportional to C_a and using the usual Arrhenius expression for the reaction rate constant, we have

$$v = C\chi_m A e^{-E/RT} \left[\left(\frac{P}{P^0} \right)^{\left\{ RT/\chi_m (1-rT) \right\}} \right] .$$

The experimental values of v are reasonably well represented by this expression with a value of 10.7 kcal/mole for E. Overall activation energies presented in ANL-5974, page 52, vary from 12.4 kcal/mole at 20 mm O_2 to 18.7 kcal/mole at 800 mm. These values, however, include the pressure and temperature-dependent factor $P^{1/n}$ which is not included in the constant value 10.7 kcal/mole. It is thus possible to develop a reasonable and consistent description of the oxidation process in these terms. This material is the subject of a publication currently being prepared.

B. Metal-Water Reactions
(L. Baker, M. Kilpatrick*)

1. Laboratory Studies: Condenser-discharge Method
(L. Baker, R. Warchal)

The condenser-discharge experiment is an attempt to obtain fundamental rate data under experimental conditions similar to those encountered during a serious accident in a nuclear reactor. Either a nuclear runaway or a sudden loss of coolant during operation of a water-cooled reactor could result in contact between very hot fuel and cladding metals with water or steam and might involve fine particles. The condenser-discharge experiment simulates the limiting case of a nuclear incident in that the heating time is very short and very fine metal particles are produced.

In the condenser-discharge experiment metal wires are rapidly melted and dispersed in a water-filled cell by a surge current from a bank of condensers. The energy input to the wire is used to calculate the initial reaction temperature. The transient pressure measures reaction rate, the amount of hydrogen generated gives the extent of reaction, and the particle size of the residue indicates the surface area exposed to reaction.

Analysis of the results is based on one of the usual laws of metal oxidation (parabolic rate law) and on calculations of the rate of heat loss. In this way an attempt is made to interpret experimental work as it proceeds. It is expected that final isothermal rate constants will be

---

* Consultant, Illinois Institute of Technology (presently Senior Chemist, Emeritus, Argonne National Laboratory).

available at the conclusion of experimental work. The final constants should be applicable to a detailed analysis of particular reactor conditions.

a. High-pressure Apparatus

The construction of the high-pressure reaction cell has been completed. There were several unusual requirements in the design of a reaction cell for metal-water reaction studies by the condenser-discharge method. The cell had to be both vacuum and pressure tight, and able to withstand thermal cycling. In addition, insulated leads of high current-carrying capacity had to be brought into the cell. A diagram of the apparatus is shown in Figure 37. The reaction cell is constructed of stainless steel; copper wire and rods are used as conductors within the cell. The discharge current is carried into the cell through eight 14-gauge wires using a large Conax Fitting. An additional machined ring was silver-soldered to the standard fitting to hold either a Teflon or a silver-plated stainless steel O-ring to effect a positive seal. An SLM piezoelectric pressure transducer is mounted in a similar fashion on the lower end of the cell. The face of the transducer is therefore under the water level.

FIGURE 37
HIGH-PRESSURE CONDENSER-DISCHARGE APPARATUS

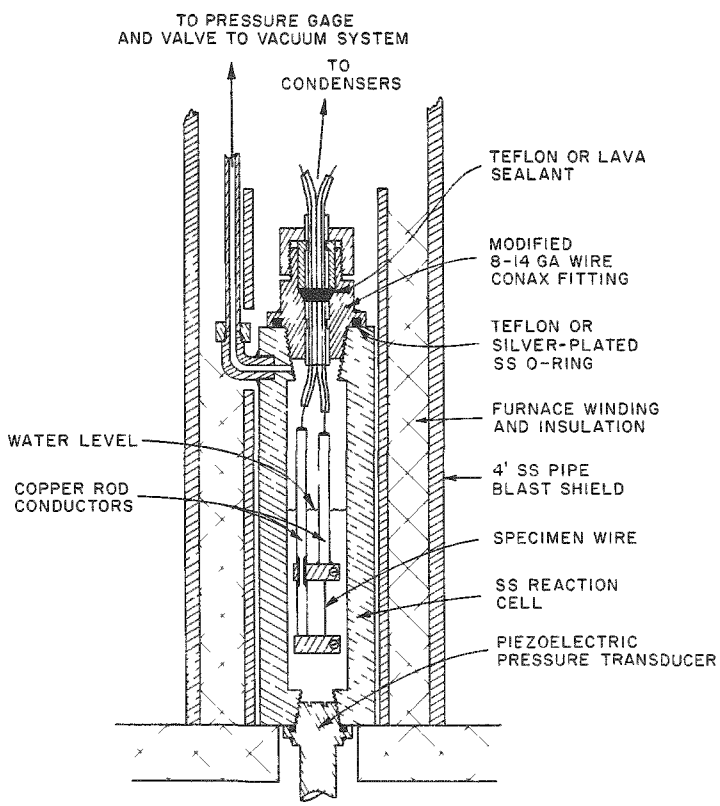

The reaction cell after assembly and leak testing is lowered into a furnace constructed of two sizes of stainless steel pipe. The annulus between the two pipes contains nichrome heater windings, asbestos insulation, and control thermocouples. Both pipes act as blast shields in the event of an accident and would direct any projectiles either up or down.

The cell is connected to a high-pressure Bourdon gage and through a high-pressure valve to a vacuum system. The cell and associated tubing are evacuated to a pressure of 0.1 micron. Degassed water (50 cc) is then poured in by the rotation of a ground glass joint. The high-pressure components are then sealed off from the glass vacuum system by closing the high-pressure valve. Heating the cell causes about 10 cc of the water to distill from the cell to fill the Bourdon tube and connecting lines with liquid water.

Following a run, the reaction cell is cooled to below 100 C; the hydrogen generated by reaction is removed from the cell to a calibrated volume by a Toepler pump. The quantity of gas collected is determined by a pressure measurement and the purity (absence of air in-leakage) by diffusion through a heated palladium tube.

b. Zirconium Runs at High Pressure

A series of runs was completed in the new high-pressure cell, using 60-mil zirconium wires. The results of the runs are given in Table 29 and plotted in Figure 38.

Table 29

ZIRCONIUM-WATER REACTION DATA FROM
HIGH-PRESSURE CONDENSER-DISCHARGE APPARATUS

Apparatus: see Figure 37
Zirconium used: 60-mil wires

Run	Energy Input (cal/g)	Calc Temp (C) and Phys State	Satd Vapor Pressure of Ambient Water (psia)	Per cent Reaction	Appearance of Residue
192	144	1700, Solid	0.5[a]	2.6	Intact
194	150	1800, Solid	5.2	8.6	Distorted
191	150	1800, Solid	22	7.8	Distorted
193	157	1840, 5% Liq	0.5[a]	3.7	Intact
195	157	1840, 5% Liq	230	9.0	Distorted
190	161	1840, 10% Liq	225	8.5	Distorted
189	169	1840, 25% Liq	215	14.5	Some Particles
197	201	1840, 75% Liq	0.5[a]	11.2	Coarse Particles
196	204	1840, 80% Liq	16	31.5	Coarse Particles
188	206	1840, 85% Liq	154	30.7	Coarse Particles

[a] Ambient water at room temperature.

FIGURE 38
RESULTS OF CONDENSER-DISCHARGE RUNS
WITH 60-MIL ZIRCONIUM WIRES
(nonexplosive runs)

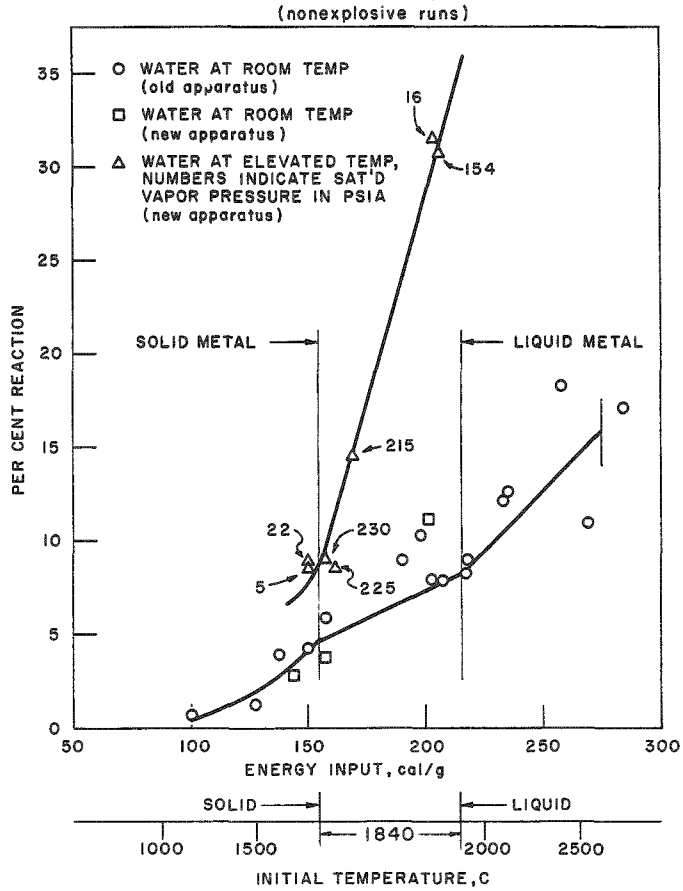

Figure 38 includes the nonexplosive runs that were reported previously for 60-mil zirconium wires heated in water at room temperature. Wires are mounted vertically in the new cell. They were mounted horizontally in the room-temperature cell. Several runs were made at room temperature in the new cell and were found to agree with results obtained previously using the horizontal mounting. Data for these runs are given in Figure 38.

The results of runs made in water at elevated pressure indicate that the overall reaction depends strongly on the pressure of water vapor up to some point between 0.5 psia (the nominal vapor pressure of water at room temperature) and 5 psia. A further increase in pressure causes no additional reaction. This limit suggests that the reaction becomes controlled by the transport of water vapor through a hydrogen film generated by reaction. This latter process would be expected to be relatively independent of pressure. None of the runs showed an explosive pressure rise.

Studies at elevated pressure will include runs with saturated water at pressures up to about 1500 psi and runs with undercooled water under inert gas pressure.

A theoretical model of a metal-water reaction is under development. This model will include the effect of a gaseous diffusion step in the overall process. Numerical solutions to the equations describing the overall process will be obtained by computer methods.

2. In-pile Testing in TREAT Reactor*
(R. C. Liimatainen, R. O. Ivins, M. Deerwester, F. Testa, J. DeAcetis**)

The program of studying metal-water reactions by simulating actual nuclear meltdown incidents is continuing. The previous report (ANL-6183, page 145) gave results on oxide-core fuel pins clad in aluminum and stainless steel; also, data were given on aluminum-uranium oxide cermet pins clad in Zircaloy-2. During this quarter, experiments were conducted on oxide-core pins clad in Zircaloy-2 and on cermet-core pins. These current results are summarized in Table 30.

Table 30

SUMMARY OF RESULTS OF RECENT IN-PILE METAL-WATER EXPERIMENTS

Oxide-core composition, w/o: 81.51 ZrO_2, 9.06 CaO, 8.69 U_3O_8, 0.74 Al_2O_3, 93% enriched

Cermet core composition, w/o: 90 Al, 10 U_3O_8, 95 % enriched

Wire composition, w/o: 100 U, 95% enriched

	CEN Transient Number							
	28	29	30	31	34	35	37	38
Fuel Pin								
core material	oxide	oxide	oxide	cermet	U	U	cermet	cermet
clad material	Zr-2	Zr-2	Zr-2	Zr-2	none	none	none	none
overall diameter, inches	0.38	0.38	0.38	0.38	0.034	0.034	0.31	0.31
overall length, inches	1.05	1.05	1.05	1.80	1.00	1.00	0.70	0.70
Environment of Pin	in Liq H_2O	in Liq H_2O	in Liq H_2O	in Liq H_2O	He	in Liq H_2O	in Liq H_2O	in Liq H_2O
Reactor Characteristics								
Mw-sec burst	320	385	550	525	98	47	440	235
Mw peak power	1630	1600	1690	1610	570	306	1650	1000
ms period	60	63	62	63	96	96	65	84
nvt Thermal Dose	2.4×10^{14}	6.0×10^{14}	10×10^{14}	8.6×10^{14}	0.97×10^{14}	0.30×10^{14}	5.7×10^{14}	3.2×10^{14}
Per Cent of Metal Reacted with Water	4.1	8.0	14.0	7.0	-	28.3	0.7	3.8
Peak Metal Surface Temp, C	840	925	~350	1210	>1500	~1500	>1500	>1500
Peak Pressure, psi	186	36	-	-	-	25	300 spike	90 spike
Appearance of Fuel Pin after Transient	hole melted in jacket; particles produced	hole melted in jacket; particles produced	hole melted in jacket; particles produced	pin melted into 3 fragments plus particles	melted into particles plus fine powder	melted into particles	melted	melted

In Experiments CEN-28, -29, and -30, the energy input to the Zircaloy-2 clad, oxide-core pins was progressively increased while the reactor period and peak power were held essentially constant. An interesting point in these three runs with the Zircaloy-2 clad, oxide-core pins

* The cooperation of the TREAT operating personnel of the Idaho Division, and of the ANL Metallurgy Division is gratefully acknowledged.

** Summer employee.

is the increase in the extent of the metal-water reaction as the reactor burst becomes more energetic. As the burst energy increases from 320 to 385 to 550 megawatt seconds, the per cent of metal reacted with the water goes from 4.1 to 8.0 to 14.0, respectively. The fission energy input is calculated to be 266 calories per gram of core at 320 megawatt seconds and 460 calories per gram at 550 megawatt seconds from measurements on other oxide core pins. Figures 39, 40, and 41 show the changes that occurred in these oxide-core pins. Another point of interest is a comparison of runs on Zircaloy-2 clad, oxide-core pins with stainless steel-clad oxide-core pins. In Experiment CEN-21 (ANL-6183, page 146), it was observed that a 420-megawatt-second burst did not rupture or melt the stainless steel jacket. For comparison, bursts of 320 Mw-sec (CEN-28) and 385 Mw-sec (CEN-29) did rupture and melt the central portion of the Zircaloy-2 jacket. To achieve melting of the stainless steel jacket, a burst of 560 megawatt-seconds was required (CEN-24 in ANL-6183, page 147). These comparisons are made for runs in which the reactor energy was systematically varied while the reactor period and peak power were held as constant as possible at 60 milliseconds and 1600 megawatt seconds, respectively.

FIGURE 39

ZIRCALOY-2-JACKETED, OXIDE-CORE PIN AFTER TRANSIENT CEN-28

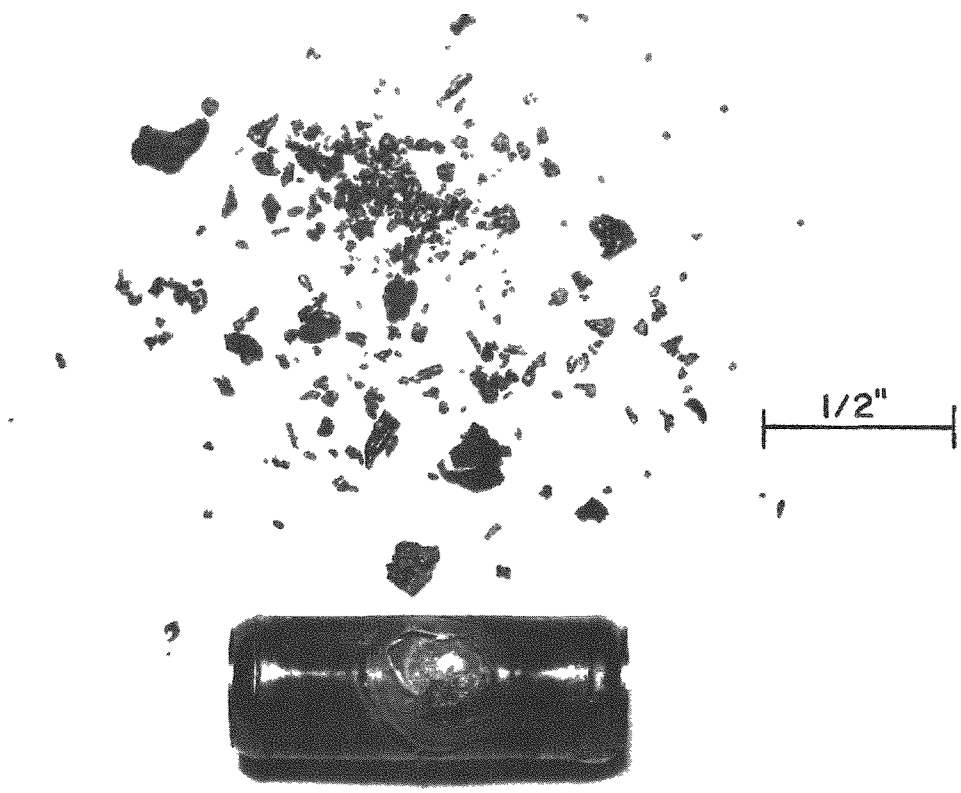

FIGURE 40

ZIRCALOY-2-JACKETED, OXIDE-CORE PIN AFTER TRANSIENT CEN-29

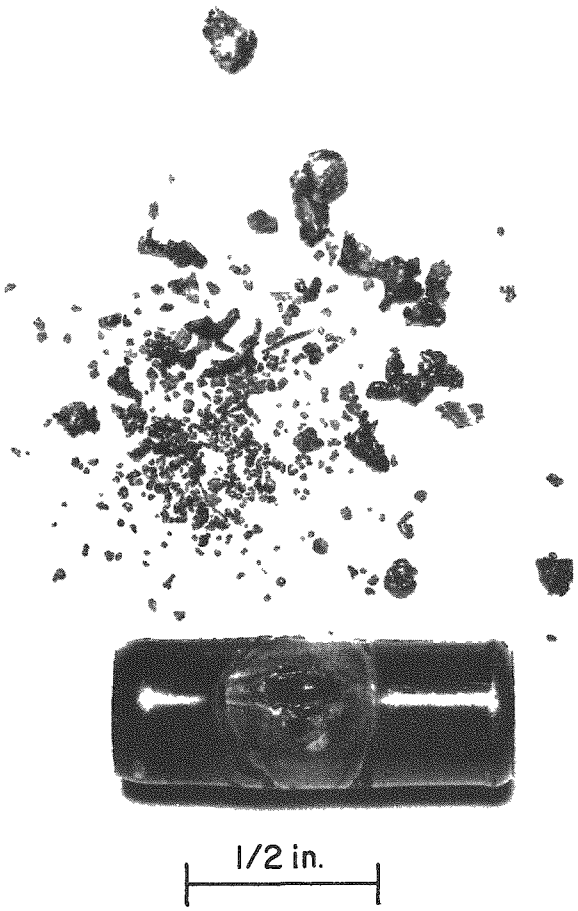

FIGURE 41

ZIRCALOY-2-JACKETED, OXIDE-CORE PIN AFTER TRANSIENT CEN-30

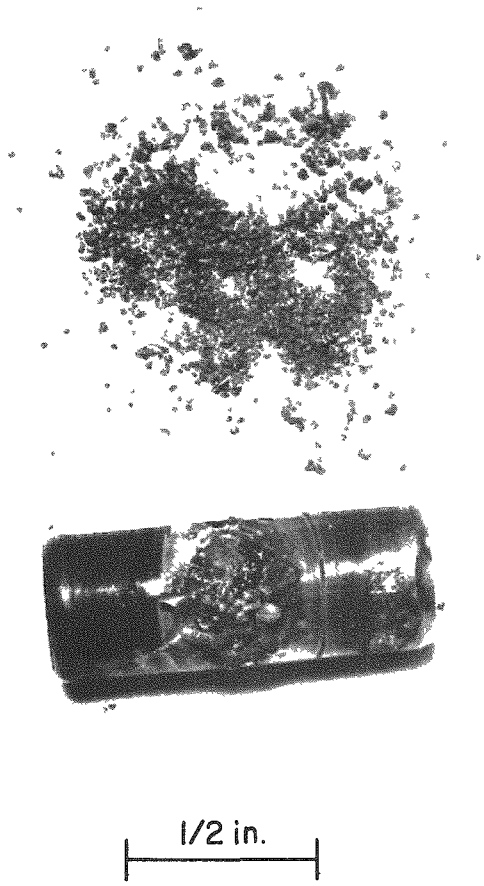

Observation has shown that a lower burst energy (~350 Mw-sec) will rupture or melt a Zircaloy-2-clad pin whereas the same energy does not rupture or melt a stainless steel jacket. This is probably due to contributions of the following two factors:

1. Heat transfers from the core by conduction through Zircaloy-2 occur more slowly than through stainless steel for the same temperature gradient; the values of thermal conductivity are $K_{Zr-2} = 0.03$ and $K_{SS} = 0.17$ cal/(cm)(sec)(C).

2. Stainless steel is the stronger metal at high temperatures; at 500 C, the values of ultimate strength are 72,000 psi for SS-304 and 32,000 psi for Zircaloy-2.

An X-ray photograph was taken of the pin from CEN-28; the photograph (Figure 42) clearly shows voids and nonuniformities in the oxide core. Radiographs of the unirradiated pins, as manufactured, showed no voids or nonuniformities in the core (Figure 35, page 146, ANL-6183).

FIGURE 42

RADIOGRAPH OF ZIRCALOY-2-JACKETED, OXIDE-CORE FUEL PIN AFTER TRANSIENT CEN-28

To obtain a closer comparison between the condenser-discharge and in-pile techniques, two experiments (CEN-34,-35 in Table 30) were run on 34-mil diameter uranium wires, 93 per cent enriched. CEN-34 was a base-line run in a helium atmosphere; the 98-megawatt-second burst resulted in complete conversion of the pin into particles and a fine dust. In CEN-35, a run with liquid water, the 47-megawatt-second burst (273 calories per gram uranium estimated energy input) also melted the pin into particles; the extent of the uranium-water reaction was 28.3 per cent as computed from the reaction

$$U + 2H_2O \longrightarrow UO_2 + 2H_2$$

and the measured hydrogen evolution. It is of interest to recall that it was previously found in Run CEN-11, made with a uranium pin, that an energy input of 182 calories per gram gave 10.1 per cent metal-water reaction (ANL-6145, page 167); thus, it appears that the positive dependence of extent of reaction on energy input is continuing.

Three runs were made on cermet-core pins to extend the information on the aluminum-water reaction. By comparing the physical changes in the jacketed pin from Run CEN-31 (Figure 43) with the unjacketed pins from Runs CEN-37 and -38 (Figures 44 and 45), there is evidence that the breakup of the pin into particles is favored by the presence of the jacket.

FIGURE 43

CERMET-CORE, ZIRCALOY-2-JACKETED PIN AFTER TRANSIENT CEN-31

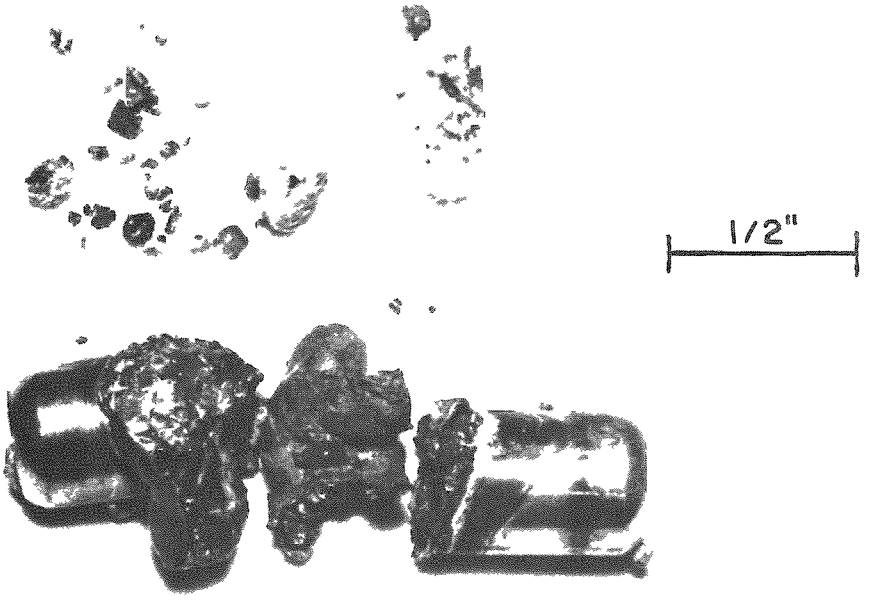

FIGURE 44

UNUSED PIN AND MELTED PIN FROM TRANSIENT CEN-37, UNJACKETED CERMET

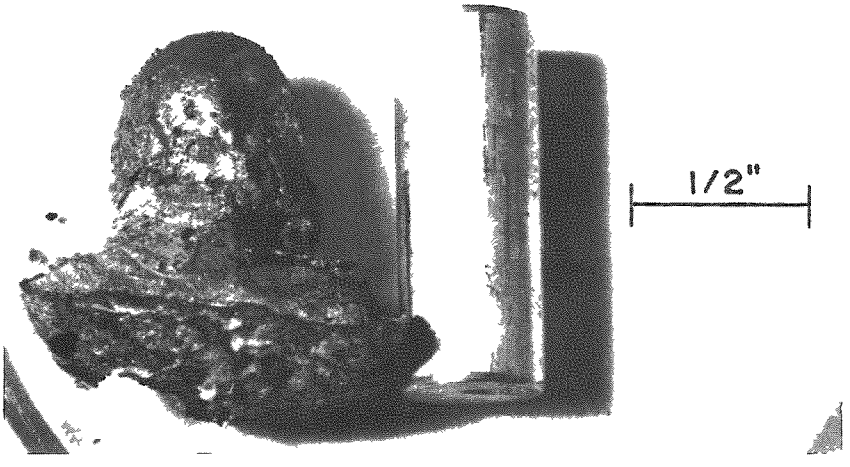

FIGURE 45

UNUSED PIN AND MELTED PIN FROM TRANSIENT CEN-38, UNJACKETED CERMET

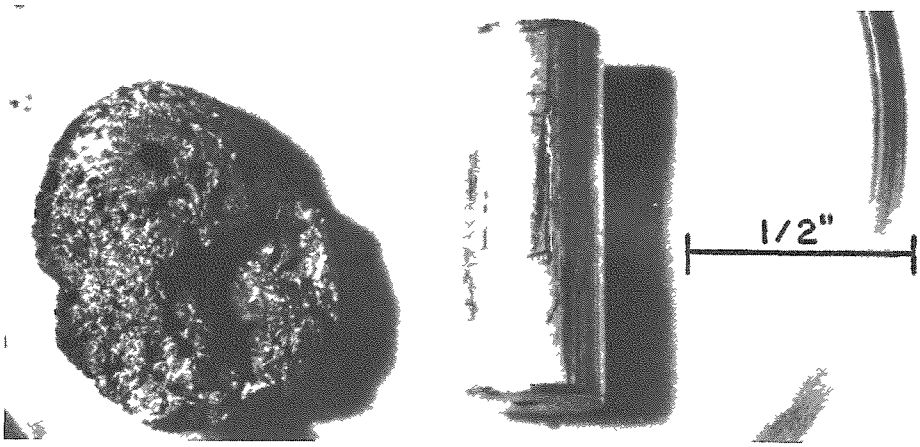

Evidently, when a hole is ruptured or melted in the Zircaloy-2 jacket, this allows the confined molten core to come out in a relatively fine spray. Reference can also be made to Runs CEN-25 and -26 (ANL-6183, page 147) in which there was extensive particle formation from the jacketed cermet-core pins. This observation of the influence of the jacket is also consistent with results from previous "pin-hole" experiments where dispersion of the uranium metal core was achieved by drilling 3- or 15-mil diameter holes in a Zircaloy-2 jacket (ANL-6145, page 166).

Experiments CEN-37 and -38 are also of interest since these are the only two runs in which a pressure "spike" has been observed. The oscillograph record from Experiment CEN-37 is shown in Figure 46.

FIGURE 46
OSCILLOGRAPH RECORD OF CEN-38

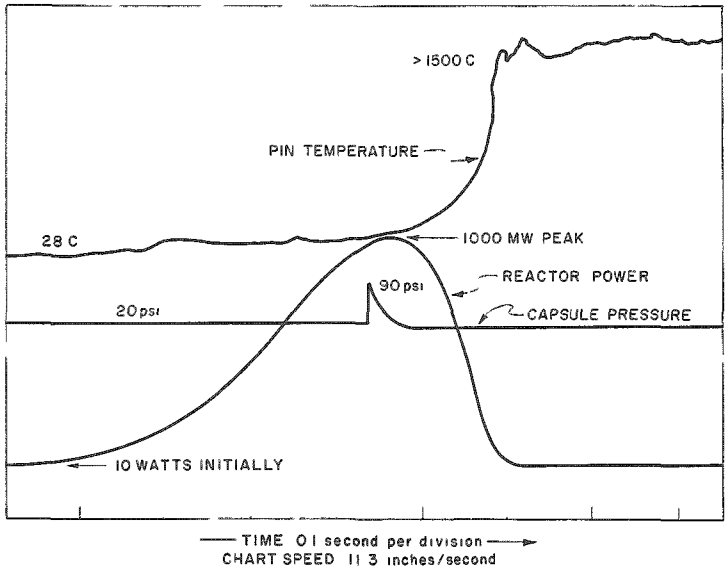

Two energetic transients, Runs CEN-27a and b, were made to determine the output of a new "radiation-resistant" (no organic materials) strain gage pressure transducer and to observe the radiolysis of water An autoclave containing water, gold foils, and 20 psia of helium was fitted with an unbonded strain gage pressure pickup type CEC-4-326-0180. The transducer had a range of 0 to 1000 psi and a full-scale output of 23.2 millivolts with a five-volt input. A 515-Mw-sec (0.75×10^{15} nvt_{th}), 1740-Mw peak, 61-ms period transient gave a maximum change in output corresponding to 160 psi with a DC input. A 500-Mw-sec (0.78×10^{15} nvt_{th}), 1670-Mw peak, 63-ms period transient gave a change of 80 psi with an AC carrier system. The pressure on the transducer was actually constant at 20 psia. It is apparent that the burst does influence the transducer. It is also evident that a considerable reduction in the radiation output results by using AC excitation rather than DC.

Another observation was on the radiolysis of water subjected to a total integrated power of 1015 Mw-sec (1.53×10^{15} nvt_{th}). The mass spectrometer analysis showed 2.4 volume per cent hydrogen in the vapor phase inside the autoclave. This corresponds to 0.007 per cent decomposition (2×10^{-4} g mole hydrogen produced) of the water as calculated from the reaction

$$2H_2O \rightarrow H_2O_2 + H_2 \quad .$$

For comparison, a previous test, CEN-7, with 25-Mw-sec energy, showed no observable decomposition of the water. A calculation based on the G value of 0.75 molecule of water decomposed per 100-ev absorbed energy and an estimated dose of 10^6 rad gives a predicted value of 3.8×10^{-4} mole hydrogen produced. This is in reasonable agreement with the observed value of 2×10^{-4} mole hydrogen.

IV. REACTOR CHEMISTRY

Data are being obtained on the neutron capture cross sections of uranium-236 as a function of neutron energy. Cross sections have been obtained for neutron energies ranging from 0.475 to 1.74 Mev.

The Slurrex Reactor chemical supporting program has been terminated and a final report is being written.

The Reactor Decontamination Program has two main objectives: 1) to determine the seriousness of fuel ruptures in boiling water reactors as measured by the quantities of radioactive materials which deposit in the steam system, and 2) to determine what methods of decontamination can be used to remove these deposited activities. The first study is being made with a stainless steel loop that simulates the action of a boiling water reactor into which mixed fission products can be introduced. Quantities and types of fission products deposited are monitored by several methods. A second study is being made in the laboratory to find suitable means of removing deposited activities.

In the laboratory, it was found that the presence of oxygen during the contamination portion of an experiment reduced the effectiveness of decontamination by the alkaline permanganate-citrate procedure. This effect was greater when 30-day-cooled uranium was used for the experiment than it was with 60-day-cooled uranium.

Corrosion studies of various turbine materials in typical decontamination reagents were continued. Pitting of chromium-molybdenum steels in citrate solutions adjusted to pH 10 was found to be appreciably reduced when hexamethylene tetramine was added as an inhibitor.

In additional laboratory runs, analyses of supernatant and uranium dioxide particulate produced by reaction of irradiated uranium with water at high temperature indicated that two per cent of the total gamma activity was extracted into the water. The latter contained 52 per cent of the iodine, 0.9 per cent of the cerium, and 0.05 per cent of the ruthenium.

In the loop runs, radioactivity was introduced in the form of irradiated uranium which reacted with the hot water to simulate a fuel rupture. Analysis of loop liquid over a 12-day period indicated that the concentrations of uranium and fission products did not remain constant but exhibited variations both upward and downward.

Total gamma activity in steam samples was low and difficult to measure accurately. Calculated disengaging factors* were 2×10^3 for

*"Disengaging factor" is defined as the ratio of activity in the liquid phase to that in the steam phase. This factor is often called a "decontamination factor" in the literature but is not so called herein to avoid confusion with the "decontamination factors" reported which are the ratios of activities on solid surfaces before and after various chemical treatments.

total gamma counts to 9×10^4 for zirconium-95. Disengaging factors for other fission products fell in between these two values.

The fission products zirconium-95, ruthenium-103, and barium-140-lanthanum-140 were deposited on the metal sample strip in the disengaging section in the same relative proportions as they were present in the circulating liquid. Cerium-141 deposition in the liquid phase was lower than that suggested by its relative content in the circulating liquid.

Gamma spectra of loop water and residual undissolved uranium oxide indicated that iodine-131 was preferentially leached into the water.

The program for studying the effects of steam on structural materials for nuclear superheaters has been terminated and a final report is being written.

A. Determination of Nuclear Constants
(C. E. Crouthamel)

1. Fast Neutron Capture in Uranium-236
(D. C. Stupegia and R. Heinrich)

The neutron capture cross sections of uranium-236 have been determined for seven neutron energies between 0.475 and 1.74 Mev, using the Van de Graaff accelerators of the Reactor Engineering Division and of the Physics Division. In this work one measures the absolute uranium-237 activity produced in a known amount of uranium-236 in a known flux of monoenergetic neutrons. The flux is measured with a fission chamber. The absolute disintegration rate of uranium-237 was determined by relating its gamma spectrum to the spectrum of a known amount of uranium-237, which was assayed by 4π beta counting. The values obtained are given in Figure 47.

The values are expected to change slightly, depending upon refinements being made in the absolute 4π beta count of uranium-237. Such changes will be in the form of a constant factor, changing each value by about 5 per cent, but not affecting the values relative to each other. It is intended to extend the curve back to about 0.3 or 0.4 Mev on the low energy end, and to obtain one or two other points on the curve.

2. Capture and Fission Cross Sections of Uranium and Plutonium Isotopes in EBR-I, Mark III
(C. E. Crouthamel, D. C. Stupegia and R. Heinrich)

Samples of uranium-233, -235, and -238, and of plutonium-239 and -240 have been irradiated in the fast breeder reactor EBR-I, Mark III, for a total exposure of 800,000 kilowatt-hours. When the samples arrive they will be analyzed for their fission and capture cross sections in the fast reactor flux.

FIGURE 47
NEUTRON CAPTURE CROSS SECTION OF URANIUM-236

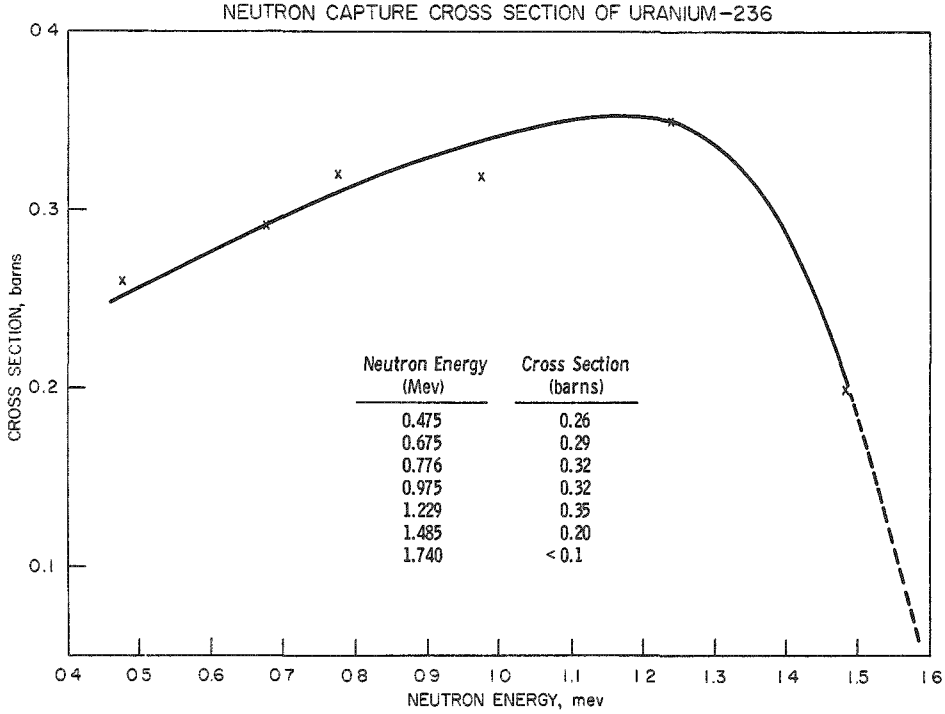

Neutron Energy (Mev)	Cross Section (barns)
0.475	0.26
0.675	0.29
0.776	0.32
0.975	0.32
1.229	0.35
1.485	0.20
1.740	< 0.1

The number of fissions in these samples will be determined by the chemical separation and absolute counting of the fission product cesium-137, whose fission yield is known in the fast neutron flux. The degree of neutron capture will be measured by comparing mass spectrographic analyses of the irradiated nuclides with similar analyses made before irradiation.

B. Slurrex Chemical Supporting Program
(C. E. Crouthamel)

This program has been terminated and a final report is being written.

C. Reactor Decontamination
(W. B. Seefeldt)

Laboratory studies are being made to evaluate decontamination methods that may be useful in boiling water reactor systems. Efforts to date have been focused on the decontamination of stainless steel type 304 with liquid reagents.

A recommended procedure for the decontamination of metallic surfaces contaminated by high-pressure steam (~600 psig) involves the use of alkaline permanganate and ammonium citrate or citric acid. Part of the investigations are aimed at exploiting the use of foam with these reagents in an effort to achieve decontamination with smaller volumes of solution than are necessary with liquid-phase decontamination.

A stainless steel type 304 loop which simulates the action of a boiling water reactor has been installed in a shielded cell in order to study the effects of fuel ruptures on the deposition of fission products in the vapor phase.

1. Laboratory Studies
(S. Vogler, H. Tyler)

a. Decontamination of Stainless Steel

Previous experiments with gross amounts of oxygen present in the autoclave during the contamination cycle produced contaminated stainless steel for which the decontamination by the alkaline permanganate procedure was markedly lower than for material contaminated in the absence of oxygen. More recent results (reported in ANL-6183, page 162) were carried out on metal contaminated in the presence of approximately 200 ppm of oxygen. These results showed a total gamma decontamination factor of four as compared with a decontamination of sixteen for metal contaminated in a steam phase in the absence of oxygen.

The procedure for these experiments was to place a piece of irradiated natural uranium in 100 ml of deionized water in a preoxidized stainless steel liner, which in turn was placed in the autoclave. The autoclave was evacuated quickly to one mm by means of a vacuum pump. Then a small amount of oxygen was expanded into the autoclave system to produce a vapor space concentration of approximately 200 ppm at operating conditions. The autoclave was heated to approximately 250 C and maintained at 600 psig for $6\frac{1}{2}$ days. Upon completion of the run and cooling of the autoclave, a sample of the residual gas was taken. This gas was chiefly hydrogen generated by the reaction of water with the uranium metal. Mass spectrometric analysis of the gas in a typical experiment gave 0.02 per cent oxygen, which was approximately 15 per cent of the oxygen originally added to the autoclave. The liner was then cut into one-inch squares for the decontamination experiments, which were performed by means of the alkaline permanganate-citrate decontamination procedure.

The metal sample pieces used in the decontamination experiments were assayed with a 256-channel gamma scintillation spectrometer both before and after the decontamination procedure. From an examination of the gamma scintillation spectrometer scans the counting rates of various fission products were computed by measuring the area under the principal peak for the individual fission products. A comparison of the counting rate before and after the decontamination experiment yielded a measure of the decontamination for that particular fission product. Examination of the gamma scintillation scans indicated four major peaks and one minor peak. The major peaks were attributed to cerium-141, ruthenium-103, zirconium-95, niobium-95, and iodine-131. The minor peak was not investigated but could represent a secondary iodine-131 peak or a cesium-137 peak.

The first two experiments were performed immediately upon the completion of the contamination segment of the experiment (produced by irradiated natural uranium with one-month cooling). The decontamination experiments were repeated one month later using the same contaminated metal. The decontamination factors for the individual fission products are summarized in Table 31.

Table 31

SPECIFIC FISSION PRODUCT DECONTAMINATION BY THE ALKALINE PERMANGANATE PROCEDURE

Effect of Oxygen during the Contamination Step

Cooling Time of Activity:[a] ~ 30 days for Expt 1 and 2
60 days for Expt 3 and 4

Expt 1 and 3: Contaminated in the presence of 200 ppm oxygen
Expt 2 and 4: Contaminated in the absence of noncondensible gases

Decontamination

Solution 1: 0.5 per cent $KMnO_4$ in 1 per cent NaOH, four hours at 25 C
Solution 2: 10 per cent ammonium citrate, $\frac{1}{4}$ hour at 85 C

Activity	Decontamination Factors[b]			
	Expt 1	Expt 2	Expt 3	Expt 4
Total Gamma	3	19	8	33
	5	13	24	46
Iodine	2.6	20	-	-
Cerium	3.0	18	4	13
			12	28
Ruthenium	7.8	7.3	12	119
			28	>200
Zirconium	-	-	66	330
			120	440

[a]The metal samples for Experiments 1 and 3 and for Experiments 2 and 4 were contaminated at the same time. As indicated, the metal samples for Experiments 3 and 4 were allowed to stand in air for an additional 30 days before being decontaminated.

[b]Pairs of numbers indicate duplicate liner specimens.

These results indicated that the limitation in the total decontamination in Experiment 1 was the result of a drop in both the cerium and iodine decontamination factors as compared with Experiment 2. The iodine

activity in Experiments 1 and 2 was by far the most prominent activity on the metal plate, representing greater than 50 per cent of the total activity upon the plate. Zirconium data were not tabulated for the first two experiments because of difficulty in fully resolving the zirconium peak. In Experiments 3 and 4 (one-month additional cooling time) similar differences in the decontamination were still noticeable. Again it appeared that a low cerium decontamination resulted in a low total gamma decontamination. In Experiments 3 and 4 differences in the ruthenium decontamination were more evident.

The results obtained indicate that the presence of oxygen during the contamination step resulted in a reduced decontamination with the alkaline permanganate-citrate procedure when compared with metal contaminated in the absence of oxygen. The improvement in the gross gamma decontamination obtained in Experiments 3 and 4 was due both to the elimination of iodine by decay and the improvement in the fission product decontamination, which was apparently due to a longer standing time of the samples between contamination and decontamination.

b. Distribution of Fission Product Activities in Contamination Runs

As an aid in evaluating the amount of contamination which might occur following a fuel rupture in a boiling water reactor, it was of interest to determine the distribution of the individual fission products between the solid uranium dioxide and the supernatant water of the autoclave, and to compare this with the distribution of the fission products deposited on the metal.

The activity in the supernatant water was determined by counting an aliquot of the solution evaporated on a metal plate. The uranium dioxide was dissolved in nitric acid, and an aliquot dried, and counted. These, as well as samples of the liner, were counted by means of the 256-channel scintillation spectrometer. The amounts of the individual activities present in a particular sample were determined by counting under the appropriate peak after the position and clarity of the peak had been established from plots of count rate against energy. The total gamma and the iodine, ruthenium, and cerium gamma activities were computed and compared. These values are given in Table 32. Zirconium gamma activity was not calculated in most cases because of the difficulty of resolving the zirconium peak on the gamma spectra.

Iodine was most readily leached from the uranium dioxide, the cerium and ruthenium being leached to a much lesser extent. Qualitatively, it appeared that the zirconium activity was leached from the uranium dioxide to the same extent as the ruthenium activity. The activities deposited on the metal specimens were determined by measuring the area

under the appropriate peak. The data indicate that the activities are depositing on the metal strips in approximately the same ratio as they are present in the supernatant water except for ruthenium in the oxygen experiment (Run 33). In this case, the ruthenium was deposited to an extent at least tenfold greater.

Table 32

DISTRIBUTION OF FISSION PRODUCT ACTIVITY AFTER AN AUTOCLAVE CONTAMINATION RUN

Uranium Weight: 2.5 g
Exposure Time: 3 d
Cooling Time: 30 d
Total Activity Present: $\sim 1.5 \times 10^{10}$ γ cpm

	% Indicated Activity Found in Supernatant		Ratio of Deposited Activity on Metal Sample to the Activity in Supernatant[a]	
Activity	Run 33	Run 34	Run 33	Run 34
Total Gamma	2.0	3.1	0.15	0.07
Iodine	52	48	0.12	0.08
Cerium	0.9	1.0	0.20	0.10
Ruthenium	0.05	0.04	4.1	0.33

[a]This ratio gives a measure of the selective adsorption of fission products.

c. Corrosion Behavior

Previously reported results (ANL-6183, page 158) had indicated that ammonium citrate or citric acid solutions resulted in excessive corrosion of mild steels. Adjustment of the pH of citrate solutions to a value of 10 with sodium hydroxide resulted in an acceptable decrease of the corrosion. However, microscopic observation of the metallic specimens indicated that the corrosion of the chromium-molybdenum steel (1 per cent chromium-0.5 molybdenum) proceeded via pitting, which makes corrosion evaluation difficult.

Attempts to minimize the pitting were attempted by the use of corrosion inhibitors such as 2-mercapto-benzo-thiazole and hexamethylene tetramine. The procedure was the following. The metallic specimen was first wet ground with 120 grit silicon carbide abrasive paper

and then weighed. The specimen was placed in a solution of 0.5 per cent potassium permanganate-one per cent sodium hydroxide for four hours at room temperature. After removal from this solution, it was placed in a sodium citrate solution for four hours at 85 C. The results are given in Table 33.

Table 33

CORROSION OF CHROMIUM-MOLYBDENUM STEEL IN ALKALINE PERMANGANATE-CITRATE SOLUTIONS

Sample: Wet ground with 120 grit silicon carbide abrasive paper
Solution 1: 0.5 per cent potassium permanganate in 1 per cent sodium hydroxide, 4 hours at 25 C
Solution 2: 10 per cent sodium citrate pH 10, temperature 85 C with indicated inhibitor and time

Time of Exposure to Solution 2 (hr)	Wt Loss[a] (mg)			
	No Additive[b]	No Additive	2 Mercapto-benzothiazole	Hexamethylene tetramine
0.25	-	0.6	0.6	1.7
4.0	17.9	4.6	7.5	4.4

[a]Average of two measurements.

[b]Solution 1 was 3 per cent potassium permanganate in 20 per cent sodium hydroxide; sample was exposed for five hours at 90 C.

From the weight loss data there appears to be little effect produced by the corrosion inhibitors. However, microscopic examination made at the end of the four-hour exposure in the citrate solution revealed differences. The samples which were subjected to the solutions without additive were severely pitted. The 2-mercapto-benzo-thiazole resulted in a large decrease in the frequency of pitting, but there still remained several deep pits. With the hexamethylene tetramine, no deep pits were visible. In places the surfaces were slightly roughened as if corrosion were first starting.

Additional corrosion tests will be carried out in which several commercial acid inhibitors will be tested.

2. Loop Operations
(D. Grosvenor, C. Bally)

A stainless steel type 304 loop which simulates the action of a boiling water reactor has been installed in a shielded cell in order to study

the effects of fuel ruptures on the deposition of fission products in the vapor phase. A description of the equipment appeared in ANL-5858, page 66.

Loop experiments are not intended to include the study of volatile fission products whose daughters are short-lived and not likely to cause reactor maintenance problems for long periods. Such experiments are best performed and have been done in reactor systems. Fuel ruptures are simulated by the addition of fission products to the loop, either in the form of tracer or as irradiated metallic uranium. Deposition of the radioactive species on surfaces in the vapor phase is monitored in two ways. A metal sample strip of the material to be studied is inserted in the water-steam disengaging section; this is removed and analyzed following a run using the 256-channel gamma scintillation spectrometer. In addition, a scintillation detector is mounted outside the disengaging section at an elevation eight inches below the steam exit line. All elevations referred to in the text, figures, and tables are measured from a common reference point, namely, the liquid sample line. The elevations of pertinent equipment items are shown in Figure 48.

FIGURE 48
DISENGAGING SECTION OF LOOP SHOWING ELEVATIONS OF COMPONENTS RELATIVE TO REFERENCE

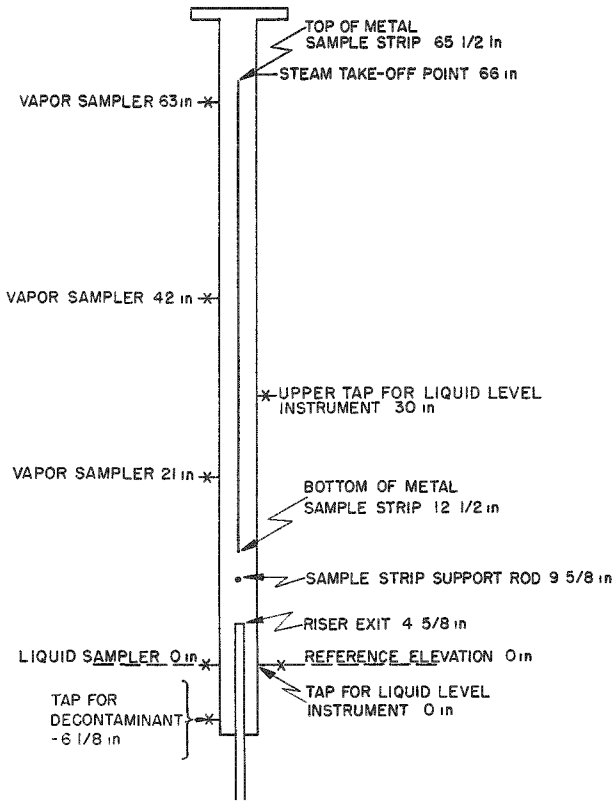

Data are reported below for two runs, U-1 and U-2, in which fission product activity was introduced into the loop as metallic irradiated uranium. Cooling times for the two runs were 37 and 52 days, respectively.

The operating conditions that were common for both runs were a steam velocity of 0.8 ft/sec, 200 psig operating pressure, and liquid levels of 17 to 20 inches. The durations of the experiments were 140 and 284 hours, respectively.

a. Loop Liquid Composition

Samples of loop liquid were taken at two-day intervals starting on the sixth day. Gamma-energy spectra were obtained with the 256-channel gamma scintillation spectrometer. A typical scan of loop water is shown in Figure 49. Six photo peaks can be identified, each of which is attributable to a single fission product. These include: cerium-141, iodine-131, ruthenium-103, cesium-137, zirconium-95-niobium-95, and barium-140-lanthanum-140. Table 34 lists the half-lives and principal gamma energies contributed by each of these isotopes.

FIGURE 49
GAMMA ENERGY SPECTRUM OF LOOP WATER FROM RUN U-I

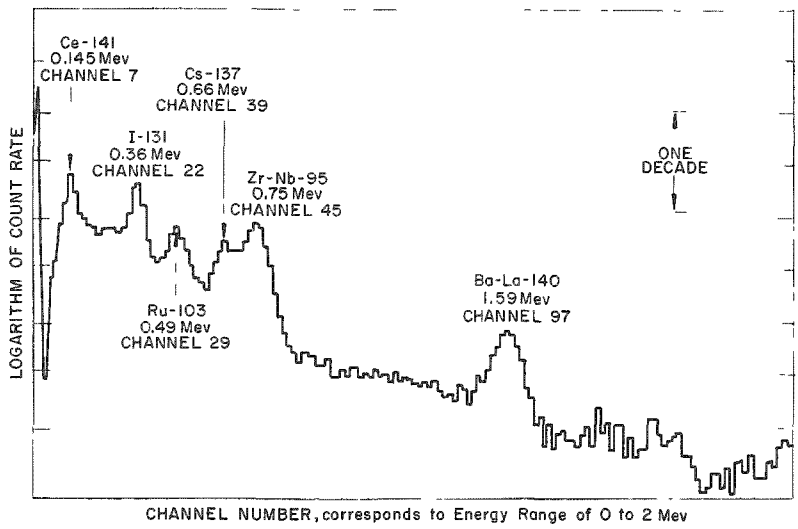

Table 34

HALF-LIVES AND PRINCIPAL GAMMA ENERGIES OF FISSION PRODUCTS OBSERVED IN LOOP RUNS

Isotope	Half-life	Principal Gamma Energies (Mev)
Cerium-141	33.1 d	0.145
Iodine-131	8.1 d	0.364
Ruthenium-103	39.8 d	0.498
Cesium-137	30.0 y	0.662
Zirconium-95	65.0 d	0.740
Niobium-95	35.0 d	0.768
Barium-140	12.8 d	0.126, 0.537
Lanthanum-140	40.2 h	0.33, 0.49, 0.82, 1.60

To determine the relative quantity of a particular isotope in various samples, the area under each photo peak was measured, background subtracted, and the result converted into counts per minute. The limitations of this method include a neglect of Compton and back-scattering contributions and their interferences with other photopeaks. In addition, merging of two photo peaks occurs, as is evident in Figure 49 with the 0.66 and 0.75-Mev contributions.

Figure 50 shows the variation of radioactive composition of the circulating liquid of Run U-2 with time. Ideally, one would desire that this composition remain constant during a run in order to maximize the reliability of the information derived from an experiment. The zirconium-95 and ruthenium-103 contents decreased between the sixth and eighth days, then remained reasonably steady to the end of the run. The uranium content dropped sharply between the sixth and eighth day, and rose to a higher value in the loop drainings. Total beta and gamma counts showed small variations.

FIGURE 50
COMPOSITION OF LOOP WATER DURING RUN U-2

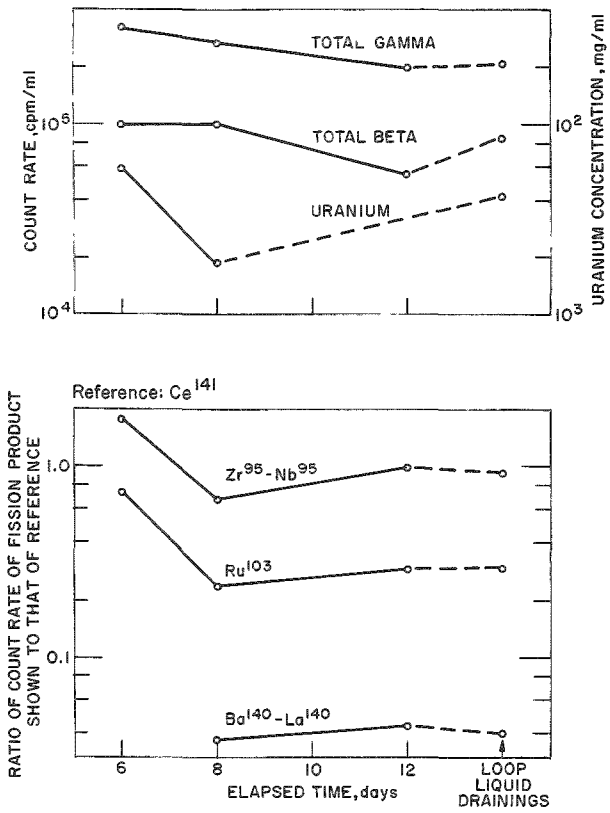

Gamma-energy spectra of both loop water and nitric acid-dissolved uranium dioxide residues were compared for Runs U-1 and U-2 to determine if there were any differences in fission product distribution. The results are shown in Table 35. The distributions of all isotopes,

except that of iodine-131, between loop water and uranium oxide residue were not significantly different. The iodine-131 content of the loop water was greater by a factor of ten than that in the uranium dioxide. Thus iodine appears to be the only fission product which is preferentially leached from the uranium specimen.

Table 35

COMPARISON OF INDIVIDUAL FISSION PRODUCT CONTENT OF LOOP DRAININGS AND RESIDUES

		Ratio: $\frac{\text{Peak Count Rate}}{\text{Total Count Rate}}$				
		Energy (Mev) and Isotope				
		0.145	0.364	0.500	0.75	1.59
Run No.	Description	Ce^{141}	I^{131}	Ru^{103}	Zr^{95}-Nb^{95}	Ba^{140}-La^{140}
U-1	Loop Drainings	-	0.216	0.080	0.185	0.017
U-1	Dissolved UO_2	-	0.032	0.129	0.231	0.023
U-2	Loop Drainings	0.112	-	0.043	0.202	0.0018
U-2	Dissolved UO_2	0.099	-	0.057	0.195	0.0018

b. Deposition on Metal Sample

The deposition of individual fission products on the removable $\frac{1}{2}$-inch wide metal sample strip from the disengaging section was determined for the two runs. Specimens of $\frac{1}{2}$-inch length were cut from the stainless steel strip at approximately 20 selected locations. Gross gamma counts were obtained on each sample, using a 50-kev threshold. About 6 of the samples of each run were selected for analysis with the 256-channel gamma scintillation spectrometer. The principal photopeaks observed in gamma-energy spectra of the metal coupons were at 0.14, 0.49, and 0.75 Mev. The 1.6-Mev photopeak was generally observed, but its contribution was smaller than that shown for the loop water in Figure 49.

The distribution of individual fission products plated on the stainless steel strip as a function of elevation in the disengaging section, as determined by the area-measuring method, is shown in Figures 51 and 52. All isotopes show the same marked reduction with elevation as does the total gamma count. The relative amounts of the isotopes appear to be nearly the same at all points on the metal strip 12 inches or more above the liquid. In Run U-1, iodine-131 was identified on a single metal sample located in the liquid phase but on no samples in the vapor phase. No cerium-141 activity was identified on samples from Run U-1, and no iodine-131 or cesium-137

activity was identified from samples in Run U-2. Because of the long cooling time, relatively little iodine-131 would be expected to be present in these runs. By examining the curves and comparing them with the isotopic content of the circulating loop liquid, it appears that the zirconium-95, niobium-95, ruthenium-103, and barium-140-lanthanum-140 deposited in both liquid and vapor phases in approximately the same relative proportions as they are present in the loop liquid. The proportion of total counts deposited on the sample strip in the vapor phase attributable to cerium-141 is somewhat higher than the relative content in the loop liquid would suggest; deposition of cerium-141 in the liquid phase is lower. It appears that cerium-141 is easily washed off in the liquid phase.

FIGURE 51
DEPOSITION OF FISSION PRODUCTS ON METAL SAMPLE STRIP DURING RUN U-2
STEAM VELOCITY 0 8 ft/sec, 200 ps g, SAMPLE SS 304
SAMPLE AREA ca 2 sq cm RUN LENGTH ca 6 days
COOLING TIME 37 days IRRADIATION 41 MWD/ton
WEIGHT URANIUM 16 2 gm

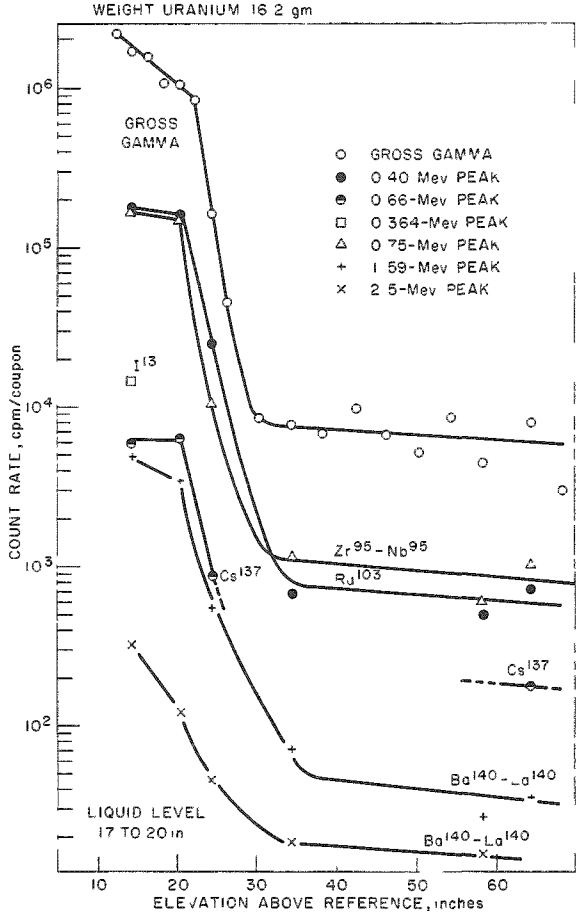

FIGURE 52
DISPOSITION OF FISSION PRODUCTS ON METAL SAMPLE STRIP DURING RUN U-2
SAME AS FIGURE 51 EXCEPT, RUN LENGTH Ca 12 days
COOLING TIME 52 days
IRRADIATION 41 MWD/ton
WEIGHT URANIUM 499 gms

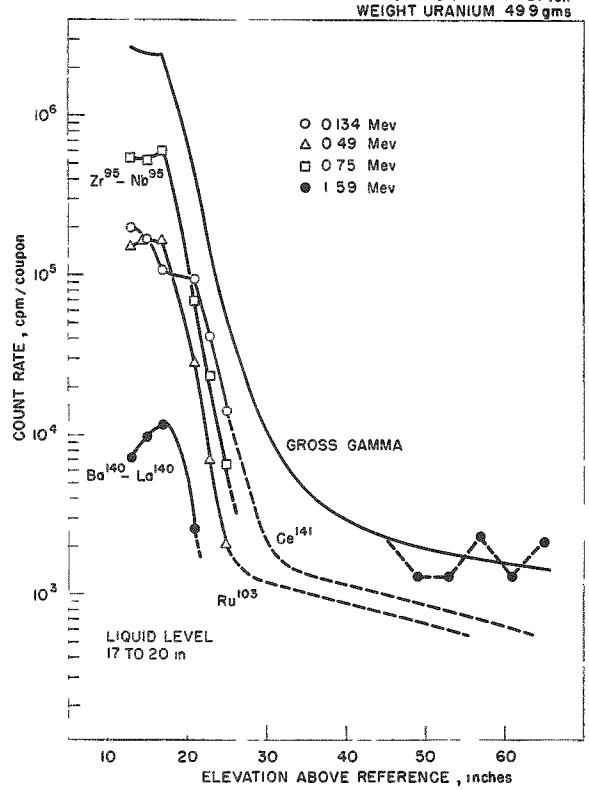

c. Steam Samples and Disengaging Factors

Gamma-energy spectra were obtained with several steam samples (elevation 63 inches), and disengaging factors were calculated. The disengaging factors varied from 2×10^3 for gross gamma counts as obtained

in a well-type scintillator to 9×10^4 for zirconium-95 based on counts under the peaks. The ruthenium-103 disengaging factor was 1×10^4. Because the activity level in the steam samples was very low, the accuracy of these data is somewhat uncertain.

d. Decontamination Results

The loop is intended primarily for contamination studies, but it must be decontaminated between experiments in order to produce meaningful contamination information. Decontamination is therefore incidental to the principal objective of contamination. To achieve the cleanest possible loop consistent with the procurement of good data, it is sometimes necessary to use stronger chemicals (such as nitric acid) than would normally be allowed in a reactor system. It is for this reason that the procedures used do not follow in detail those that are under development in the laboratory. Following the procurement of useful contamination data, the procedures which have been developed in the laboratory and which take into account reactor system integrity, volumes, waste handling, and waste processing will be tested in the loop. The data shown below should not be interpreted as being part of the systematic development program of decontaminants, but rather as information accumulated in the process of preparing the loop for a subsequent contamination run.

The results obtained with respect to the removal of uranium, and beta and gamma activities from the loop during decontamination operations is shown in Tables 36 and 37. In Run U-1, the alkaline permanganate procedure was used following a nitric acid step, and in Run U-2 the same procedure following a peroxide-carbonate-bicarbonate step. The bulk of the uranium recovery in Run U-1 was accomplished with nitric acid, while half of the recovery in Run U-2 was attributed to the basic peroxide mixture. Both runs confirm the fact that the alkaline permanganate solutions remove little uranium or beta and gamma activity. Ammonium citrate in Run U-1 likewise removed little uranium or activity, but in Run U-2, it removed considerable amounts of both. Also of interest is the fact that the uranium dioxide residue of Run U-1 contained 31 per cent of the recovered beta counts, while the same material of Run U-2 contained 2.5 per cent of the recovered gamma counts.

3. Present Status of the Work

The efforts in the Reactor Decontamination program to date have been directed primarily at modifying known decontamination procedures for use in boiling water reactors. Factors that guide modification include the large volumes of vapor space inherent in this reactor type, the possible difficulties of heating large volumes of solution by non-nuclear means to near boiling temperatures, the possible inability of system components to withstand liquid loading, and the handling and disposal of the resulting wastes.

Table 36

REMOVAL OF URANIUM AND BETA ACTIVITIES FROM LOOP FOLLOWING RUN U-1

	Uranium Removed		β Counts Removed	
	(g)	(per cent)[a]	(cpm x 10^{-9})	(per cent)[a]
Removed from Loop after Run				
Loop Drainings	0.006	0.04	1.26	2.41
Dissolved UO_2 from Sample Holder	4.28	28.6	15.8	30.2
Removed from Loop During Decontamination				
10% nitric acid	10.50	70.3	32.2	61.6
Alkaline permanganate 1[b]	-	-	1.1	2.1
Alkaline permanganate 2[b]	-	-	0.67	1.3
Water rinse (vapor section)	-	-	0.23	0.44
Water rinse (liquid section)	-	-	0.29	0.55
Ammonium citrate[c]	0.121	0.81	0.54	1.03
Water rinse	0.035	0.23	0.14	0.27
Totals	14.94		52.2	
Amount of U charged to loop	16.24			

[a]Based on total quantity removed.

[b]Composition 3.0% $KMnO_4$, 10% NaOH; temp 65 to 75 C; time 2 to 3 hr.

[c]Composition 10% ammonium citrate; temp 65 to 75 C; time 2 to 3 hr.

Table 37

REMOVAL OF URANIUM AND GAMMA ACTIVITIES FROM LOOP FOLLOWING RUN U-2

	Uranium Removed			γ Counts Removed		
	(g)	(per cent)[a]		(cpm x 10^{-9})	(per cent)[a]	
Removed from Loop after Run						
Loop drainings	0.02	-		0.89	0.19	
Dissolved UO_2 from sample holder	7.60	13.5		16.2	3.5	
Removed from Loop During Decontamination						
Peroxide-carbonate[b]	25.2	43.3	68.3	205	44.4	81.0
Alkaline permanganate[c]	1.16	2.0		8.8	1.91	
Water rinse	0.28	0.5		0.7	0.15	
Ammonium citrate[d]	11.08	19.0		139.0	30.1	
Water rinse	1.94	3.5		203	4.4	
10% nitric acid	9.4	16.1	18.7	64.7	14.0	14.1
Water rinse	1.48	2.6		0.3	0.06	
Miscellaneous solutions	-	-		5.7	1.23	
Totals	58.16			461.6		
Amount of U charged to loop	49.37					

[a]Based on total quantity removed.

[b]Composition: 0.5 M H_2O_2, 0.25 M Na_2CO_3, 0.25 M $NaHCO_3$, 3.5 g/gal EDTA, 1 g/gal 8-hydroxyquinoline; 2 hours at room temperature, 2 hours at 50 C.

[c]Composition: 3% $KMnO_4$, 10% NaOH; 2 to 3 hr at 65 to 75 C.

[d]Composition: 10% Ammonium Citrate; 2 to 3 hr at 65 to 75 C.

The alkaline permanganate decontamination procedure as used by Hanford Laboratories, Westinghouse Bettis, Westinghouse Atomic Power Division, and others has been the principal basis for study. The first step has been modified by lowering temperatures, reducing concentrations, and extending contact times. This has resulted in reduced decontaminating ability, which, though reduced, appears sufficiently good to be attractive for a reactor system. The laboratory data obtained thus far pertain to stainless steel type 304 surfaces. Experience at other laboratories has usually shown that data of this kind are optimistic relative to subsequent tests on practical systems. There is evidence that suggests that the presence of oxygen during contamination and the aging of contaminated surfaces affects decontamination capability - the oxygen decreases it, whereas aging appears to improve it. Zirconium is most easily removed by the alkaline permanganate procedure; ruthenium is removed less readily but the removal is still good. Cerium and iodine removals have been variable, with decontamination factors between two and thirty.

Corrosion experiments have shown that the alkaline permanganate procedure is, in general, compatible with mild and low alloy steels provided that the pH of the citrate solution used in the second step is increased to 9, or an inhibitor used. The procedure is not useful in systems containing aluminum or its alloys. This study has not to date included procedures that are simultaneously compatible with aluminum, mild steels, and stainless steels.

The use of foam to transport liquid decontaminants has been explored in a preliminary manner as a method to overcome or reduce the problems of waste volumes and the inability of system components to sustain liquid loadings. Early tests suggested that decontamination with foam was feasible; a possible limitation being foam stability at temperatures of 60 C or higher. This work was interrupted in order to clarify the effects of oxygen during contamination or decontamination.

D. Structural Materials for Nuclear Superheaters
(E. H. Dewell)

This program has been terminated and a summary report is being written.

V. ROUTINE OPERATIONS
(H. G. Swope)

A. Radioactive Waste Processing
(J. Harast, K. Bremer, G. Teats, R. Jarrett, and V. Lemke)

There were 31,415 gallons of liquid radioactive wastes processed from July through September, 1960. The processing methods used were as follows:

Process	Gallons
Evaporation and Concentration	22,074
Filtration	4,240
Ion Exchange (cation only)	4,240
Neutralization of HF Wastes	105
Absorption on Vermiculite	756
Total	31,415

B. High-level Gamma Irradiation Facility
(H. G. Swope, J. Harast, N. Ondracek, B. Kullen, R. Juvinall, C. Ryberg, and D. Santelli)

A summary of irradiations performed in Rack M-1 for July through September, 1960 is given in Table 38.

Table 38

SUMMARY OF IRRADIATIONS PERFORMED IN RACK M-1 DURING JULY THROUGH SEPTEMBER, 1960

Month	No. of Samples[a]	No. of Special Dosimetry Samples	Total Urn Units[b]	
			Day	Night
July	559	246	1240	3552
August	1061	658	1785	2092
September	983	800	1612	2467
Total	2603	1704	4637	8111

[a]Equivalent to a No. 2 sized can ($3\frac{7}{16}$ in. diam x $4\frac{9}{16}$ in. high).

[b]1 urn unit = 2×10^6 rad.